ABSTRACT

Title of dissertation: The Cellular Basis for Hearing

Bora Sul, Doctor of Philosophy, 2010

Dissertation directed by: Professor Rajarshi Roy
Department of Physics

Doctor Kuni H. Iwasa
National Institute on Deafness
and Other Communication Disorders

Hair cells constitute the cellular basis for hearing. Their primary role is to convert mechanical signal into electrical signal through the ion channels, called "mechano-electrical transducer (MET) channels", in the hair bundles of hair cells. Another important function of hair cells is to reciprocally amplify the mechanical input signal by working against damping due to viscous fluids in the organ. This thesis consists of theoretical investigations on hair cell function as the mechano-electrical transducer and as the cochlear amplifier.

First, we examine gating of two MET channels that are coupled to each other. While gating of MET channels has been successfully described by assuming that in a hair bundle, one MET channel is associated with one tip link, recent reports indicate that a single tip link is associated with more than one channel [7, 8]. To address the

discrepancy between the earlier models with the recent experimental observations, we describe gating of MET channels by assuming that each tip link is associated with two identical MET channels, which are connected either in series or in parallel. We found that series connection model predicts double minima of the hair bundle stiffness with respect to the hair bundle displacement if the minimum is below a certain positive value. In contrast, the parallel connection model makes predictions similar to the previous model that assumes a single channel for each tip link, within the physiological range of parameters. This explains how the earlier models assuming a single channel for each tip link has been successful in describing gating of MET channels. The parallel connection model of MET channels is, therefore, a reasonable assumption to explain most experimental observations. However, we show that turtle hair cell data may be compatible with the series connection model.

Second, we examine roles of hair cells as an amplifier in the cochlea. Hair cells are responsible for high sensitivity and frequency selectivity of hearing. This is attributed to motile mechanisms in hair cells, "electromotility" which indicates length change of outer hair cell driven by AC electrical potential across the membrane, and "hair bundle motility" which is an active movement of the hair bundle of hair cells. We first investigated the amplifying role of hair cells in the mammalian ear, including studies of both electromotility and hair bundle motility.

Electromotility is driven by the receptor potential, which is an AC electrical potential generated by gating of MET channels. Thus, the frequency characteristics of electromotility are determined by a low-pass filter, represented by the product of membrane resistance R and capacitance C with frequency roll off at about 0.1

of the highest audible frequency. This filter significantly decreases the efficiency of electromotility as an amplifier. In the thesis, we examine a proposal that the cochlear microphonic, the voltage drop across the extracellular medium by the receptor current, contributes to overcome this problem. We found that this effect can improve the frequency response. However, this effect alone is too small to enhance the effectiveness of electromotility beyond 10 kHz in the mammalian ear.

It has been experimentally found that the hair bundle motility in the mammalian ear is based on a "release mechanism", which is the fast component in the hair bundle's response to mechanical stimulation. In the release mechanism, the hair bundle responds in a way to reduce applied tension, similar to common mechanical relaxation with a damping. This observation is puzzling because hair bundle motility based on the release mechanism is expected to have an amplifying role. In the thesis we show that a release mechanism can indeed have a role in amplification if it takes place in a range where effective hair bundle stiffness has a negative value.

Finally we expand scope of investigation to avian hair cells, which must rely on hair bundle motility for amplification due to lack of electromotility. Specifically we evaluate the effectiveness of hair bundle motility in mammalian and avian ears. If hair bundle motility works for amplification, energy generated by the hair bundle must be, at least, greater than energy lost due to damping in the viscous fluid of cochlea. We compare work done by the hair bundle motility with the energy loss due to shear in the sub-tectorial gap during one cycle of small sinusoidal hair bundle displacement. This condition gives a frequency limit where the hair bundle motility can work as an amplifier in the cochlea. We obtain frequency limits for

two mechanisms for hair bundle motility; one is based on the interaction between calcium and the MET channel and the other is based on the interplay between gating of the channel and the myosin motor. We show that the frequency limit obtained for each of these models is an increasing function of a factor that is determined by the morphology of hair bundles and the cochlea. Primarily due to the higher density of hair cells in the avian inner ear, this factor is about 10-fold greater for the avian ear than the mammalian ear, which has much higher auditory frequency limit. This result is consistent with a much greater importance of hair bundle motility in the avian ear than that in the mammalian ear.

THE CELLULAR BASIS FOR HEARING

by

Bora Sul

Dissertation submitted to the Faculty of the Graduate School of the
University of Maryland, College Park in partial fulfillment
of the requirements for the degree of
Doctor of Philosophy
2010

Advisory Committee:
Professor Rajarshi Roy, Chair/Advisor
Doctor Kuni H. Iwasa, Co-chair/Co-advisor
Professor Michael A. Coplan
Professor Theodore R. Kirkpatrick
Professor Wolfgang Losert

Dedication

To my God who is the source of life, power, and wisdom

Acknowledgments

This research project would not have been possible without the support of many people.

I thank my research advisor, Dr. Kuni H. Iwasa who has been patient and offered invaluable assistance, and support. Working with him has been a wonderful experience.

I thank my advisor Professor Rajarshi Roy who has been always patient and supportive. His advices and encouragements have been a great support throughout my research.

I thank my dissertation committee members, Professors Michael Coplan, Kuni H. Iwasa, Theodore Kirkpatrick, Wolfgang Losert, and Rajarshi Roy. Their comments and suggestions were particularly helpful in improving my thesis.

I thank Professor Wolfgang Losert and Dr. Bruce Kane. Professor Losert gave me the opportunity to participate in experimental biophysics research in his lab. Dr. Kane gave me the opportunity to participate in quantum computing research in his lab.

I thank Professors Robert J. Dorfman and Michael Coplan who are wonderful teachers. They received me always with patience, encouragement, and good resources even when I approached them with stupid questions.

I thank Dr. David Robinson. I appreciate his encouragement as well as useful comments in improving my work.

I thank Physics Department in University of Maryland and NIDCD (National

Institute on Deafness and Other Communication Disorders) for supporting my graduate studies and research.

I also thank all of my friends. My lab members, Dr. Ghanshyam P. Sinha, Dr. Fang Jie, and Dr. Chisako Izumi, always gave me useful advices and support. All my church members have supported me with sincere prayers. I thank my friends in Korea, especially Sungbin Cho who has supported me in many ways. I thank my dear friend Dr. Anand Banerjee. He has helped me throughout my Ph.D studies, with useful comments and wonderful support. Time spent with him is one of the most precious moments in graduate school.

Special thanks to my family. Their love and support give me strength to overcome any trouble in my life.

Most importantly, I give special thanks to my God who is the source of life, power, and wisdom in my life. How amazingly and faithfully He has guided me throughout my life is unimaginable.

Table of Contents

List of Tables

List of Figures

List of Abbreviations

AC	alternating current
ADP	adenosine di-phosphate
ATP	adenosine tri-phosphate
BM	basilar membrane
Ca	calcium
CAP	compound action potential
CM	cochlear microphonic
dB	decibel
DC	deiters' cell (in chapter 1)
	direct current (in chapter 3)
EM	electron micrograph
K	potassium
NIDCD	National Institute on Deafness and Other Communication Disorders
NIH	National Institutes of Health
MET	mechano-electrical transducer
Myo1c	myosin 1c
OHC	outer hair cell
pRP	pseudo-receptor potential
RL	reticular lamina
RP	receptor potential
SPL	sound pressure level
TM	tectorial membrane

List of Publications

1. B. Sul and K.H. Iwasa,"Gating of two mechanoelectrical transducer channels associated with a single tip link," Biophys. J. 99(4):1027-1033 (2010).

2. B. Sul and K.H. Iwasa, "Effectiveness of hair bundle motility as the cochlear amplifier," Biophys. J. 97:2653-2663 (2009).

3. B. Sul and K.H. Iwasa, "Amplifying effect of a release mechanism for fast adaptation in the hair bundle," *J. Acoust. Soc. Am.* 126:4-6 (2009).

4. K.H. Iwasa, B. Sul, J. Fang and G.P. Sinha, "Cellular basis of the cochlear amplifier," *In Concepts and challenges in the biophysics of hearing*, N.P. Cooper, and D.T. Kemp, editors, World Scientific, Singapore, 303-309 (2009).

5. C. Köppl, K.H. Iwasa and B. Sul, "Big and powerful: a model of the contribution of hair bundle motility to mechanical amplification in hair cells of the bird basilar papilla," *In Concepts and challenges in the biophysics of hearing*, N.P. Cooper, and D.T. Kemp, editors, World Scientific, Singapore, 444-450 (2009).

6. K.H. Iwasa and B. Sul, "Effect of the cochlear microphonic on the limiting frequency of the mammalian ear," *J. Acoust. Soc. Am.* 124(3):1607-1612 (2008).

Chapter 1

Introduction

The beginning of hearing process takes place in the ear by the function of hair cells. Hair cells are located in the inner ear cochlea (Fig. 1.1). Their primary role is to convert the mechanical signal originated from sound into electrical signal to be sent to the brain. Due to their strategic morphology and location in the inner ear, hair cells can detect the external stimuli even with 1nm displacement at their apical tips.

Another important function of hair cells is to amplify mechanical signal from external stimuli, which otherwise would be diminished due to severe damping in the ear. The amplifying function of hair cells enables the ear to cover a remarkable range of sound with high frequency selectivity and this will be discussed in the later section of this chapter.

The main theme of the thesis is the cellular basis of hearing, particularly studies of how different mechanisms in hair cell work for mechano-electrical transduction and amplification. In this chapter, I will introduce a brief overview of the anatomy and auditory function of the ear.

1.1 Anatomy of the inner ear

The figure 1.1 shows anatomy of the human ear. The sound collected in the external ear is funneled into the middle ear. At the middle ear, sound induced vibration of the tympanic membrane is transferred to the inner ear, cochlea, through the bones attached to the tympanic membrane, called malleus, incus, and stapes, in adjacent to the windows of the cochlea. The cochlea is a spirally coiled organ, embedded within the tympanic bone. Its coiled passage has an internal diameter of about one and a half millimeters in humans and a total length of about 35 mm measured along its spirally curved centerline. In the middle of the cochlea, a partition, called cochlear partition, is located along the entire length of the cochlea dividing it into two chambers of fluids, the scala vestibuli and scala tympani, which are called perilymph, and ends at the helicotrema (Fig. 1.1B). The cochlear partition shows a systematic change in its stiffness and width from the window region (i.e. base) to the helicotrema (i.e. apex); the width of the cochlea increases from 0.04 mm to 0.5 mm and its stiffness decreases by two orders of magnitude from the base to apex (Fig. 1.1C).

The cochlear partition consists of three major elements: tectorial membrane, basilar membrane, and organ of Corti (Fig. 1.2A). The tectorial membrane is a gelatinous and fibrous flap and the basilar membrane is an elastic membraneous structure. The organ of Corti, which contains hair cells and nerve fibers, is covered by the tectorial membrane, sitting on the basilar membrane. A space, called subtectorial space, between the tectorial membrane and the organ of Corti is sealed by

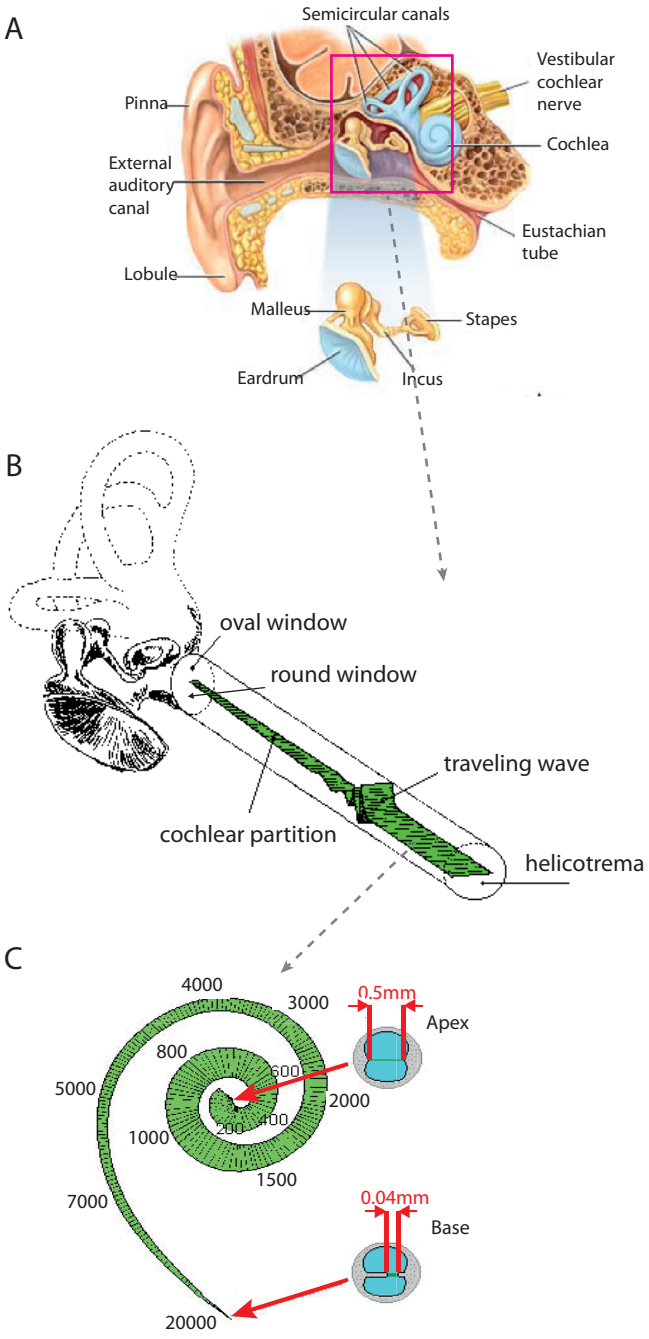

Figure 1.1: (A) Anatomy of the human ear. (B) Schematic representation of uncoiled cochlea. (C) Cochlear partition and frequency to which the cochlear partition responds most. Numbers are frequencies in Hz. Figure (A) reprinted from mdconsult.com and (B), (C) from [105].

reticluar lamina of the organ of Corti. The reticular lamina separates the chemical compounds of the fluid, perilymph, which the organ of Corti is submerged in, from the endolymph that fills the sub-tectorial gap. The difference in the chemical compounds of the two media is important for keeping the electrical potential across the media as well as for the cells' survival.

The structure of the cochlear partition is important for delivering sound induced vibration of the cochlear partition to hair cells effectively. The rigidity of the organ of Corti is given by reticular lamina and an arch of rods, which may possibly serve as a pivot point for bending of the organ of Corti. Traveling wave along the cochlea causes up-down motion, pivoted at the rigid point of the organ of Corti, of the basilar membrane and the organ of Corti (Fig. 1.2B). This is coupled with motion of the tectorial membrane in the horizontal direction. As a result, shear motion in the sub-tectorial space is induced. The shear motion has significance because it stimulates hair cells directly and also it is a major source of damping of the entire vibration, which will be described more in details in the following sections.

Most of all, the organ of Corti contains hair cells, which is the main subject of the thesis. In the mammalian cochlea, three rows of outer hair cells and one row of inner hair cells are arranged in each segment of the cochlear partition (Fig. 1.2A). They have a cylindrical body and hair-like structure at their apical surface. The diameter of the cell body is about 10μm and its length varies from about 15μm to about 100μm, depending on its location. Hair cells are surrounded by supporting cells and specifically outer hair cells sit on the Deiter cells so that the up-down movement of the basilar membrane can be transferred to them. Their apical surface

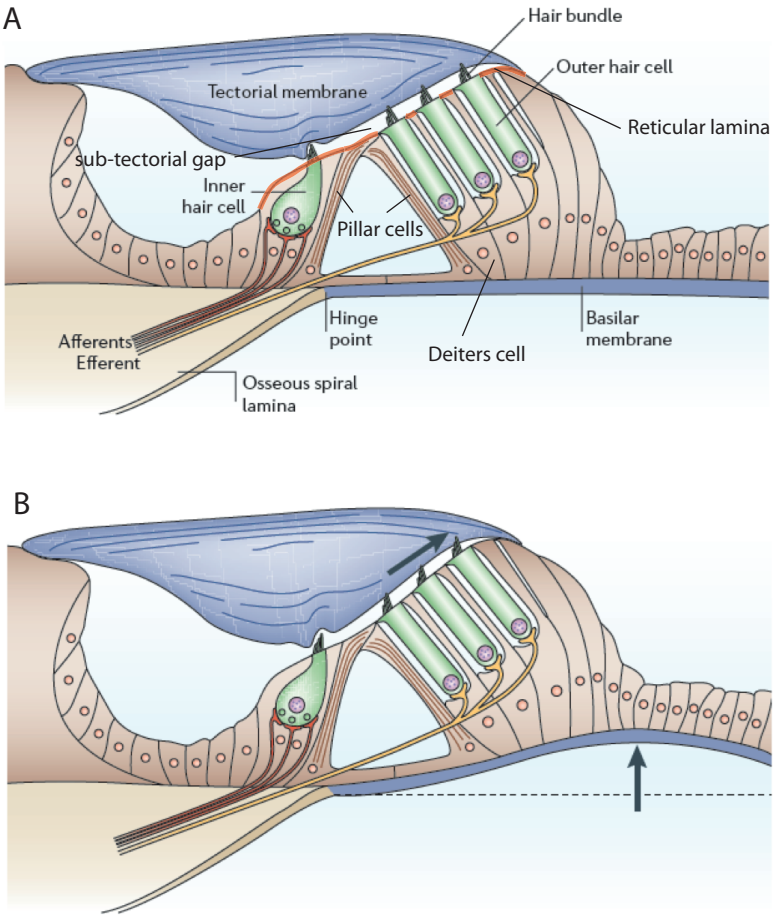

Figure 1.2: (A) Anatomy of the organ of Corti, which is a cross section of the cochlear partition. The organ of Corti contains three rows of outer hair cells and one row of inner hair cell in the cross section. At the ends of hair cells, afferent and efferent nerve fibers are attached to deliver electrical signal from the brain to the cell (efferent) and from the cell to the brain (afferent). The rigidity of the organ of Corti is given by the reticular lamina and the pillar cells, which may serve as a hinge point. (B) Local vibration of the organ of Corti. While the basilar membrane moves up-down pivoted at the hinge point, the tectorial membrane moves in a horizontal direction. This induces bending of the hair bundle in the sub-tectorial space. Figures reprinted from [47]

is exposed to the sub-tectorial gap and at the basal ends of hair cells, auditory nerve fibers are attached so that the electrical signal is sent from hair cells to the auditory cortex and the auditory cortex to hair cells. The former is called afferent nerves and the latter efferent nerves. Efferent nerves are dominant for the outer hair cells and the afferent nerves are dominant for the inner hair cells, suggesting differentiated functions for the cells.

The hair cell function depends on their highly specialized structure at their apical surface, called the hair bundle. The hair bundle is a bundle of actin filled microvilli, called stereocilia, which protrude at the apical surface of the cell and are exposed in the sub-tectorial gap. Stereocilia are arrayed in increasing heights like a staircase. The length of the tallest stereocilia in hair bundles ranges from $\sim 0.7\mu$m to 5.5μm (in chinchilla [1]). Each stereocilium is connected to its neighbors through interciliary connectors in the horizontal direction. The tip links, which connect the tip of the shorter stereocilia to the side of the taller ones along the staircases, play an important role in mechano-electrical transduction. They consist of two protein links, protocadherin 15 and cadherin 23. Near the ends of the tip links, mechano-sensitive channels are located, possibly connected in series with them [8, 86]. The morphology of the tip links and staircase stereocilia are quite well adapted to the transmission of the mechanical signals [121]. Because the tip links are tilted with a sharp angle with respect to the apical surface of the cell, deflection of the hair bundle in a direction along the staircase effectively applies tension to the tip link

[1] Chinchillas are crepuscular rodents, slightly larger and more robust than ground squirrels, and are native to the Andes mountains in South America. [Wikipedia.org]

and to the channels in series with it. This will be introduced more in detail in the section of mechano-electrical transduction.

1.2 Mechano-electrical transduction by hair cells

In order to "hear" sound, the mechanical signal which is the sound itself, should be converted into the electrical signal that brain can perceive. This conversion is called "mechano-electrical transduction" and is a major function of hair cells.

1.2.1 Mechano-electrical transduction

Deflection of hair bundle toward the tallest stereocilia along the staircase gives rise to current flowing inside the hair cell, mainly carried by K^+ ions and by smaller amount of Ca^{2+} ions and deflection in the opposite direction lowers the amount of the current from the resting level [24, 82, 129, 136]. Deflection orthogonal to the staircase direction does not make any change in the current [85].

Current due to the opening of the transducer channels, which is called "transducer current" or "receptor current", alters the electrical potential across the membrane. The change in the membrane potential, called "receptor potential", triggers the nerve fibers attached at the bottom ends of the cells and the electrical signal generated by the deflection of hair cells are sent to the brain. This process is mechano-electrical transduction.

A simple description of the mechano-electrical transduction can be made as follows. On deflection of the hair bundle, tension is applied dominantly to the tip

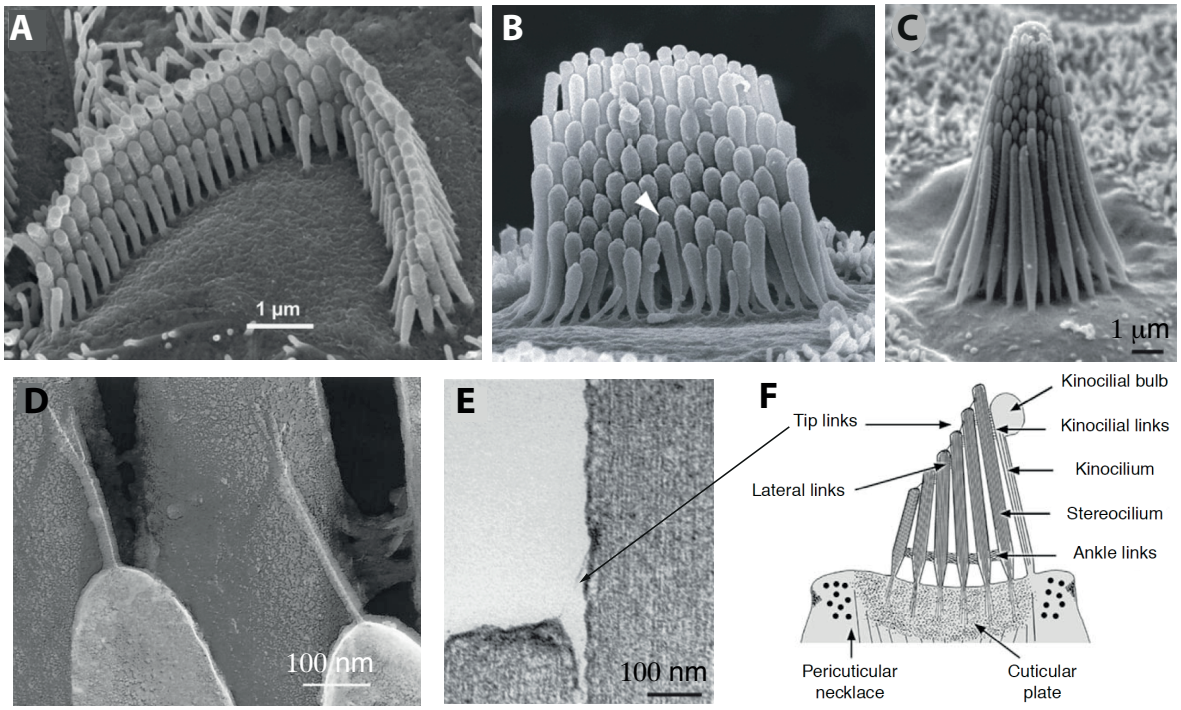

Figure 1.3: Hair bundles of guinea pig outer hair cell (A), chicken hair cell (B), and frog saccular hair cell (C). Each hair cell has a bundle of stereocilia arranged as a staircase. (D) Freeze-etch image of guinea pig tip links. (E) Tip link connects the tip (in (B), shown as a triangle) of the shorter stereocilia to the side of the longer one along the staircase. Stereocilia are filled with actin filaments. (F) Schematic illustration of links in the frog saccular hair bundle. Stereocilia are anchored at the cuticular plate and connected in the horizontal direction to their surrounding neighbors through side links such as ankle links. Pictures in (A)–(C), (E) taken by scanning electron microscope. Figures are reprinted from Dr. D. Furnace http://www.keele.ac.uk/emunit/galleries for (A), [72] for (B), [165] for (C) and (E), [83] for (D), and [60] for (F).

link due to its sharp angle along the staircase [80, 85, 121]. Because the channels sensitive to the force applied are connected in series with the tip link, the force will gate the mechano-sensitive channels. Because the electrical potential of the external medium where the hair bundles are exposed is higher by ∼150mV than the internal medium of hair cell [171], on the opening of the channel current flows inside the cell. Thus periodic deflection of the hair bundle by external mechanical stimuli causes alternating current and the electrical potential across the membrane that triggers the nerve fibers.

The molecular identity of the mechano-electrical transducer (MET) channels has not been found yet [20, 22], its mechano-sensitivity has been found from the relationship between the transducer current and the force for applied displacement of hair bundle as described below.

In a typical experiment, hair bundles are deflected by a flexible glass probe. One end of the probe is attached to a piezoelectric bimorph and the other end to the tallest stereocilia or kinocilium (Fig. 1.4A). While the piezoelectric controller gives displacement x_p, the other end of the probe, which is the displacement of the hair bundle, x is observed by a photo-detector. If the bending stiffness of the glass probe is k_p, then, the force applied to the hair bundle is given by $F = k_p(x_p - x)$.

With an electrode in the patch clamp setup, the transducer current I is measured for a given displacement x while clamping the electrical potential across the membrane. Then the open probability P_o of the MET channels is given by normalizing I with the maximum value I_{max} (i.e. $P_o = I/I_{max}$) and is plotted against x. In the same way, the force applied to the hair bundle for a given displacement x is

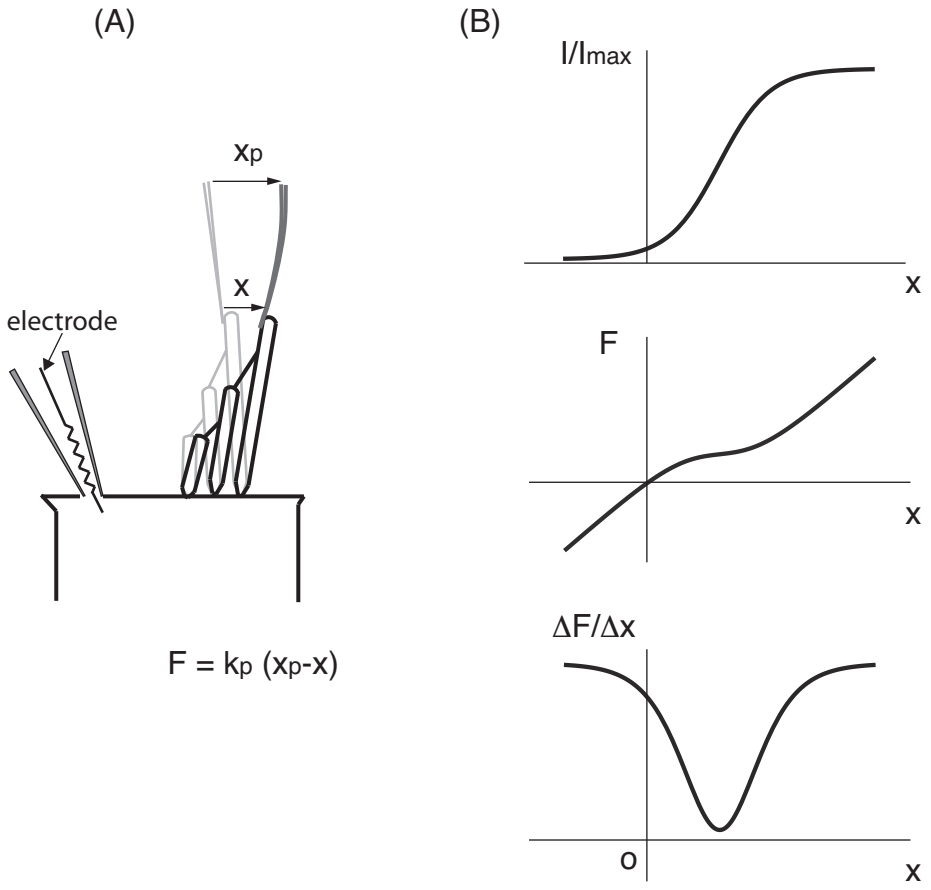

Figure 1.4: (A) Schematic representation of a setup for gating experiment. Hair bundle is stimulated by a flexible probe attached to the kinocilium or to the tallest stereocilia. Probe is displaced by a piezoelectric bimorph. Hair bundle displacement x is measured by photodiodes. When hair bundle displacement is x, probe displacement x_p and stiffness k_p, force applied to hair bundle is $F = k_p(x_p - x)$. Current is measured using a patch clamp technique with an electrode penetrating the cellular membrane. (B) Normalized transducer current I/I_{max}, hair bundle force F, and effective hair bundle stiffness $\Delta F/\Delta x$ are plotted against hair bundle displacement x. Effective hair bundle stiffness $\Delta F/\Delta x$ is obtained by taking slope of F-x plot. Notice a non-linear domain of $F-x$ plot. Where the I is around half of its maximum I_{max}, the effective stiffness becomes minimum.

plotted. Figure 1.4B shows that open probability is a sigmoid function of the hair bundle displacement, with a resting level of open probability reduced for hair bundle deflected toward the lower staircase and increased for deflection in the opposite direction. At the same time, the force–displacement plot shows interesting phenomena (Fig. 1.4B). First of all where the open probability is closer to 0 and 1, force is linear to displacement, following Hooke's law. This shows the channel's elastic property. However, where the open probability is close to 1/2, the linear relationship does not hold. Rather, the slope of the force-displacement plot decreases [71]. Also it was found that the slope, which is the effective stiffness of the hair bundle, becomes negative (Fig. 1.5C) if the displacement x of the hair bundle is clamped using the feedback circuit of the controller (Fig. 1.5A) [111]. This is interesting because the mechanical property of the channels is not likely to change for the size of the stimulation. Such a reduction of the effective stiffness is named "gating compliance" and found that it is due to the gating of MET channels. Negative values of the effective stiffness, named "negative stiffness", has a significance in not only being a source of spontaneous oscillation of the hair bundle, which may result in amplification of the external signal, (Fig. 1.5B) but in also amplification of the hair bundle movement, which will be discussed in the chapter 4.

1.2.2 Model for gating of MET channels

The simplest description of gating of the MET channels as well as gating compliance has been made by assuming two states, open and closed [71] (Fig. 1.6).

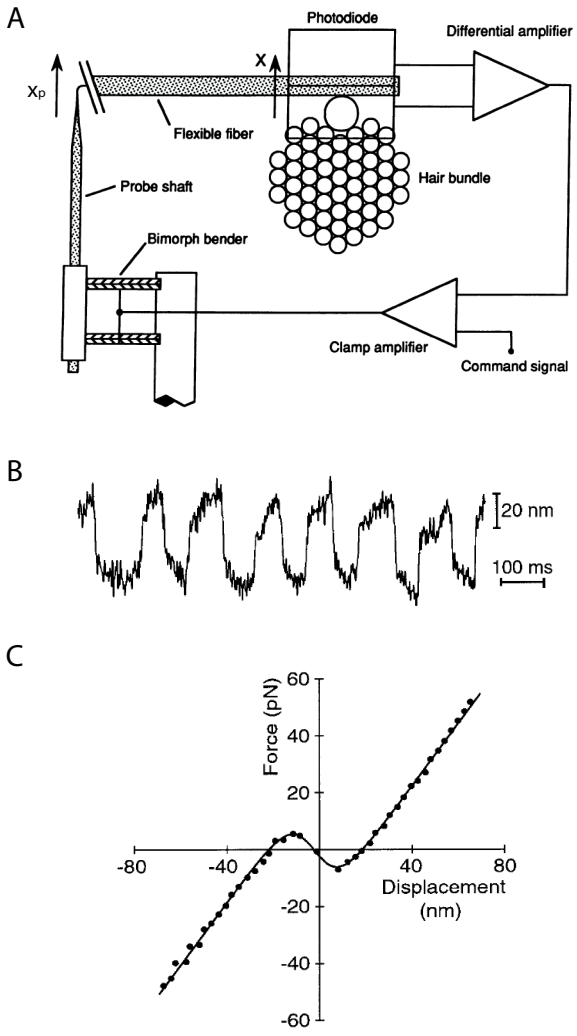

Figure 1.5: (A) Experimental set-up for hair bundle displacement clamp. Because the hair bundle avoids being located in the negative stiffness region, it is not possible to observe such a domain unless the hair bundle is forcefully located there. Using the feedback circuit, the set-up constantly adjust displacement x_p of the probe so that a hair bundle displacement x can be maintained. (B) When negative stiffness exists at the operating point, the hair bundle oscillates spontaneously with a frequency. In this cell the frequency is $\sim$7Hz. (C) The relationship between the force and hair bundle displacement x. At the operating point, the hair bundle shows negative stiffness. Figures reprinted from [111].

In this model, the MET channel is represented by a spring, called gating spring, attached to the gate. When the gating spring is pulled by distance x, the energy difference ϵ between open and closed states is

$$\epsilon = k_g x_g (x - x_g/2) \tag{1.1}$$

where k_g and x_g are gating spring constant and displacement given by opening of the gate. At the equilibrium, open probability P_o of the channel is, then, expressed as

$$P_o = \frac{1}{1 + \exp(-k_B T \epsilon)}. \tag{1.2}$$

The effective stiffness $\tilde{k}$ of gating elements, which appears as a slope of the averaged force $\langle F \rangle$ for a given displacement x, is shown below.

$$\tilde{k} \;\; = \;\; k_g - k_g^2 x_g^2 P_o(1 - P_o)/(k_B T). \tag{1.3}$$

Therefore the minimum value of $\tilde{k}$ occurs when P_o is $1/2$ and $\tilde{k}$ can take negative value only if $k_g x_g^2 > 4 k_B T$ [77].

This model, which assumes existence of one channel with two states, has been successful to explain most of the experimental data related to channel gating. However recent reports with fluorescence images of the transducer current show that more than one channel exist together as a unit. To resolve the discrepancy between the model and observation, we examined the issue by modeling coupled systems of two identical channels. This will be discussed more in detail in the chapter 2.

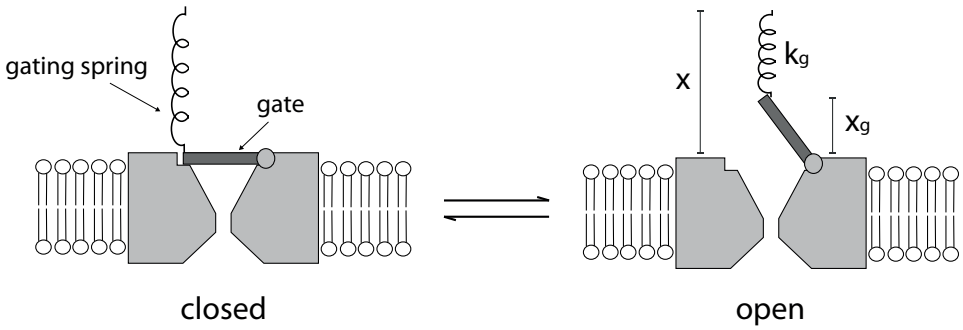

Figure 1.6: Schematic representation of two-state model of the MET channel gating. The MET channel is represented by gating spring with spring constant of k_g and gate with a size of x_g. The model assumes that MET channel has two states, open and closed for a given displacement x. Figure adapted from [71]

1.3 Cochlea, the frequency analyzer

The location of the local vibration, described in the section of mechano-electrical transduction, along the cochlea is related to the frequency component of the sound. In other words, the cochlea is analogous to a frequency analyzer.

Sound funneled into the middle ear causes vibration of the tympanic membrane. Attached to the tympanic membrane, middle ear bones deliver the vibration to the cochlea by hitting the oval window. Consequently the disturbance in the cochlear fluids propagates away from the oval window along the cochlea while inducing local vibration of the cochlear partition in the transverse direction (Fig. 1.1B). The pattern of the vibration along the cochlea in the relationship with its frequency is well described by George von Békésy [169].

George von Békésy first measured the traveling wave in human cadaver ears.

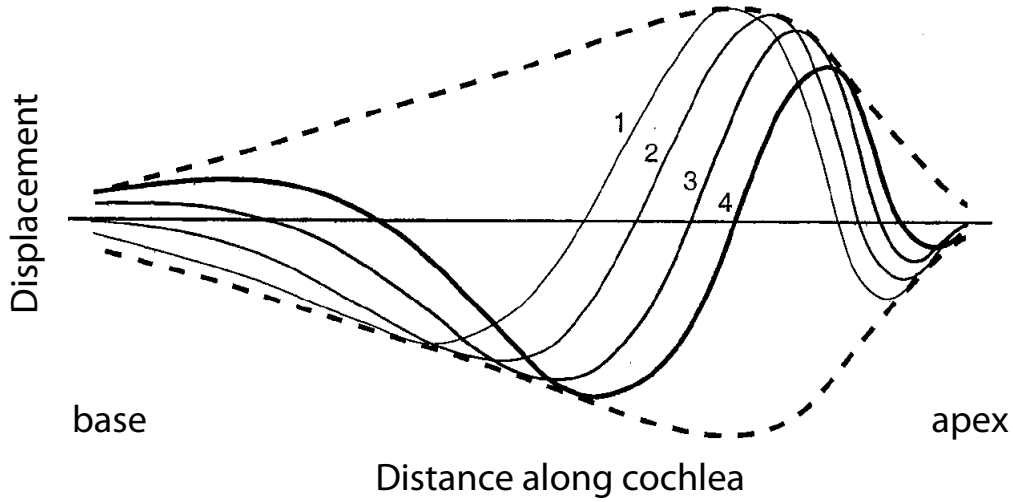

Figure 1.7: Traveling waves in the cochlea were first shown by von Békésy. The full lines are the pattern of the deflection of the cochlear partition at successive instants, as numbered. The envelope of the waves is static (dotted lines). Stimulus frequency, 200Hz. Plots reprinted from [120] and orginated from von Békésy [168].

For observation, he substituted rubber windows for the oval and round windows of the cochlea and attached a mechanical vibrator to one of them. The movement of the cochlear partition was traced by observing silver particles on it through the opening of the cochlear wall under water. First he found the propagation of the wave along the cochlea. For a stimulus of fixed frequency, the cochlear partition vibrated with a wave that gradually grew in amplitude as it traveled away from the windows and reached a maximum stalling at a certain location as if a local resonance takes place. Afterwards the wave rapidly declined (Fig 1.7).

Interestingly, the location of the resonance on the frequency of the wave. Figure 1.8 was made by plotting the envelope of the cochlear partition displacement along the cochlea while giving different tones of the stimulus with the same intensity.

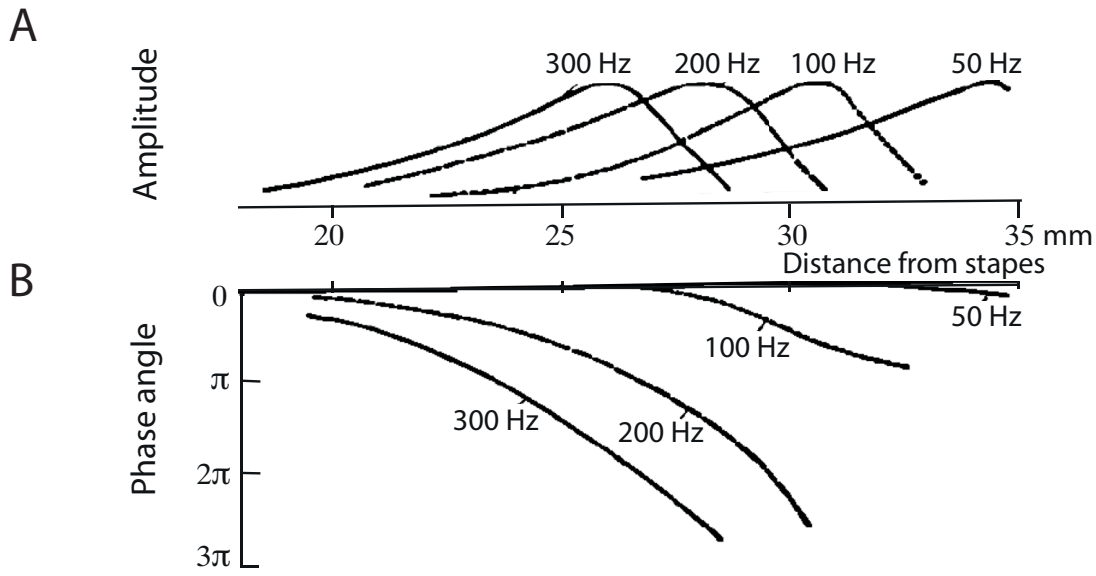

Figure 1.8: (A) Displacement envelopes on the cochlear partition are shown for different stimulus frequencies (marked on each curve). (B) The relative phase angle of the displacement. Plots reprinted from von Békésy [166].

It shows that as the frequency stimulus increases, the position of peak displacement moves toward the windows. In other words, for higher frequencies the cochlear partition nearer to the windows vibrates with the maximum amplitude and for lower frequencies the cochlear partition vibrates with the maximum amplitude further from the windows.

While the cochlear vibration is shown in panoramic view for individual tones of stimulus (Fig. 1.8), it can be also represented in local views. By putting six holes along the cochlea, von Békésy observed the vibration pattern while varying frequencies with the same intensity of the stimulus (Fig. 1.9). Figure 1.9 shows that, as in the figure 1.8, it is the nearest point to the windows that responds best

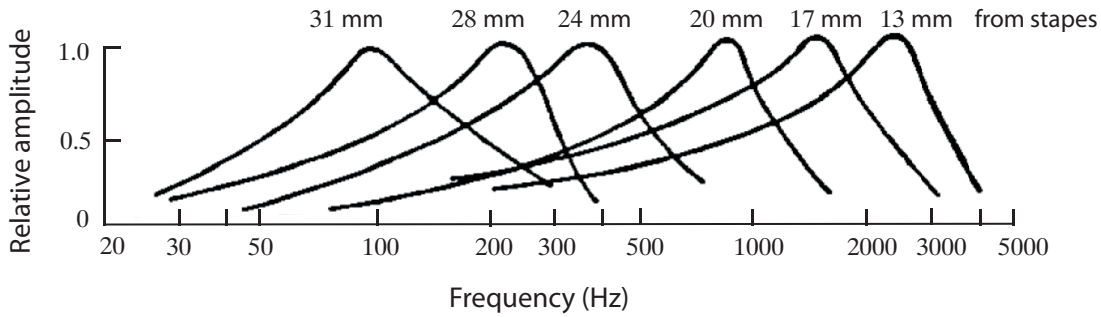

Figure 1.9: Frequency responses at six different locations of the cochlear partition. The amplitude envelope was measured as the stimulus frequency was varied with constant peak stapes displacements. The position of the point of observation is marked on each curve. Plots reprinted from von Békésy [167].

to the highest frequencies. This illustrates a mapping of frequency to place in the cochlea, analogous to the frequency analyzer.

Even though the frequency map in the cochlea has been measured more accurately and physiologically in later studies with more technological developments, the basic features of the cochlea as the frequency analyzer have been observed consistently (Fig. 1.1C). Differences between dead cochlea and living cochlea will be introduced in the following section. Similar to the cochlear frequency map, it was found that space dependent frequency map exists in the auditory nervous system [113].

1.4 The cochlear amplifier

The need for an amplifier in the cochlea, the cochlear amplifier, was predicted by Gold in 1948 [62]. He proposed that, in order for the cochlea to show sharp tuning and high sensitivity in the presence of high viscous damping, an active process must exist. Even though damping is not so high as Gold's prediction, several experiments prove the existence of the active mechanism in the cochlea, characterized by four phenomena in vertebrate ears ([72, 106, 107]).

First, the tuning curves of the living cochlea are sharper than for the dead one and the sharpness depends on the intensity of input signal [125, 147]. Such an example is shown in the figure 1.10 A. Fig. 1.10A is a plot of the velocity of the basilar membrane for various input intensities of stimuli as a function of input frequency at a given location along the cochlea. It shows that the curves are more sharply tuned at the characteristic frequency of $\sim$10kHz for lower input intensity. At higher levels of stimuli, the curves are broad, similar to von Békésy's measurement. It has been shown that highly tuned responses in live cochlea become poorly frequency tuned upon death of the animal [132, 133, 147].

Second, the sensitivity of the living ear is higher than that of the dead ear Sellick1982,Robles1986,rugg-rich1991. In many species, the threshold of normal hearing is around zero decibels of sound pressure level, which corresponds to a limit of thermal vibration in the ear. However with disrupted active process the threshold goes up by 40 to 60 dB [133]. Furthermore, the sensitivity becomes higher at the lower level of stimuli. In the figure 1.10B, sensitivity of the basilar membrane

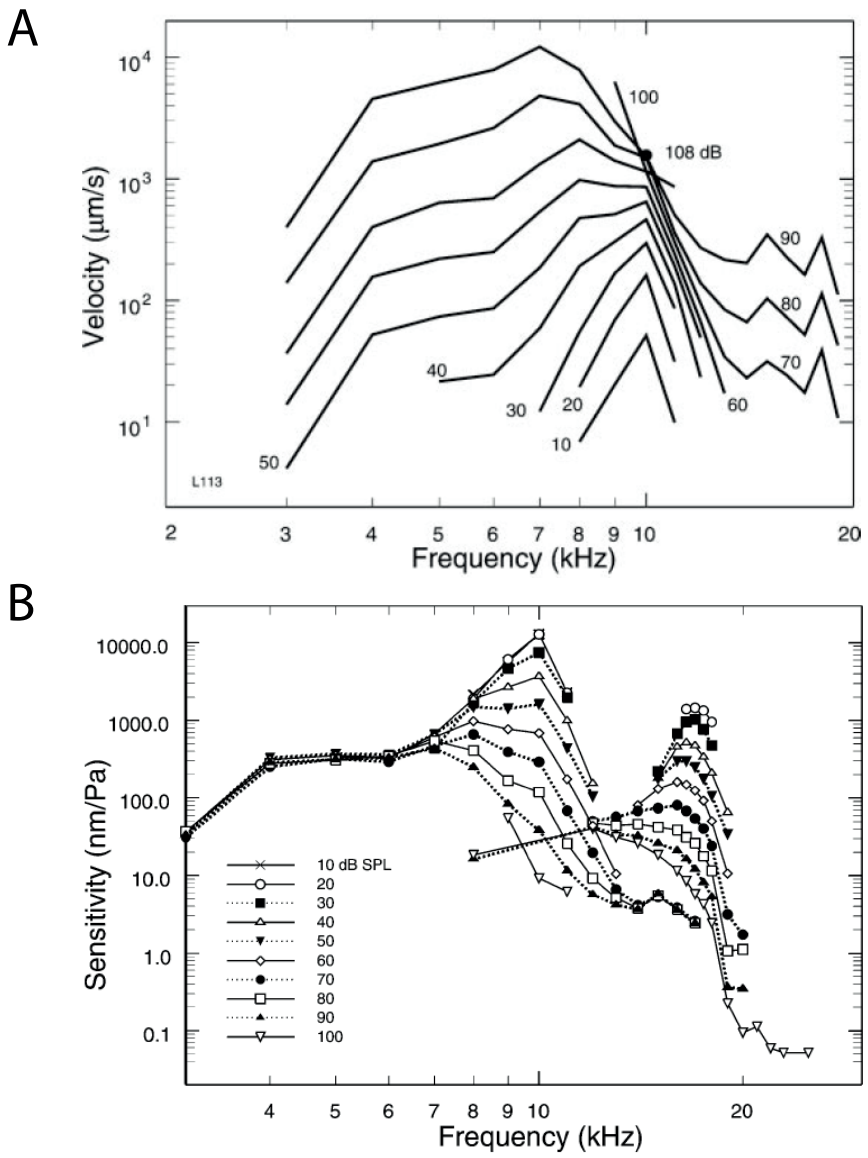

Figure 1.10: Mechanical responses of the living cochlea. Families of isointensity curves for representing the velocity of basilar membrane (BM) responses (A) and sensitivity (B) to tones as a function of frequency and intensity (in dB SPL). Figure (A) reprinted from [134] and (B) from [131].

movement is highest for 20dB input intensity level and decreases monotonically as the intensity level becomes higher.

Third property of the active process is non-linear amplification. In mammals, threshold 0dB gives 0.1nm amplitude of the basilar membrane motion. In the other limit 120dB, which corresponds to the sound of jet plane heard on tarmac, the basilar membrane moves only with 10nm amplitude. In other words, million times input amplitude difference gives only hundred-fold difference in output amplitude. This means that the sensitivity of the basilar membrane follows a power law instead of linear relationship. It was observed that power of the one-third law holds [134]. This enables for ears to detect soft sound and at the same time to protect the ear from damage by loud sound.

Finally, the strongest evidence for existence of the active mechanism in the cochlea is spontaneous otoacoustic emission. In a quiet environment, the ears of many species from all tetrapod classes can emanate sound continuously at one or more frequencies. It was experimentally first demonstrated by Kemp in human ears [87] and later it was found that many other vertebrate ears also emit sound spontaneously at one or more frequencies [108, 122]. It has been hypothesized that either local resonance or resonance created by the entire cochlea like a laser [178] may create the spontaneous otoacoustic emission even though the exact mechanism for the spontaneous otoacoustic emission is not clear yet. However at least, it clearly shows that energy generation mechanism should exist in the ears.

Several models have been proposed to explain different aspects of the tuning curves for the living cochlea. They commonly show that the sharp tuning cannot

be achieved in the passive system [36, 116, 177]. As Gold pointed out, the living cochlea must have an active mechanism that provides energy to boost the vibration of basilar membrane at the location matching with the input frequency. This concept was introduced as "negative damping" [116] or "negative impedance" [177] and has been basis for the study of the cochlear amplifier.

1.5 Hair cell, the cochlear amplifier

The presence of an active process was proposed by Gold [62], "The degree of resonance in the cochlea is not compatible with the heavy damping which must arise from the viscosity of the liquid. ...it is suggested that an electro-mechanical action takes place whereby electrical energy is employed to counteract the damping." and proven by existence of spontaneous otoacoustic emission. It has been shown that such active mechanisms should exist in hair cells in the vertebrate ears. When the outer hair cells are damaged in the mammalian cochlea, the characteristics of the active mechanisms are lost. In other words, the hearing threshold is elevated [137] and the tuning curve is broadened [32, 98]. Such an example is illustrated in the figure 1.11. It shows that the neural responses of the cochlea is broader and has higher threshold than the normal ones if the outer hair cell are damaged.

If hair cells amplify basilar membrane vibration, they must provide mechanical energy back to the system; in other words, hair cells must have motile mechanisms in them. Indeed it was found that hair cells have such motile mechanisms in their hair bundles, which are called "hair bundle motility", and in the cell body of the

outer hair cells, which are called "electromotility". Electromotility indicates a motile property of the outer hair cell, which changes its cell length as a function of electric potential applied in its membrane. Membrane potential more positive from the resting level (i.e. depolarization) shortens the outer hair cell and membrane potential more negative from the resting level (i.e. hyperpolarization) elongates the outer hair cells. With electromotility, outer hair cells converts the electrical energy applied to the cell membrane into mechanical work. Hair bundle motility means active movements of the hair bundle, which induce re-closure of the MET channels. The energy source of the hair bundle motility is the chemical energy of adenosine-triphosphate (ATP) and calcium, which is converted into mechanical work by the hair bundle's active movements.

While electromotility is uniquely present in the cell body of the outer hair cells in the mammalian ears, hair bundle motility, which indicates active movements of the hair bundle induced by action of calcium ions, is commonly shared throughout the various vertebrate animals, including frogs, lizards, birds and mammals [107]. The relative importance of the hair bundle motility and electromotility is still controversial for mammalian ears, however hair bundle motility must play a critical role for non-mammalian ears because they do not have electromotility.

1.5.1 Hair bundle motility

Hair bundle motility takes place during the process called "adaptation" in the hair bundle. On deflection of hair bundles, a steep rise of the level of current

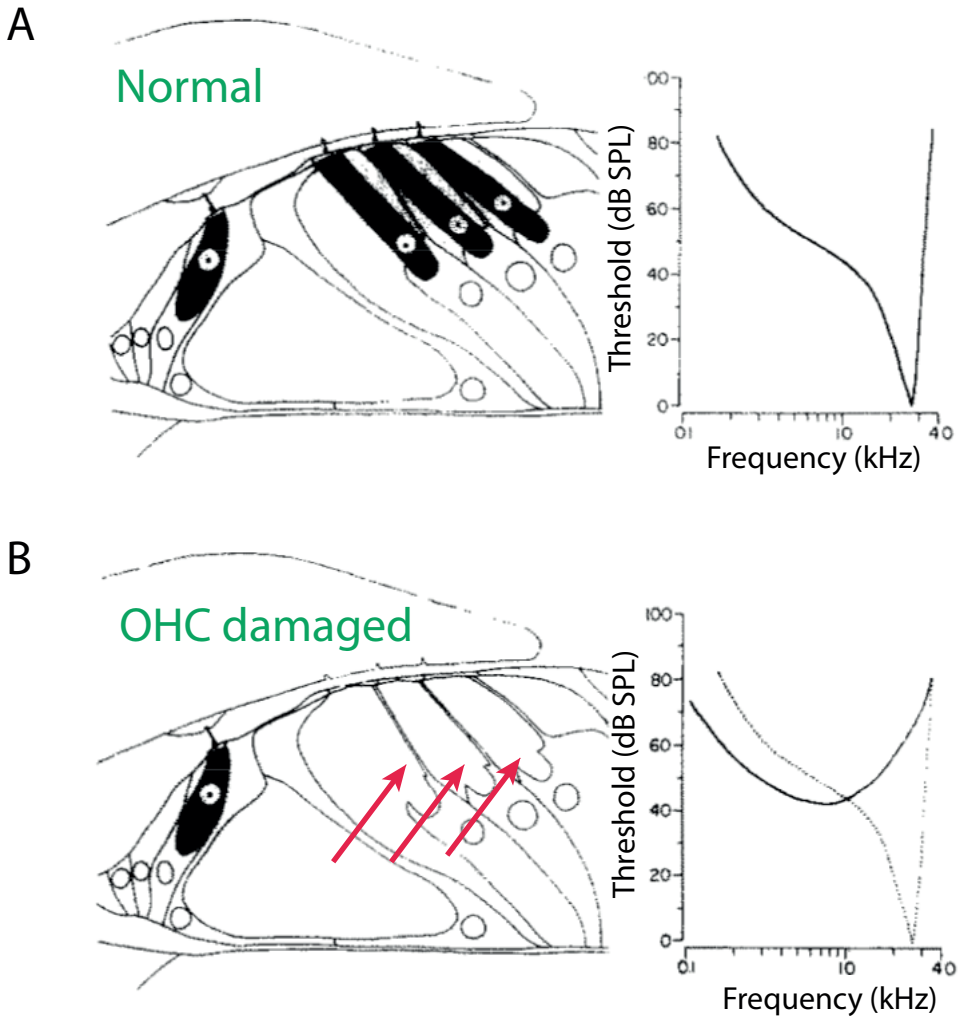

Figure 1.11: Neural tuning curves of normal (A) and damaged hair cells (B). Arrows emphasize that the outer hair cells are damaged. Figures reprinted from [98]

flowing inside the hair cell is followed by a reduction with two time constants. Reclosure of the MET with a few milliseconds is called fast adaptation and within tens of milliseconds is slow adaptation (Fig. 1.12). It has been observed that both of fast and slow adaptation accompany active movements of the hair bundle, which called hair bundle motility. The hair bundle motility is highly dependent on calcium [13, 28]. The intracellular calcium level is likely to increase with the calcium level of the extracellular medium where the hair bundle is exposed. It was found that lowering the calcium level of the solution, which the hair bundle is exposed to, slows the adaptation process as well as reduces degree of the adaptation. Even with a high concentration of calcium in the external medium, adaptation disappears if the internal calcium is lowered by depolarization of the cell. The adaptation process requires calcium in the internal medium of the cell [28].

Active movements of the hair bundle can be observed in a typical gating experiment. While the probe displacement that stimulates the hair bundle is maintained constant, the hair bundle shows different phases of movement during slow and fast adaptation. Slow adaptation was first found in the hair bundles of frog hair cells by Howard and Hudspeth [70]. They observed that the hair bundle moves toward the direction of stimulus during the time course of slow adaptation and proposed that mechanical relaxation mediates slow adaptation (Fig. 1.12). The time course of the slow adaptation can be understood if a motor is attached to the MET channel and applies force similar to a damper.

Because stereocilia are actin filled filaments, it would be natural to think that myosin motors, which generates force, be related to such a relaxation process [4].

This idea was confirmed by experiments. With the interference of ATP (adenosine triphosphate) cycle of myosin by administrating ADP (adenosine diphosphate) analog and ATPase inhibitors in the hair bundle, adaptation was blocked, increasing open probability at rest and slowing the kinetics of adaptation [57, 173]. Further investigation identified myosin 1c (myo1c) as an adaptation motor [68, 170]. Also it was revealed that myo1c is mainly localized near the tip links where the MET channels are presumed to be located [54, 59, 65, 155].

Myo1c is an unconventional myosin, which climbs toward the tips of the hair bundle along the actin filaments consuming ATP when calcium is unbound. Therefore it has been hypothesized that myo1c is connected to the channels and mediate the adaptation process by giving negative feedback. On the opening of the channel, the increase of internal calcium induces the myosin motors to slip down the actin filaments, resulting in re-closure of the channel due to reduction of tension applied to the channel (Fig. 1.13). However, a recent finding shows that the MET channels are located at the lower ends of the tip links [8]. This contradicts the above hypothesis and the way the adaptation takes place and the role of myo1c have become open to questions.

For fast adaptation, different phases of the hair bundle movement, called "twitch" and "release," have been observed. Twitch was first observed in frog hair cells [6, 70]. When frog hair bundles are deflected by flexible fibers, the hair bundle moves in the opposite direction of the given stimulus within few milliseconds in advance to the slow adaptation (Fig. 1.12A). This forceful re-closure of the channel has been modeled and considered as an amplifying mechanism in the relation to

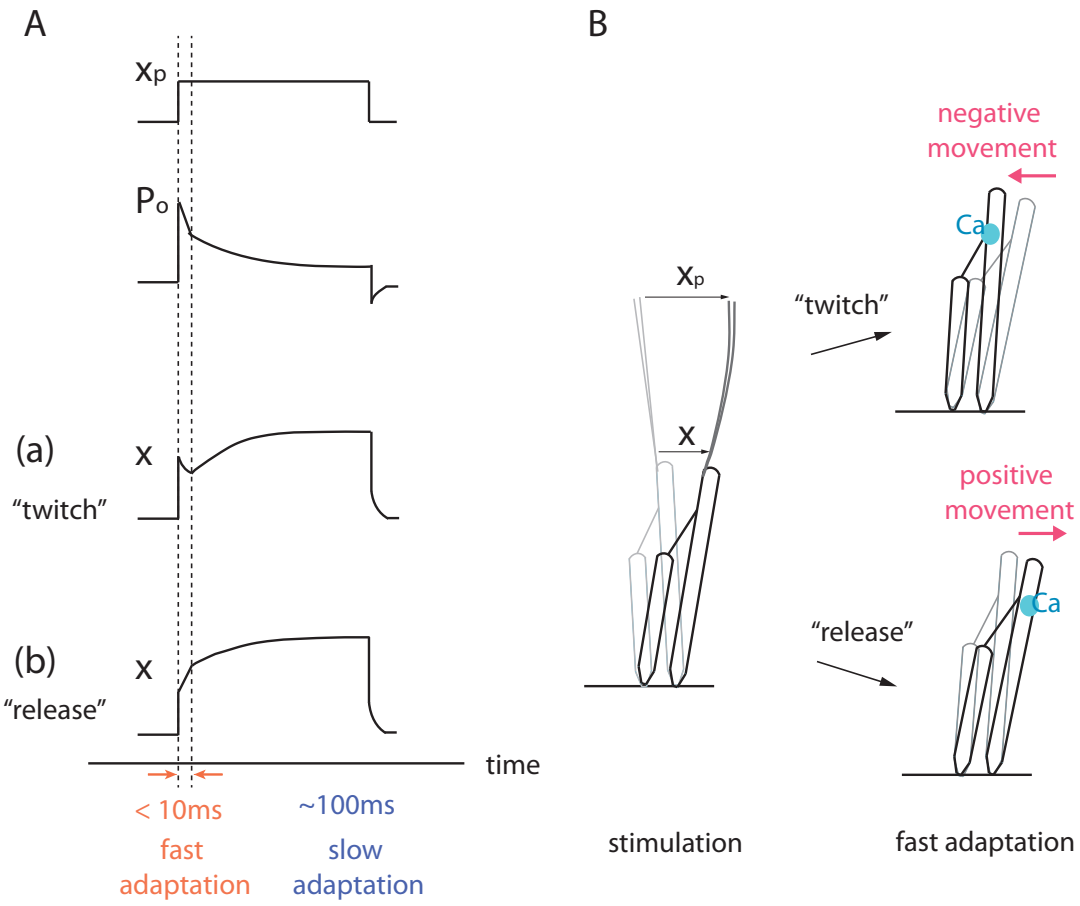

Figure 1.12: (A) Response of the hair bundle when hair bundle stimulated by a flexible fiber attached to the tip of the tallest stereocilia. Probe is displaced by x_p and hair bundle by x. At a constant probe displacement, the current falls with two time constants of sub-milliseconds (fast adaptation) and tens of milliseconds (slow adaptation). During slow adaptation, the hair bundle moves toward the stimulated direction, similar to relaxation. (B) Movements of the hair bundle. During fast adaptation, the hair bundle moves in the stimulated direction (release) or in the opposite direction (twitch), depending on the animals and experimental conditions. Calcium is involved in both adaptations.

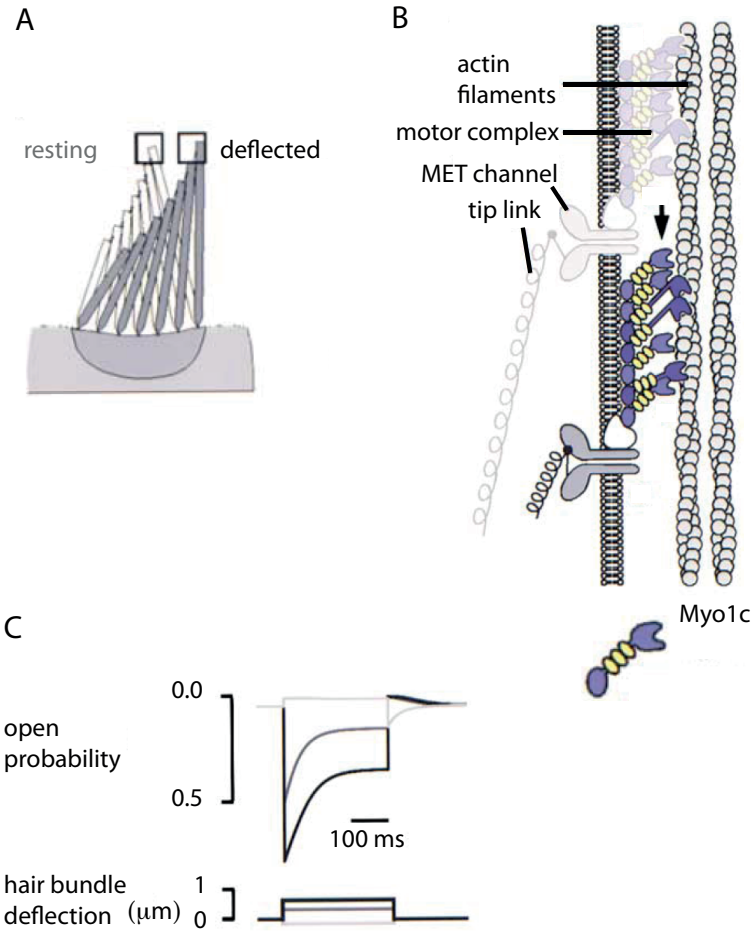

Figure 1.13: Illustration of adaptation by myosin 1c in the hair bundle. (A) Hair bundle before (light colors) and after (dark colors) deflection by a probe. (B) A model for adaptation by myosin 1c. (C) Time courses of open probability for different levels of hair bundle deflections. Figures reprinted from [68]

Hopf bifurcation [19, 162].

The release mechanism has been observed in different experiments. It was observed that during fast adaptation, the hair bundle of rat outer hair cells does not only yield in the same direction of the stimulus but also moves further pulling the stimulating fiber [89] (Fig. 1.12B). This means that the hair bundle generates force in the opposite direction of the twitch. The similar responses of hair bundles were observed in different hair cells such as those of mouse and frog and found to be related to act of myo1c [154].

How both of twitch and release mechanism can work for amplification is not clear. While the release mechanism, which hair bundle motility is based on, must result in amplification, in terms of phase of force production, the release mechanism in a characteristic of a relaxation process, resulting in damping. This issue will be discussed in the chapter 4.

Even though mechanisms for hair bundle motility have been studied, effective limit, in which hair bundle motility works as the cochlear amplifier, has not been quantified. Even though studies have been done on non-mammalian systems in relation to Hopf bifurcation [19, 40], it is not clear whether it can be applied to the hair bundles of mammalian hair cells as well. So far there is no report that mammalian hair bundles show negative stiffness or spontaneous oscillation. Instead the frequency limit where hair bundle motility works for amplification can be obtained considering the energy balance between the energy supply from the hair bundle and the energy lost by viscous damping. This will be discussed in the chapter 5 of the thesis.

1.5.2 Electromotility

Among all hair cells, outer hair cells have a unique property, called electromotility, in their cell body. It was discovered that the cylindrical shaped cell body becomes shorter and wider if the outer hair cell is depolarized and longer and thinner if hyperpolarized [2] (Fig. 1.14) [11]. The amplitude of the length changes is up to 5% of the cell length in isolated cells without load [75]. The cell generates force of 0.1 nN/mV with voltage pulse applied on the cell membrane [76], which is similar to the predicted value of 0.15 nN/mV from an area motor model [74]. The source of the electromotility is the receptor potential generated by the gating of the MET channels in the outer hair cell. When the outer hair cell is excited by an external stimulus, it may give mechanical feedback by applying force in a way to amplify the motion of the basilar membrane [118].

Electromotility of the outer hair cells shows characteristics of piezoelectricity. It was observed that the length change of the cell is accompanied by transfer of charge across the plasma membrane [3]. The charge movement is elicited by changing the membrane potential and, thus, it is observed as non-linear membrane capacitance [140] (Fig. 1.15). The length change of the outer hair cell is plotted as a sigmoid function of membrane potential applied and its derivative fits with the plot of membrane capacitance, which appears as a bell shape on top of the constant

[2] In biology, depolarization is a change in a cell's membrane potential, making it more positive, or less negative. In neurons and some other cells, a large enough depolarization may result in an action potential. Hyperpolarization is the opposite of depolarization, and inhibits the rise of an action potential. Wikipedia.org

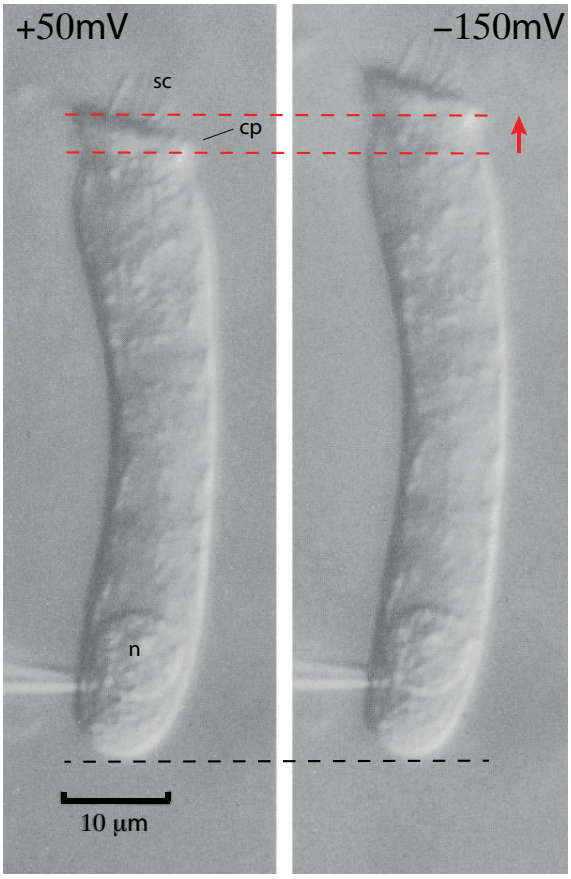

Figure 1.14: Apical OHC from the guinea pig dissociated with the enzyme trypsin. The membrane potential is held at +50mV (left) and -150mV (right) via the patch electrode next to the nucleus (n).The basolateral membrane refers to the entire cell membrane except for that surrounding the stereocilia (sc) and cuticular plate (cp). Length change of the basolateral membrane is indicated by dotted line and the arrow. Scale bar = 10μm. Figure modified from [67]

value that would be proportional to membrane area and inversely to its thickness (Fig. 1.15A). This can be described by a two state model that assumes membrane area change is coupled with movement of an internal charge, whose value is 0.5 to 1 electrons, as a function of the electric potential applied [3, 140] (Fig. 1.15B).

It was found that the molecular identity of the piezoelectric material is protein prestin (SLC26A5) [176]. When mice are genetically modified so that the prestin is not expressed in them (i.e. prestin knock-out mice), the outer hair cells were not motile [15, 81] and the electro-physiological phenotype of the mice was consistent with the lack of amplification [99]. The length of outer hair cells without prestin is shorter than wild type (normal mice), which may have affected feedback between outer hair cells and the basilar membrane. To eliminate this possibility, prestin knock-in mouse was made that does not change the cell length but modifies prestin function [15, 16, 99]. Outer hair cells from these mice did not have electromotility in the physiological membrane potential and showed elevated hearing threshold and broad tuning curve even with a normal function of hair bundle [34].

The molecular structure of the prestin and details of the conformation change are not clear yet [37, 115], however electron microscopy (EM) and atomic force microscopy (AFM) studies show that prestin is embedded in the basolateral membrane of the outer hair cell with size of $\sim$10nm and its density is 5,000 – 10,000 μm^{-2} for mid turn outer hair cells [84, 140, 143, 150].

The frequency response of outer hair cell electromotility has been examined in various ways. When the voltage waveforms that drive the motile response is delivered to the membrane without significant frequency-dependent attenuation, the

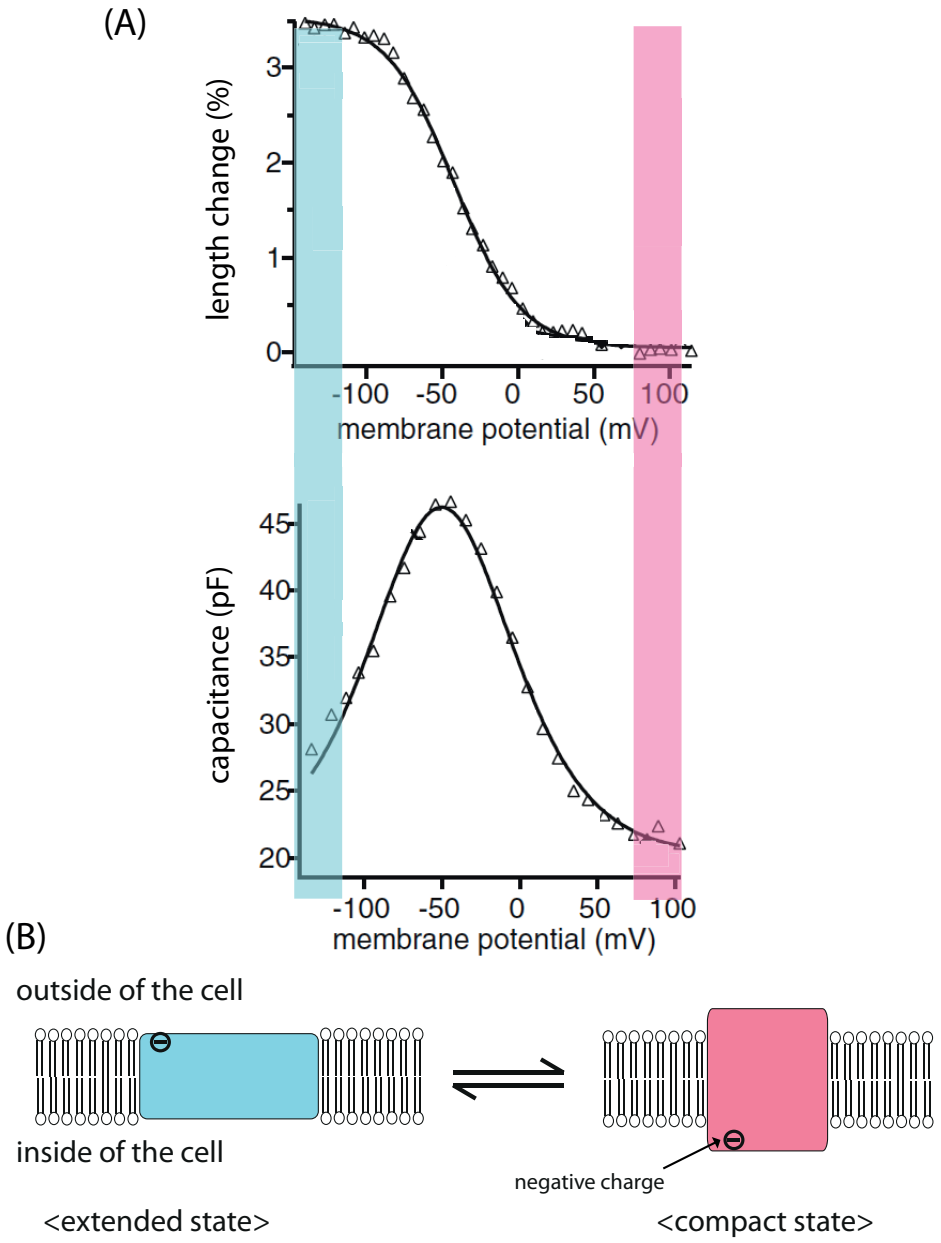

Figure 1.15: (A) Outer hair cell length change and membrane capacitance as a function of the membrane potential. (B) Two-state model. Area change of the motor is coupled with transfer of negative charge (). Blue and red color correspond to extended and compact state, respectively. Figure (A) reprinted from [45] and (B) from Dr. Kuni H. Iwasa.

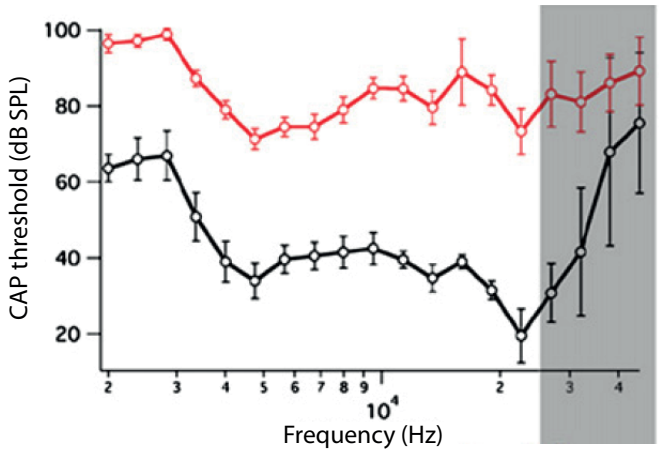

Figure 1.16: Compound action potential (CAP) data obtained from prestin knock-in mouse which modifies prestin function. Average thresholds (sound pressure level required to measure 10μV CAP) as a function of stimulus frequency for prestin knock-in (red) and wild type mice (black). Shaded region approximately corresponds to extent of age-related hair cell loss. Figure reprinted from [34].

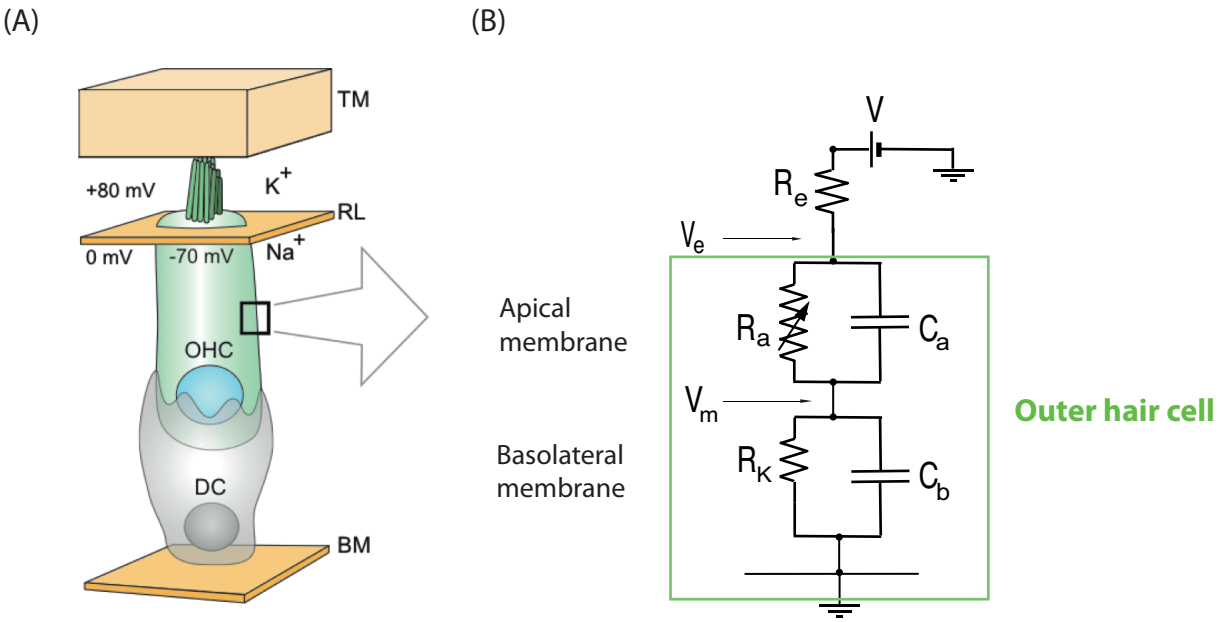

Figure 1.17: An outer hair cell (OHC) and its equivalent circuit. (A) The environment of an OHC. The apical surface is exposed to the endolymph, which is high in K^+. The lateral surface is exposed to the perilymph. (B) An equivalent circuit of an OHC (boxed). V is potential difference without external stimulation between the medium where hair bundle is exposed and inside the hair cell. The apical membrane has the membrane capacitance C_a and resistance R_a, which is dominantly determined by the MET channel conductance. The basolateral membrane has the membrane capacitance C_b and membrane resistance R_k. Receptor current through an external resistance R_e creates the cochlear microphonic. The time constant of the OHC is $\sim R_bC_b$. TM: tectorial membrane, RL: reticular lamina, DC: Deiters' cell, BM: basilar membrane.The figures (A) reprinted from [75].

amplitude of outer hair cell displacement does not roll off up to ∼20kHz in load-free condition and ∼50kHz [51]. Frequency response of charge movement of electromotility rolls off at about 10kHz [39, 53]. These experiments show that electromotility is functional at least up to 20kHz if electrical potential change is directly applied to the basolateral membrane [172]. However, whether this limit is realizable *in vivo* or not is questionable. The the electromotility is driven by the receptor potential, generated by the receptor current at the apical part of the cell, and only a portion of it is loaded on the basolateral membrane like a voltage divider. The cell membrane can be electrically represented by a capacitor and resistor with a value that is the inverse of the conductance of the channels connected in parallel (Fig. 1.17B). It is expected that the basolateral membrane acts as a low pass filter with the voltage across it declining at high frequencies, which, in turn, will decrease the effectiveness of electromotility at high frequencies because length change of outer hair cell increases with voltage across the membrane. This is called RC time constant problem. Here R is a resistance value of the apical part of the cell and C is a capacitance value of the basolateral membrane. Even though their values change depending on the location of hair cell, typical value of the resistance is ∼10MΩ [104] and capacitance is ≥15pF [69] for the outer hair cell at the basal end of the cochlea. From these values, the corner frequency can be estimated to be ∼1kHz.

Even though RC time constant problem [69, 141] is predicted for an isolated outer hair cell, whether the electromotility *in vivo* is limited by this or not is questionable. One of the theoretical proposals of circumventing RC time constant problem is to assume that endocochlear potential is given as an AC (alternating current)

potential that is not dependent on frequencies [30]. This is not realistic assumption because the source of endocochlear potential is receptor current and cannot be the same for different frequencies. The effect of the endocochlear potential shared by multiple outer hair cells is discussed and the effectiveness of the electromotility is evaluated in the chapter 3 of the thesis.

Which of the two motile mechanisms, the electromotility or the hair bundle motility, is more significant as an amplifier for mammalian system has not been resolved. The effective limit of the hair bundle motility will be obtained in the chapter 5 and electromotility in the chapter 3.

1.6 Outline of the thesis

The thesis consists of two parts. First, I addressed the question how to model the gating of two MET channels that are mechanically coupled. Earlier models assumed that one MET channel is associated with each tip link and described mechano-electrical transduction by ensemble average of single MET channel gating [71]. However, recent experimental finding suggests that about two MET channels exist for each tip link, in conflict with earlier models [7, 8]. In the chapter two, simple models for two MET channels are examined and their connectivity are discussed in the context of experimental data.

The second part of the thesis examines the role of hair cells as the cochlear amplifier. First, I focus on the hearing of mammals that have both electromotility and hair bundle motility in their outer hair cells. One of the important issues in

electromotility is the RC time constant problem, which limits the frequency response of the outer hair cell because the cell membrane acts as a low-pass RC filter [69, 141]. Earlier reports proposed that cochlear microphonic, the voltage drop across the extracellular medium by the receptor current, overcomes RC time constant problem [30]. The chapter 3 obtains the effective limit of the electromotility as the cochlear amplifier while examining the effect of the cochlear microphonic, which is an AC potential in the endolymphatic media, created by the receptor current.

Next, I examined hair bundle motility in mammalian systems. It has been found that the hair bundle motility of the mammalian hair cell is mediated by the release mechanism, a relaxation-like phenomena [89, 154]. This observation is puzzling because the release mechanism is expected to work for amplification even though mechanical relaxation usually results in damping. This issue is addressed in the chapter 4.

In chapter 5, I expand the scope of investigation to avian system. The chapter 5 examines whether hair bundle motility is effective as the cochlear amplifier both in mammalian and avian systems. I have obtained a quantitative upper bound of the frequency at which hair bundle motility can overcome viscous drag in the system. I found that the upper bound of the frequency is related to a factor reflecting the morphology of hair cell. The map of the morphological factor and the map of hearing frequency along the cochlea are compared for chicken and barn owl in the chapter 5 and 6, respectively.

Chapter 2

Gating of two mechanoelectrical transducer channels associated with a single tip-link

2.1 Introduction

Gating of the mechano-electrical transducer (MET) channels in the hair bundles of hair cells is a critical process in mechanoreception, including hearing. This process is usually described by theoretical models that assume only one MET channel associated with each tip link in the hair bundle [17, 71, 89]. Recent experimental data suggest that the number of channels are significantly greater than the number of tip links [7, 8].

Beurg and others in 2006 obtained the number of MET channels by dividing the total current flowing inside one hair cell by current for a single MET channel. They found that the MET channels outnumber tip links by $\sim$20% for inner hair cells and by $\sim$70% for the outer hair cells of rats [7]. In this experiment, the number of tip links was obtained by counting tip links seen with electronmicroscopy images. Because it is possible that all the MET channels may not have been stimulated in the experiment, the ratio of the number of the MET channels to the number of tip links may be an overestimation. To improve this point, Beurg and others in 2009 counted the number of tip links that show an increase of calcium fluorescence when

the hair bundles are stimulated. In this experiment they found that the number of MET channels is 2.3 times the number of tip links for rat inner hair cells [8]. These observations suggest that at least some of the tip links are associated with two or more MET channels.

So far, to our knowledge, this discrepancy on the number of MET channels associated with one tip link has not been addressed. A recent report does describe two channels associated with one tip-link [164]. However, rather than examining the consequences of having two channels, it re-interprets asymmetrical gating of MET channels, which has been described by a model with two closed states and one open state, by assuming two non-identical interacting channels with two states, open and closed.

What is the consequences of two identical MET channels associated with a single tip link? There are two simple cases of connectivity between these two channels, series and parallel. One of the physical implications of series connection is that each end of a tip link is associated with a MET channel [38]. Parallel connectivity requires that both channels are on one end of the tip link. Each of two strands of the tip link may be associated with a MET channel [23, 58, 153], which shares a link to the myosin motor, responsible for adaptation [59, 70, 154]. The series and parallel connectivities do not contain asymmetry in activation and saturation as will be shown later.

The issue of connectivity is related to whether the MET channel is at the upper or lower end of the tip link or both. A calcium fluorescence study of hair bundles from frog saccular hair cells indicates that the channels are at both ends

[38]. However, a recent study on mammalian cochlear hair cells demonstrates that these channels are only at the lower ends of tip links because the rise of calcium fluorescence of the tallest row stereocilia is delayed and is much less than the other rows [8]. It is not yet clear whether this feature is specific to the mammalian cochlea or is generally applicable to all hair bundles of vertebrates.

The localization of the gating spring can be also an issue for a physical model. Because the main body of the tip link is too stiff to be the gating spring, as determined by electrophysiological studies [151], either the channel itself or a part of the plasma membrane may serve as the gating spring.

Here we examine the effect of series and parallel connections of two identical MET channels on gating. We assume that these channels are independent and respond only to the force applied to them. These are simplifying assumptions and the real systems may be more complex. In our analysis the exact localization of the channels or the identification of the gating spring is not so important as the connectivity of the springs involved in the transduction process.

2.2 Formal description

Consider a system of two identical channels that are connected by springs (Fig. 2.1). Let the connectivity be symmetric with respect to the two channels. If each channel has two states, either open (o) or closed (c), the system of two channels has four states, {o,o}, {o,c}, {c,o}, and {c,c}, which will be represented by an index j. The state {c,o} is equal to {o,c} because of the two channels are identical. Let the

free energy of state j be ϵ_j and the number of open channels n_j. Then the statistical weight that the system is in state j is then given by

$$P_j = e^{-\beta\epsilon_j} \tag{2.1}$$

where $\beta = 1/(k_B T)$, k_B is the Boltzmann constant, and T is temperature. For a given displacement x of the system, the force F_j exerted in state j is equal to $-d\epsilon_j/dx$. Thus we obtain

$$\frac{dP_j}{dx} = -\beta \frac{d\epsilon_j}{dx} e^{-\beta\epsilon_j} = \beta F_j P_j. \tag{2.2}$$

The mean open probability P_o of the channels is expressed as

$$P_o = \frac{1}{2}\langle n \rangle \tag{2.3}$$

by using a notation,

$$\langle y \rangle = \frac{1}{Z} \sum_j y_j P_j$$

where $Z = \sum_j P_j$ and $\langle y \rangle$ is the mean value of an arbitrary quantity y with y_j being the value of y in state j. The open probability defined by Eq. 2.3 is the same as individual channel and is given by

$$P_o = \frac{P_{oo} + P_{oc}}{Z}. \tag{2.4}$$

The stiffness $\tilde{k}$ of the system, which includes the effect of channel gating in response to displacement x, is given by

$$\tilde{k} = \frac{d}{dx} \langle F \rangle. \tag{2.5}$$

By using Eq. 2.2, the stiffness $\tilde{k}$ can be transformed into

$$\tilde{k} = \langle k \rangle - \beta(\langle F^2 \rangle - \langle F \rangle^2) \tag{2.6}$$

where $\langle k \rangle (= \langle dF/dx \rangle)$ is the mean stiffness that does not include the effect of gating. Since $\langle F^2 \rangle \geq \langle F \rangle^2$, gating reduces the stiffness $\tilde{k}$. This effect is known as gating compliance [71]. For convenience, we introduce a dimensionless quantity $\kappa = \tilde{k}/\langle k \rangle$,

$$\kappa = 1 - \frac{\beta}{\langle k \rangle}(\langle F^2 \rangle - \langle F \rangle^2), \tag{2.7}$$

which represents the ratio of stiffness reduction due to gating. We will later refer to this quantity as the stiffness reduction ratio for brevity.

2.3 Series connection

First, we consider a case in which two channels are connected in series by a spring of stiffness k_a, which is the tip link (Fig. 2.1A). If each channel has its own gating spring with stiffness k_g and gating distance x_g, then k_s, the effective stiffness of the spring assembly, is $k_s = (k_g k_a)/(k_g + 2k_a)$. The effective stiffness becomes $k_g/2$ in the limit of stiff tip link (i.e. $k_a \to \infty$) [151].

The free energy ϵ_j of the system in each state j for a given displacement x is

$$\epsilon_{oo} = 2\mu_o + \frac{1}{2}k_s(x - 2x_g)^2, \tag{2.8}$$

$$\epsilon_{oc} = \mu_o + \mu_c + \frac{1}{2}k_s(x - x_g)^2, \tag{2.9}$$

$$\epsilon_{cc} = 2\mu_c + \frac{1}{2}k_s x^2. \tag{2.10}$$

Here μ_o and μ_c are energy of the channel independent of displacement x in open and closed configurations, respectively. The statistical weight P_j (Eq. 2.1) of each state j can be written as

$$P_{oo} = c^2 e^{-\frac{1}{2}\beta k_s (x - 2x_g)^2}, \tag{2.11}$$

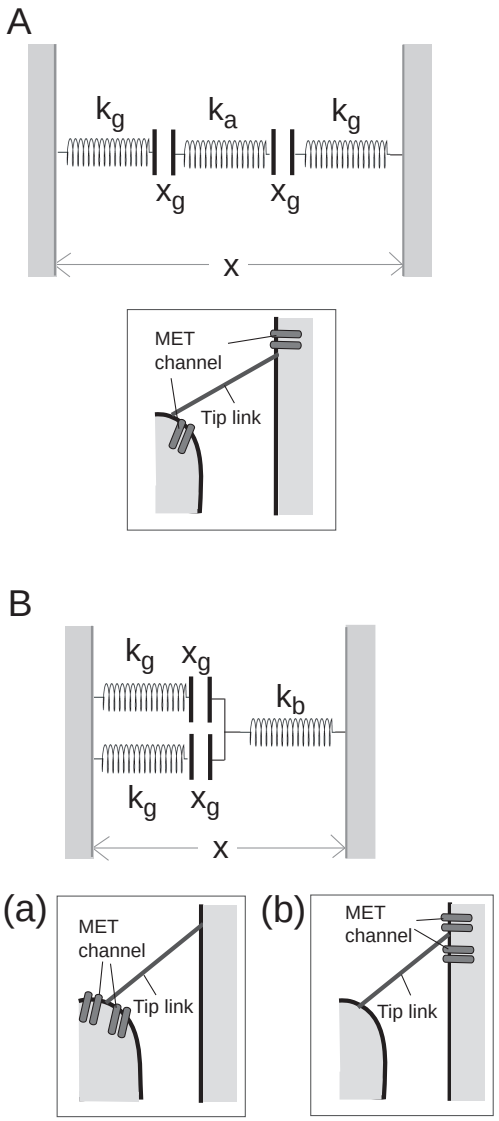

Figure 2.1: Schematic representation of two channels connected in series (A) and in parallel (B). Each channel is associated with gating distance x_g and gating spring of stiffness k_g. In (A), the likely physical picture is that two channels are located at each end of the tip link. In (B), both channels are connected to an elastic element with stiffness k_b. The likely physical picture of such connectivity is that two channels are either (a) at the lower or (b) at the upper end of the tip link. (a) is supported by a recent report [8].

$$P_{oc} = c\, e^{-\frac{1}{2}\beta k_s (x-x_g)^2}, \tag{2.12}$$

$$P_{cc} = e^{-\frac{1}{2}\beta k_s x^2} \tag{2.13}$$

where c ($\equiv e^{-\beta(\mu_o - \mu_c)}$) is a constant.

Using Eqs. 2.11–2.13, the stiffness reduction ratio (Eq. 2.7) for series connection, κ_s can be expressed

$$\kappa_s = 1 - \frac{2\gamma\,(P_{oc}P_{oo} + 2P_{oo}P_{cc} + P_{oc}P_{cc})}{(P_{oo} + 2P_{oc} + P_{cc})^2}, \tag{2.14}$$

where $\gamma = \beta k_g x_g^2/2$. This quantify could be called "reduced gating energy" because it is the energy required to open the channel divided by thermal energy $k_B T$.

It can be shown that the stiffness reduction ratio κ_s is related to open probability $P_{o,s}$, which is given by Eq. 4.2 with Eqs. 2.11–2.13. By taking derivative of $P_{o,s}$, we obtain

$$\kappa_s = 1 - 2x_g \frac{dP_{o,s}}{dx}. \tag{2.15}$$

This relationship will be examined later where the predictions of the models are compared to experimental data.

To find the number of minima of κ_s, we set $d\kappa_s/dx = 0$. This condition leads to

$$(c^2 Y_s^2 - 1)[c^2 A_s Y_s^2 + 2c(2 - A_s^2)Y_s + A_s] = 0 \tag{2.16}$$

where $Y_s = \exp[\beta k_s x_g (x - x_g)] > 0$ and $A_s = \exp(\gamma/2) > 1$. Equation 2.16 always has a root where $Y_s = 1/c$. In addition, if the discriminant of the quadratic equation is positive, it has two more roots and κ_s has double minima in x-axis. This condition is simplified as $A_s > 2$, which is equivalent to $\gamma > 2\ln 2$.

Thus, only if $\gamma \leq 2\ln 2$, the reduction ratio κ_s has a single minimum $\kappa_{s,min}$,

$$\kappa_{s,min} = 1 - \frac{\gamma}{1 + e^{\gamma/2}}$$

at

$$x = x_g(1 - \frac{\ln c}{\gamma}).$$

Note that $\kappa_{s,min}$ is a decreasing function of γ and at $\gamma = 2\ln 2$ it takes a positive value $1 - 2\ln 2/3 (= 0.5379...)$. A further increase in γ splits the single minimum into two equal minima, $\kappa_{s,min} = 1 - \frac{\gamma}{4(1-e^{-\gamma})}$, which turn negative if γ is larger than 3.92... (Fig. 2.2).

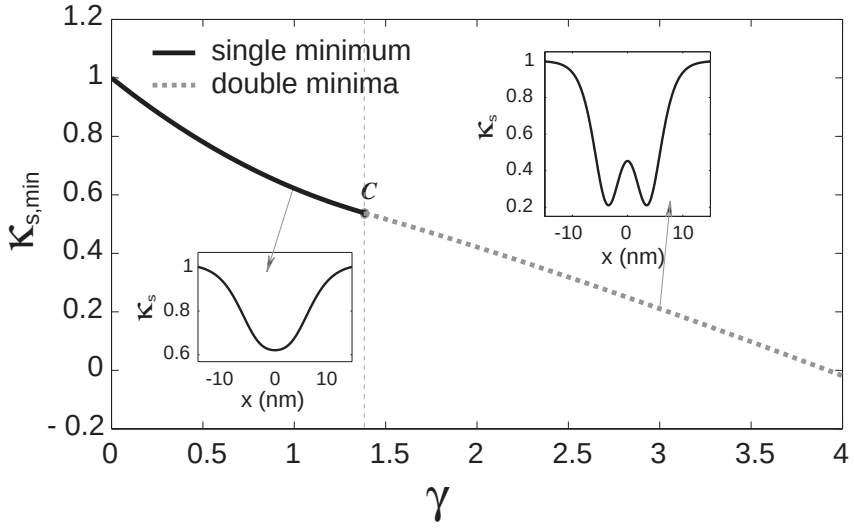

Figure 2.2: Predictions of the series connection model. The minimum value $\kappa_{s,min}$ of the stiffness reduction ratio κ_s is plotted against γ $(= k_g x_g^2/(2k_BT))$. The single minimum (solid line) splits into double minima (grey dotted line) at the critical point C $(2\ln 2,\ 1 - (2/3)\ln 2)$. Insets show the profiles of a single minimum at $\gamma = 1.08$ (left) and double minima at $\gamma = 3$ (right) plotted against displacement x.

2.4 Parallel connection

Next, we examine the case in which two identical channels are connected in parallel. Suppose the two channels connected in parallel are linked with an elastic element with stiffness k_b (Fig. 2.1B).

The energy ϵ_j in each state j for a given displacement x is expressed as follows (See Appendix A.1).

$$\epsilon_{oo} = 2\mu_o + \frac{1}{2}k_p(x - x_g)^2, \tag{2.17}$$

$$\epsilon_{oc} = \mu_o + \mu_c + \frac{1}{2}k_p(x - \frac{x_g}{2})^2 + \frac{1}{4}k_g x_g^2, \tag{2.18}$$

$$\epsilon_{cc} = 2\mu_c + \frac{1}{2}k_p x^2, \tag{2.19}$$

where $k_p = 2k_g k_b/(2k_g + k_b)$. Here μ_c and μ_o are intrinsic energy of the channel in closed and open configurations, respectively. The statistical weights of corresponding states can be given by

$$P_{oo} = c^2 \exp[-\frac{1}{2}\beta k_p(x - x_g)^2], \tag{2.20}$$

$$P_{oc} = c \exp[-\frac{1}{2}\beta k_p(x - \frac{x_g}{2})^2 + \frac{1}{4}k_g x_g^2], \tag{2.21}$$

$$P_{cc} = \exp[-\frac{1}{2}\beta k_p x^2] \tag{2.22}$$

where c $(= e^{-\beta(\mu_o - \mu_c)})$ is a constant.

Using Eqs. 2.20–2.22, the stiffness reduction ratio (Eq. 2.7) for parallel connection, κ_p, is expressed as

$$\kappa_p = 1 - \frac{\beta k_p x_g^2 \,(P_{oo}P_{cc} + P_{oc}P_{cc} + \frac{1}{2}P_{oo}P_{oc})}{(P_{oo} + 2P_{oc} + P_{cc})^2}. \tag{2.23}$$

Similar to series connection, using Eqs. 4.2, 2.20–2.22, the relationship between

the reduction ratio κ_p and open probability $P_{o,p}$ is expressed

$$\kappa_p = 1 - x_g \frac{dP_{o,p}}{dx}. \tag{2.24}$$

To find the number of minima of κ_p, we put $d\kappa_p/dx = 0$. This condition leads to

$$(c^2 Y_p^2 - A_p^4)[c^2 B_p Y_p^2 - 2cA_p(A_p^2 - 2B_p^2)Y_p + A_p^4 B_p] = 0 \tag{2.25}$$

where $Y_p = \exp[\frac{1}{2}\beta k_p x_g x] > 0$, $A_p = \exp[\frac{1}{8}\beta k_p x_g^2] > 1$, and $B_p = \exp[\frac{1}{4}\beta k_g x_g^2] > 1$. Eq. 2.25 has only one root $Y_p = A_p^2/c$ because the second quadratic equation in Eq. 2.25 does not have a solution due to the condition $k_p < 2k_g$ (i.e. $A_p < B_p$). This means that for the parallel connection, the stiffness reduction ratio κ_p has always only one minimum,

$$\kappa_{p,min} = 1 - \frac{\alpha\gamma}{(\alpha+2)(1+\exp[-\frac{\gamma}{\alpha+2}])} \tag{2.26}$$

at

$$x_{p,min} = \frac{1}{2} x_g (1 - \frac{\alpha+2}{\alpha} \frac{\ln c}{\gamma})$$

where $\alpha = k_b/k_g$, the stiffness ratio of the shared spring to gating spring. Note that $\kappa_{p,min}$ is a function of γ, the reduced gating energy which also appears in Eq. 2.14.

The dependence of $\kappa_{p,min}$ on gating energy γ and the stiffness ratio α is illustrated in Fig. 2.3A. Gating compliance increases with increasing gating energy γ. For a given value of α, the minimum value $\kappa_{p,min}$ of the stiffness reduction ratio decreases with γ and can become negative if γ is greater than 2 (see Appendix A.2).

Gating compliance increases with the stiffness ratio of the shared spring, α (Fig. 2.3A, B) for a given γ. If the link between the channels and the tip link is

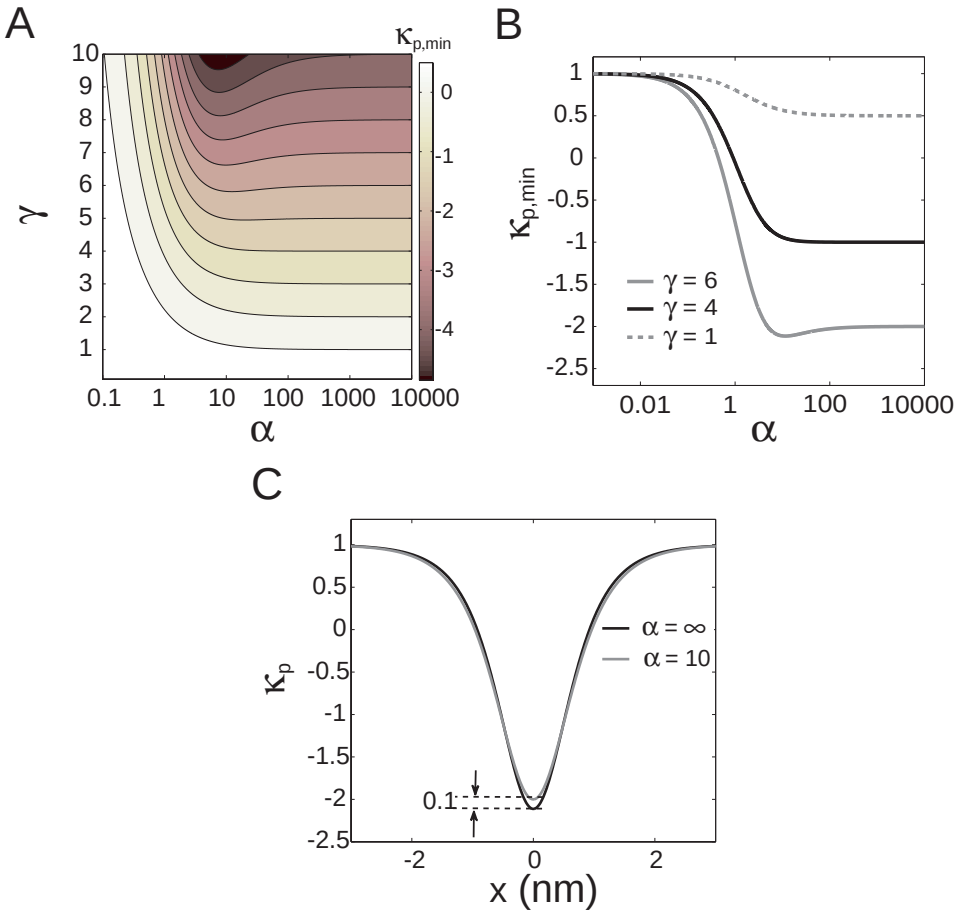

Figure 2.3: Predictions of the parallel connection model. (A) Contour plot of minimum value $\kappa_{p,min}$ of the stiffness reduction ratio κ_p that is a function of γ $(= k_g x_g^2/(2k_BT))$ and α $(= k_a/k_g)$. (B) $\kappa_{p,min}$ plotted against α for $\gamma = 1$ (dotted), $\gamma = 4$ (black solid), and $\gamma = 6$ (grey solid). (C) κ_p plotted against hair bundle displacement x for $\alpha = \infty$ (black) and optimal $\alpha = 10$ (grey) at $\gamma = 6$. The difference between the minimum value of κ_p for $\alpha = 10$ and for $\alpha = \infty$ is 0.1.

soft, the stiffness of the hair bundle will remain constant because gating does not happen. This situation corresponds to the behavior where α value is close to zero in Fig. 2.3A, B. In the other extreme, if α is infinitely large, the two channels will become independent of each other and gating of these channels will be same as that of the single channel. This explains why for large α, $\kappa_{p,min}$ approaches $1 - \gamma/2$, the value for a single channel [71], in Fig. 2.3B.

If the gating energy γ is greater than 4 (see Appendix A.3), for intermediate values of α, the stiffness reduction ratio κ_p of the two channels has lower minimum than that of a single channel (Fig. 2.3A, B). This can be attributed to an effect of the two channels being coupled by an elastic element.

The cooperative effect increases with the gating energy. In the limit of infinite γ, the minimum of κ_p of the two channels with optimized α is twice of κ_p for the single channel model (see Appendix A.3). However, experimental values for γ are less than 10 [163]. Indeed, a large value for gating energy γ makes the MET channel insensitive to applied force. For this reason, this cooperative effect cannot be significant and the gating compliance of the two identical channels connected in parallel should be similar to that of a single channel (Fig. 2.3C).

Why does parallel connection of MET channels have so little effect? One might expect that increasing stiffness k_b of the shared spring increases steric interaction between the MET channels and thus these channels become more cooperative. However, such a change brings the gating of the channels closer to that of a single channel. Steric interaction between channels is built-in in the standard description of the MET channel proposed by Howard and Hudspeth [71], which assumes that

bending of a hair bundle imposes an equal displacement on all MET channels in the hair bundle [77].

2.5 Comparison with experimental data

To compare experimental data with the theoretical predictions, we discuss briefly how to obtain experimental values for the open probability of the channel and the stiffness reduction ratio.

The open probability P_o of the MET channels is obtained by dividing the transducer current by its maximum value. Errors in this quantity are minor if transducer current shows saturation in the current-displacement plot.

To obtain a stiffness reduction ratio κ (Eq. 2.7), hair bundle stiffness must be obtained as the displacement derivative of bundle force F,

$$F = k_\infty x - k_t x_g P_o \tag{2.27}$$

where x is displacement, k_t the stiffness of transduction elements, and k_∞ the hair bundle stiffness in non-gating range. The stiffness reduction ratio κ is then obtained by

$$\kappa = (1 - \frac{k_\infty}{k_t}) + \kappa_h \, (\frac{k_\infty}{k_t}), \tag{2.28}$$

where κ_h is the normalized hair bundle stiffness, i.e. $\kappa_h = (dF/dx)/k_\infty$.

The data of open probability and the stiffness reduction ratio are plotted against hair bundle displacement (Fig. 2.4, 2.5). In the figure, the curves are the theoretical fits obtained from the two models. The fits were calculated using the optimization toolbox (lsqcurvet) of Matlab (version 7.8, The Math Works). This

curve fitting algorithm minimizes the mean squared error between the data and the theoretical prediction.

2.5.0.1 Rat outer hair cells

Experimental data on rat outer hair cells [89] do not show a good fit with the series connection model (Fig. 2.4(c)). The stiffness reduction ratio has a single minimum, which is lower than the critical value of $1 - 2\ln 2/3 (= 0.5379...)$ for the series connection model. Thus the data are inconsistent with the series connection model, which predicts double minima. The parallel connection model can provide a reasonable fit, which is similar to that of the one-channel-per-tip-link model (Fig. 2.4(d)). This observation is compatible with the report that these cells have two or more channels and that channel is not located at the higher ends of tip links [8].

The curve-fits of the open probability, however, are not sufficiently sensitive to distinguish the two models (Fig. 2.4(a), (b)), as predicted in Eqs. 2.15 and 2.24.

This analysis of the stiffness data is consistent with other experimental observations as described above. However, the parameter values of the optimal fit may not be realistic. The relatively weak displacement dependence of gating requires the combination of relatively large gating distance of 190 nm and weak gating spring, requiring a rather large number of channels. That makes it hard to rule out the possibility that the experimentally obtained stiffness changes and transducer current may be affected by the distribution of operating points of the channels in the hair bundle rather than the characteristics of the gating of individual channels. This

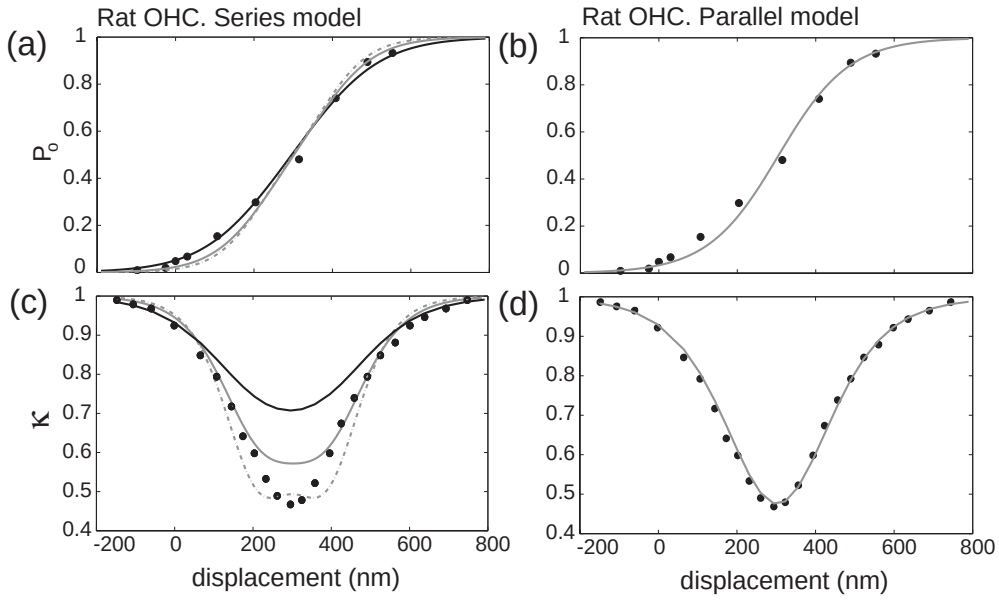

Figure 2.4: Open probability P_o and the stiffness reduction ratio κ compared with the series connection and the parallel connection models. Data points (•) are from rat outer hair cells [89]. Lines in left column represent the series connection model and in right column the parallel connection model, which is, in effect, indistinguishable from the classical one channel per tip link model. For details of comparison, refer to the text. Parameter values used in (a), (c): $k_s = 0.70$ μN/m, $k_\infty/k_t = 1.0$, $x_g = 65$ nm (black solid line) with $c = 0.080$, $x_g = 85$ nm (grey solid line) with $c = 0.045$, and $x_g = 100$ nm (grey broken line) with $c = 0.035$. Parameter values used in (b), (d): $k_g = 0.25$ μN/m, $x_g = 190$ nm, $c = 0.10$, $\alpha = 50$, and $k_\infty/k_t = 1.0$.

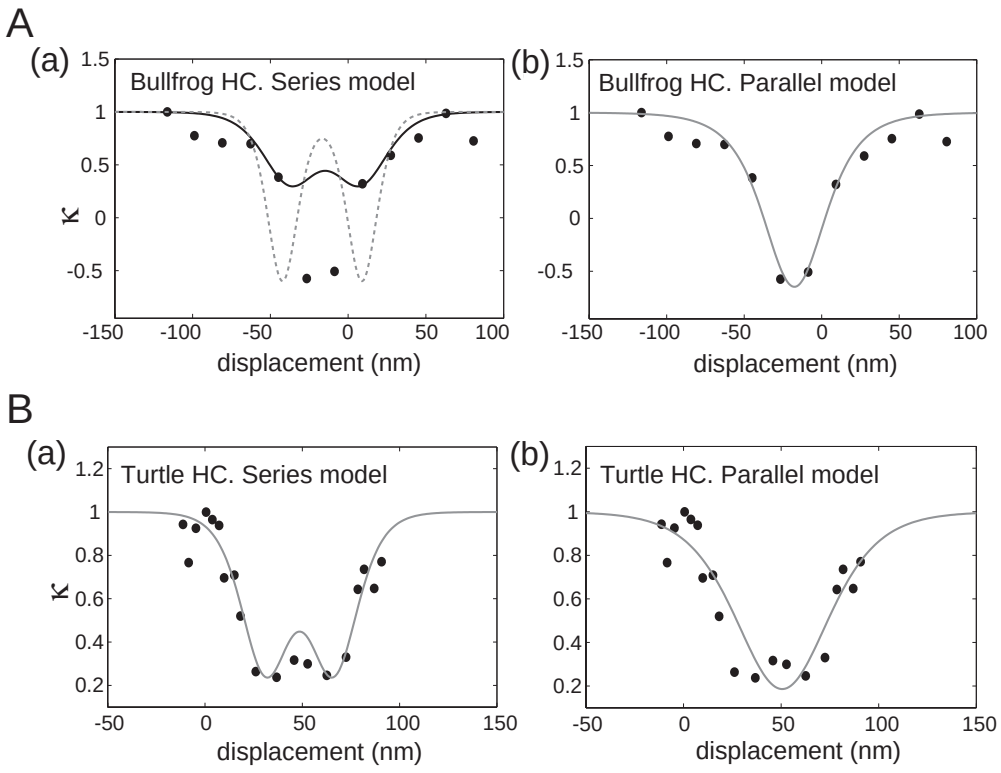

Figure 2.5: Open probability P_o and the stiffness reduction ratio κ compared with the series connection and the parallel connection models. Data points (•) in (A) bullfrog saccular hair cells [96], and in (B) turtle auditory hair cells [128]. Lines in left column represent the series connection model and in right column the parallel connection model, which is, in effect, indistinguishable from the classical one channel per tip link model. For details of comparison, refer to the text. Parameter values used in A-(a): $k_s = 12.0$ μN/m, $x_g = 30$ nm, and $c = 49$ (black solid line), $k_s = 15.0$ μN/m, $x_g = 42$ nm, and $c = 7500$ (grey broken line) with $k_\infty/k_t = 1.0$. Parameter values used in A-(b): $k_g = 3.7$ μN/m, $x_g = 92$ nm, $c = 31$, $\alpha = 3.7$, and $k_\infty/k_t = 1.0$. Parameter values used in B-(a): $k_s = 21$ μN/m, $x_g = 24$ nm, $c = 0.050$, and $k_\infty/k_t = 1.0$. Parameter values used in B-(b): $k_g = 4.9$ μN/m, $x_g = 53$ nm, $c = 0.22$, $\alpha = 250$, and $k_\infty/k_t = 1.0$.

issue was already present in the initial interpretation of the experimental data using the classical model [89]. If that is the case, our analysis regarding the connectivity of channels may not be relevant to these data.

2.5.0.2 Frog saccular hair cells

For the bullfrog saccular hair cells, experimental values for the stiffness reduction ratio have a single minimum, which is negative far below the critical value for single minimum in the series connection model [96]. Therefore, this feature is consistent with the parallel connection model and incompatible with the series connection model (Fig. 2.5A). This result is also consistent with the well-established analysis of mechanotransduction of bullfrog hair cells with one-channel-per-tip-link model [71].

Table 2.1: Parameters used for figure 2.6

	I.(a)	I.(b)	II.(a)	II.(b)	III.(a)	III.(b)
k_g (μN/m)		8.00		6.00		5.54
k_s (μN/m)	21.4		37.0		15.1	
x_g (nm)	15.9	31.0	12.0	51.0	14.1	33.4
c	0.39	0.50	0.59	1.80	0.75	0.76
k_∞/k_t	1.00	1.00	1.42	2.67	1.00	1.20
α		153		8.92		53.9

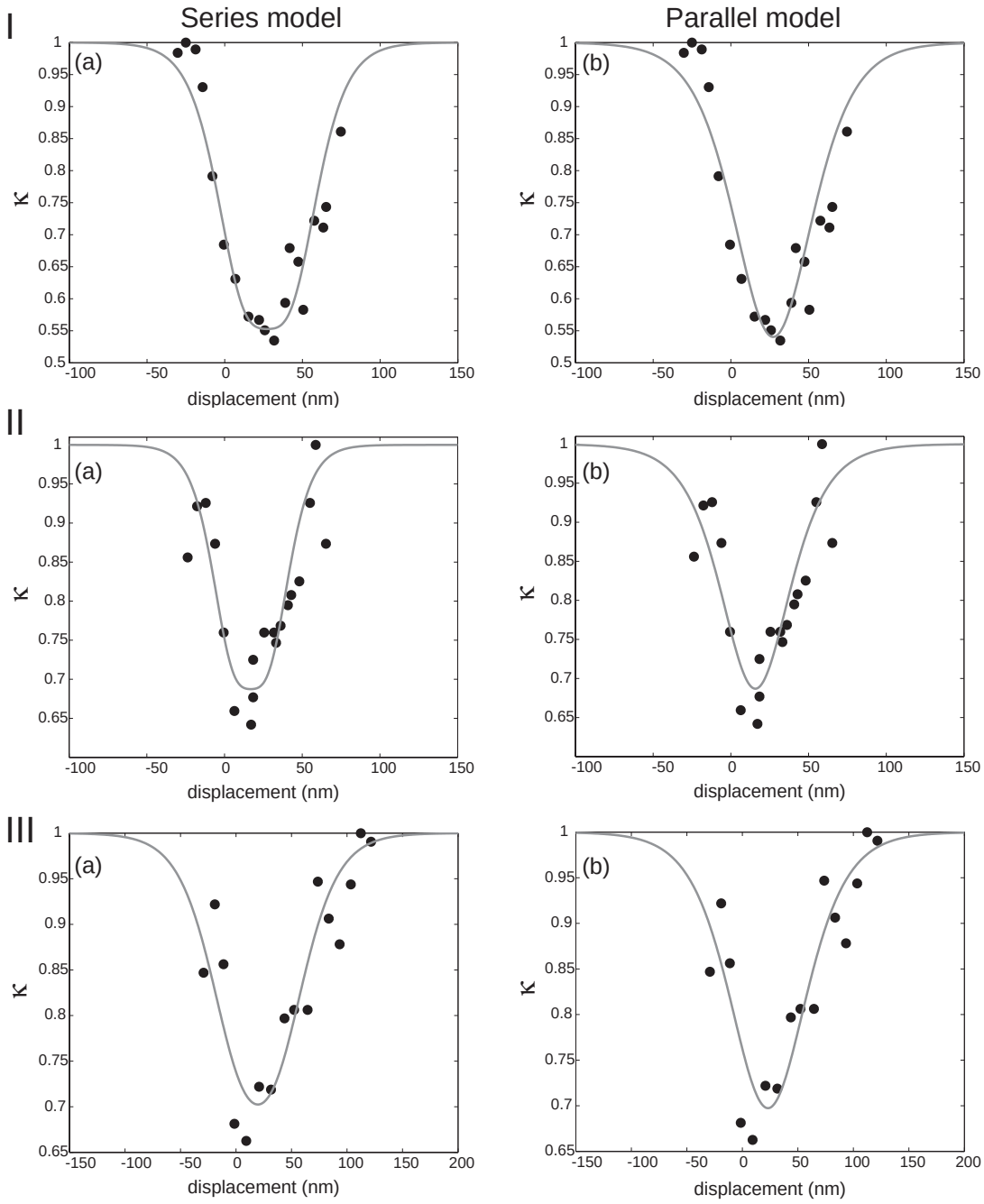

Figure 2.6: Curve-fits of turtle hair cell data to the series (left column) and the parallel (right column) models. Data (•) in (I) are taken from Fig. 2A. 2.8mM Ca, in (II) from Fig. 2A. 0.25mM Ca, and in (III) from Fig. 2B control experiment, presented in [127]. Parameters used are shown in the table 2.1.

2.5.0.3 Turtle auditory hair cells

The most of existing datasets for the hair bundle stiffness of turtle hair cells [128] show a minimum of the stiffness reduction data above the critical value of 0.54... and differences between the series and parallel connection model are not so clear because both models predict a single minimum of the stiffness reduction value under this condition (Fig. 2.6). Among these datasets, only one dataset shows a minimum of the stiffness reduction data lower than the critical value of 0.54..., the condition at which the series connection must show double minima and thus advantageous to distinguish parallel and series connection. This dataset fits slightly better to the series connection model than to the parallel connection model (Fig. 2.5B). Even if we disregard the double minima as the result of noise, the stiffness data still have a broad minimum, which is still more consistent with the series connection than the parallel connection. For this reason, we cannot rule out the possibility that turtle hair bundles have series connection of the two channels.

Finally, we make a simple remark on the significance of our findings on hair bundle organization. The observation that two channels are likely to be in a parallel connection is consistent with the report that mechanoelectric transducer channels are located at the lower end of tip links [8]. However, the localization of the adaptation motor must be also important. If the adaptation motor is located at the higher end of the tip link [41], the operating points of mechanotranducer channels may not be identical, which is unfavorable for negative stiffness [77]. Such an organization of hair bundles may not be advantageous for negative stiffness, which is expected

to be essential to function as an amplifier [156, 162]. This issue could be related to possible variability in the localization of myosins in hair bundles [65].

2.6 Conclusions

In this chapter, we examined gating of two identical channels, connected either in series or in parallel. We found that the difference is most pronounced in gating compliance. If two identical channels are connected in series, negative stiffness leads to double minima when plotted against displacement. In contrast, parallel connection of two identical channels results in gating similar to that of a single channel. Our results confirm that the prevailing approach for analyzing the gating of MET channels is, in effect, compatible with the existence of two or more channels per tip link. However, we found that experimental data on turtle hair cells does not rule out the series connection model.

Acknowledgement

This work was directed by Dr. Kuni H. Iwasa and supported by NIDCD.

Chapter 3

Effect of the cochlear microphonic on the limiting frequency of the mammalian ear

3.1 Introduction

The sensitivity and frequency selectivity of the mammalian ear depend on the motile activity of outer hair cells (OHCs) as described in the chapter 1. Electromotility of OHCs is likely responsible for this function [33, 99, 102, 114]. However, its dependence on the receptor potential (RP) may limit its efficiency because the RP is attenuated by the intrinsic low-pass RC filter of the cell, the corner frequency of which is significantly lower than the operating frequency. This is known as the RC time constant problem [69, 141] [1]. To evaluate the significance of this problem, we will need a scale to measure force production by electromotility. In an earlier report [118], Ospeck and others assumed that this motility must counteract viscous drag [62], specifically the shear drag in the gap between the tectorial membrane and the reticular lamina [1]. They found that this leads to a frequency limit and that the limiting frequency obtained for the ear geometry of chinchillas was about 10 kHz, reasonable but still short of covering the known auditory frequency. This result suggests the presence of factors that enhance the effectiveness of electromotility.

To address the RC time constant problem, several mechanisms that can en-

[1] This is explained in the page 35.

hance the efficiency of electromotility have been proposed. Those mechanims include piezoelectric resonance [118, 152], modulation by a stretch-sensitive Cl^- current [138, 144], fast voltage-gated K channels [118, 119], and the effect of the cochlear microphonic (CM) [30, 31]. Of those mechanisms, the analysis by Ospeck and others [118] showed that pure piezoelectric resonance that does not involve the mechano-electric transducer channel is not effective and that fast voltage-gated K channels, which can counteract the capacitive current, are capable of extending the frequency limit beyond 10 kHz. Now it appears possible to extend this analysis to include the effect of the CM on unstimulated outer hair cells [30, 31] because recent experiments [52, 124] have provided details regarding traveling waves and the CM.

Dallos and Evans [30, 31] posit the following. The CM, which is the voltage drop generated by the receptor current of outer hair cells across the extracellular medium, has relatively flat frequency response. In addition, unstimulated outer hair cells should act as voltage dividers with relatively flat frequency response because at low frequencies their performance is determined by the resistance ratios of their apical and basolateral membranes and at high frequencies the performance is determined by the capacitance ratios [30, 31]. Thus the oscillatory membrane potential in unstimulated OHCs induced by the CM has relatively flat frequency response and this potential can be larger than the receptor potential of stimulated OHCs at high frequencies.

Here we examine whether or not the CM can contribute to overcoming the RC problem by constructing a simple theoretical model that sets an upper bound to efficiency.

First, we assume that stimulus level is low enough to consider that the cochlear microphonic (CM) is locally produced by the receptor current of OHCs [29]. This calculation can be justified for the following reasons. Since the responses of the cochlea to stimuli with very low intensity are extremely localized [125, 131], we estimate the external potential near the locus of the characteristic frequency assuming that the major current source is local. This assumption, which is rather approximate, appears to be compatible with the value of ~ 200 μm [124] for the wavelength of the traveling wave near the peak and estimates of >300 μm [55] and 40 μm [52] for the space constant of the CM. Second, instead of detailed model of cochlear mechanics, we assume that electrical energy generated by the CM is optimally converted into mechanical energy. We further assume that mechanical energy made available from electromotility is optimally used to counteract viscous drag. Then by considering energy balance we examine whether or not this effect increases the frequency limit that is imposed by viscous drag.

3.2 Equivalent circuit for hair cells

Following Dallos and Evans [30], we consider two kinds of OHCs (Fig. 3.2). One kind of OHCs is those cells, which are stimulated at their characteristic frequency. These cells have receptor currents, which generate the receptor potential (RP) across their plasma membrane and the cochlear microphonic (CM) in their vicinity in the extracellular space. Although these cells convert electrical energy made available by the RP into mechanical energy, let us refer them as *sensor* cells

for convenience. Another kind is unstimulated OHCs. These cells have oscillating potential not because of stimulation to their hair bundles but because of the CM. Let us call this potential "pseudo-receptor potential" (pRP). We refer to those cells as *actuator* cells because their pRP drives those cells. For simplicity, we assume that these two kinds of cells, *sensors* and *actuators*, share the same electrical properties that include the apical capacitance C_a, the basal capacitance C_b, the resting apical resistance R_0 and the basal resistance R_K.

Since the resting potential of OHCs is about -70 mV [21], close to the reversal potential e_K of about 100 mV for K^+ [2], the basal conductance is dominated by K^+ current. The apical membrane is exposed to the endolymph with endocochlear potential e_{ec} of about 100 mV [139], measured from the perilymph, which surrounds the basolateral membrane.

The circuit in the figure 3.2 is described by

$$I_1 = \frac{V_1 - e_K}{R_K} + C_b \frac{d}{dt} V_1 = \frac{V_e - V_1}{R_a} + C_a \frac{d}{dt}(V_e - V_1), \tag{3.1}$$

$$I_2 = \frac{V_2 - e_K}{R_K} + C_b \frac{d}{dt} V_2 = \frac{V_e - V_2}{R_0} + C_a \frac{d}{dt}(V_e - V_2), \tag{3.2}$$

$$I_1 + nI_2 = \frac{e_{ec} - V_e}{R_e}, \tag{3.3}$$

where V_1 and I_1 are the membrane potential and current of sensor cells and V_2 and I_2 are those for actuator cells. The voltage drop $e_{ec} - V_e$ is produced by currents through the external resistance R_e. The factor n is the ratio of actuator cells to sensor cells.

We placed the extracellular resistance R_e on the apical side of OHC's (i.e. in

[2]The Nernst potential with 140 mM K^+ inside and 2.7 mM K^+ outside the cell.

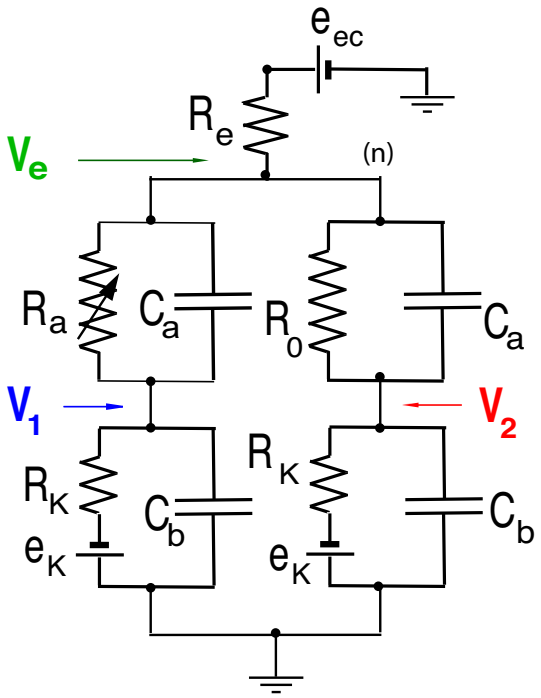

Figure 3.1: An equivalent electric circuit that represents the configuration in which two kinds of outer hair cells are connected. On the left is the sensor cell, which has mechanotransducer conductance represented by the resistance R_a. The transducer current induces the receptor potential V_1 in the cell as well as the cochlear microphonic V_e across the external resistance R_e. The apical capacitance is C_a, the basolateral membrane has resistance R_k and capacitance C_b. On the right is the actuator cell. The properties of the actuator cell are identical to the sensor cell with the exception that the apical resistance is constant at R_0. The cochlear microphonic induces pseudo-receptor potential V_2 in the actuator cell.

quantity	used	measured (estimated)
C_a	5 pF	(3 pF)†
C_b	10 pF	(10 pF)†
$C_a + C_b$	15 pF	$\geq$15 pF [69]
R_K	10 MΩ	10 MΩ [104], 20 MΩ [69]
R_0	60 MΩ	(60 MΩ)‡
R_e	1 MΩ	(0.7 MΩ)§
g	1 nS/nm	1 nS/nm¶

Table 3.1: Parameter values. The values used reflect properties of basal cells. †Estimation based on the membrane area. ‡Assumes 50% opening of the maximal hair bundle conductance, which is 9.2 nS in a perilymphatic medium [95] multiplied by 3 to account for low Ca^{2+} endolymph [94]. §The amplitude of cochlear microphonic near outer hair cells is 0.1 mV for basilar membrane motion with 1 nm amplitude [52] which elicits 0.15 nA given the sensitivity of 1 nS/nm and 150 mV potential drop. This gives 0.7 MΩ for R_e. ¶Obtained by multiplying the steepest slope for hair bundle open probability 1/(25 nm) multiplied by 28 nS conductance [94, 95], assuming 1:1 ratio of hair bundle displacement to basilar membrane displacement. This value is also consistent with the peak sensitivity of 0.7 nS/nm [66] obtained from the hemicochlea preparation, considering the blocking effect of high Ca^{2+} concentration in the perilymph-like medium.

the scala media) in the equivalent circuit diagram. However, it is also reasonable to have the extracellular resistance on the basolateral side of the OHCs. These two cases give the same result for the AC voltage drop because the circuit is closed at the ground.

Let us assume that the basilar membrane moves sinusoidally with a small amplitude x at an angular frequency $\omega(= 2\pi f)$. The reason for this assumption is that the sensitivity of the basilar membrane is largest for small signals [131] and therefore examining the case of small signal must be sufficient for examining the RC time constant problem. The resistance of the apical membrane, R_a responds to the motion of the basilar membrane without a phase delay due to fast gating of mechanotransducer channels. It can be described by

$$R_a(t) = R_0(1 - \epsilon \exp[i\omega t]), \tag{3.4}$$

with $\epsilon \ll 1$. The relationship between x and ϵ can be given by using the sensitivity g of the mechanoelectric transducer (MET) channel to basilar membrane displacement,

$$\epsilon = gR_0x. \tag{3.5}$$

The potentials V_1, V_2, and V_e can be expressed by,

$$V_1(t) = V_{10} + e_K + v_1 \exp[i\omega t], \tag{3.6}$$

$$V_2(t) = V_{20} + e_K + v_2 \exp[i\omega t], \tag{3.7}$$

$$V_e(t) = V_{e0} + e_K + v_e \exp[i\omega t], \tag{3.8}$$

where v_1, v_2, and v_e are small complex amplitudes.

Although the membrane capacitance C_b depends on the membrane potential due to the membrane motor, we treat it as constant. Because the voltage changes are small, the voltage-dependent component of the capacitance contributes only to second- and higher-order terms.

Perturbation solution

The zero-th order terms lead to,

$$V_{10} = V_{20} = \frac{R_K V_0}{R_0 + R_K + (1+n)R_e} \tag{3.9}$$

$$V_{e0} = \frac{(R_0 + R_K)V_0}{R_0 + R_K + (1+n)R_e}, \tag{3.10}$$

where $V_0 = e_{ec} - e_K$. Here $V_{10}(= V_{20})$ is the resting potential of OHCs. The DC component of the membrane potential of both types of cells are equal because it is determined by the time independent part of the resistance, which is equal in both.

The fist-order terms in the perturbation method lead to,

$$\begin{aligned} \frac{v_1}{\epsilon} &= i\frac{R_0 V_{10}}{D_n}[nR_e + R_K(1 + i\omega C_b n R_e) \\ &\quad + R_0(1 + i\omega C_b R_K + i\omega C_a(R_K + nR_e \\ &\quad + i\omega C_b n R_K R_e))] \end{aligned} \tag{3.11}$$

$$\frac{v_2}{\epsilon} = -\frac{iR_0 R_e V_{10}}{D_n}(1 + i\omega C_a R_0)(1 + i\omega C_b R_K) \tag{3.12}$$

$$\frac{v_e}{\epsilon} = -\frac{R_0 R_e V_{10}}{R_K D_e}(1 + i\omega C_b R_K) \tag{3.13}$$

with

$$D_n \equiv -i[R_K + R_0(1 + i\omega(C_a + C_b)R_K)]D_e \tag{3.14}$$

$$
\begin{aligned}
D_e \equiv & -(1+n)R_e - R_K(1+i\omega C_b(1+n)R_e) \\
& -R_0[1+i\omega C_b R_K + i\omega C_a((1+n)R_e \\
& +R_K(1+i\omega(1+n)C_b R_e))]
\end{aligned} \tag{3.15}
$$

Here v_1 is the AC component of the RP, v_2 is the AC component of the pRP, and v_e is the CM.

In the special case of $R_e = 0$, both CM and pRP disappear, i.e. $v_e = v_2 = 0$. The RP v_1 of the sensor cell turns into v_0 and

$$
\frac{v_0}{\epsilon} = \frac{R_0 V_{10}^{(0)}}{R_0 + R_K + i\omega R_0 R_K (C_a + C_b)}, \tag{3.16}
$$

where $V_{10}^{(0)}$ is V_{10} with $n = 0$.

3.3 Magnitudes of oscillating potentials

Here we numerically examine the phase and the magnitude of the pRP and compare them with those of the RP. A set of typical parameter values is given in Table 3.2.

Numerical examination (Fig. 3.3) shows that the magnitude of the pRP is less than that of the RP if $n \geq 1$ for the entire frequency range. However, the pRP increases with decreasing n and a reversal takes place at a high frequency range if $n < 1$. The reason for the reversal is the phase. The phase of the pRP is similar to that of the CM, which differs in phase from the RP by about π. Namely, the RP suffers destructive interference from the CM.

These observations are consistent with the high frequency asymptotes. For

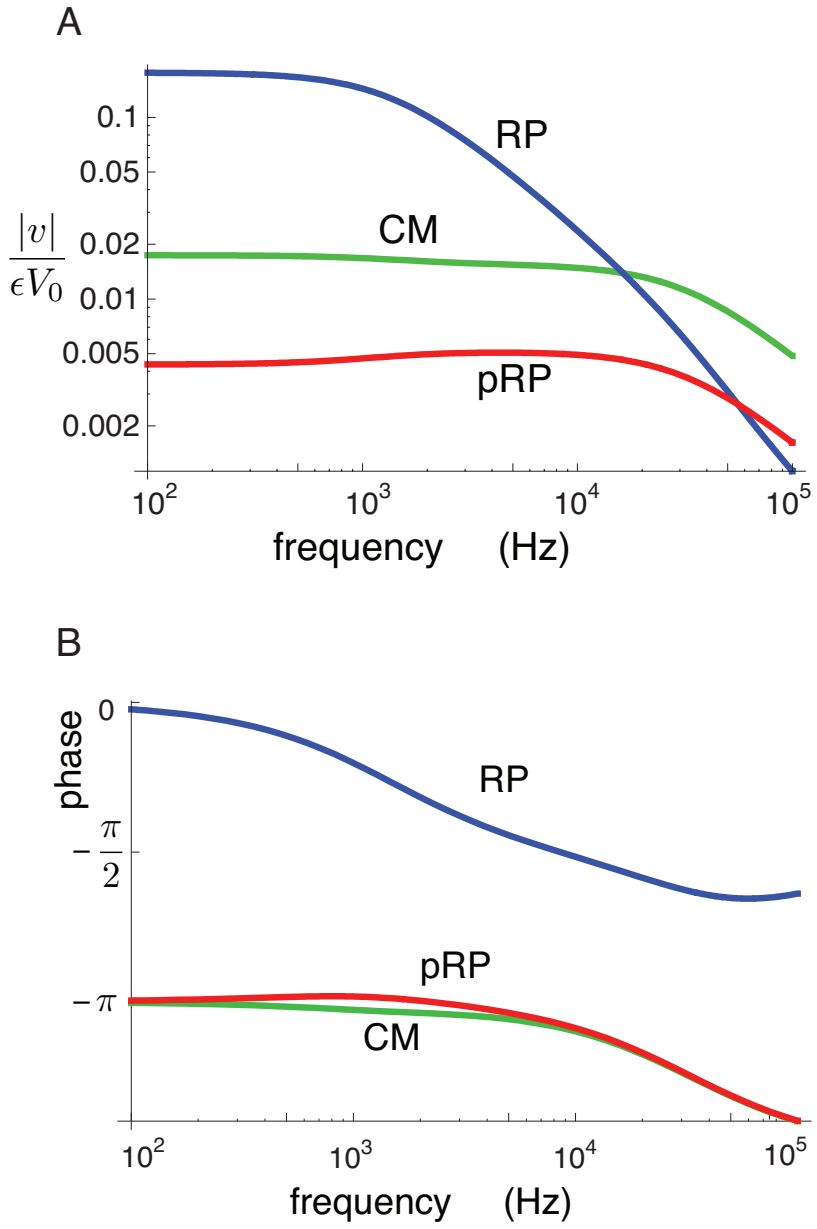

Figure 3.2: The magnitude (A) and phase (B) of the receptor potential (RP), the cochlear microphonic (CM), and pseudo-receptor potential (pRP). The values of the parameters are shown in Table 3.2. The value for n is 0.5.

high frequency, Eqs. (3.11) and (3.11) yield,

$$\frac{v_1}{\epsilon V_{10}} \approx -i\frac{n}{n+1}\cdot\frac{1}{\omega(C_a+C_b)} \tag{3.17}$$

$$\frac{v_2}{\epsilon V_{10}} \approx i\frac{1}{n+1}\cdot\frac{1}{\omega(C_a+C_b)}. \tag{3.18}$$

These equations show that at high frequencies the inequality $|v_1| > |v_2|$ holds for $n > 1$ and $|v_1| < |v_2|$ for $n < 1$. They also show the phase difference of π.

3.4 Co-localization of two types of OHCs

If actuator cells are co-localized with sensor cells, what is expected? Since electromotility is proportional to the oscillating potential of OHCs, its effect on CM can be assessed by the ratio of the weighted mean of the receptor potential and the pRP $|v_1 + nv_2|/(1+n)$ to the RP $|v_1|$. Since the phase of v_2 differs from that of v_1 approximately by π, the RP and the CM interfere destructively. Thus we expect

$$|v_1 + nv_2|/(1+n) < |v_1|, \tag{3.19}$$

which is illustrated in Fig. 3.4A. This inequality is obvious for the high frequency asymptotes. For this reason, having both actuator cells in the immediate neighborhood of the sensor cells is not only inconsistent with morphological observations, it also reduces the effectiveness of electromotility.

3.5 Upper-bound of CM utilization

Following Dallos and Evans [30], here we assume that the sensor cells are in the location characteristic of frequency ω and the cells that use the CM are more

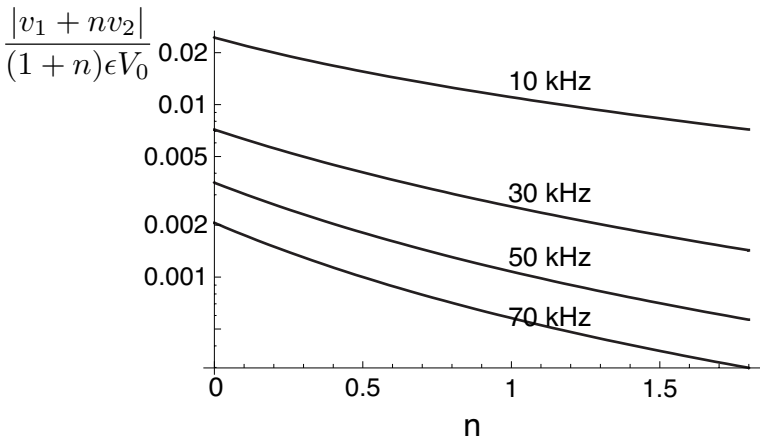

Figure 3.3: The dependence of the mean amplitude $(|v_1 + nv_2|)/(n + 1)$ on the number ratio n of the actuator cells to the sensor cells. The n-dependence of the mean amplitude depends on the frequency f. The top trace is for 10 kHz and the bottom trace is for 70 kHz, with frequency incremented in 20 kHz steps.

basal to the characteristic location.

Because we are interested in finding the frequency limit of the ear, we consider energy balance at the most basal part of the cochlea. We examine an upper bound of the efficiency with which actuator cells use the pRP by considering energy balance alone. Specifically, the CM generated by OHCs in the location of peak amplitude is used exclusively by those cells in a slightly more basal location to convert electrical energy into mechanical energy to be sent back to those cells that generate the CM.

Where is the location of the actuator cells in this hypothesis? The conditions for optimal location for the actuator cells would be:

1. The mechanical energy output of the actuator cells depends on cell displacement, which is associated with basilar membrane movement. For this reason, a

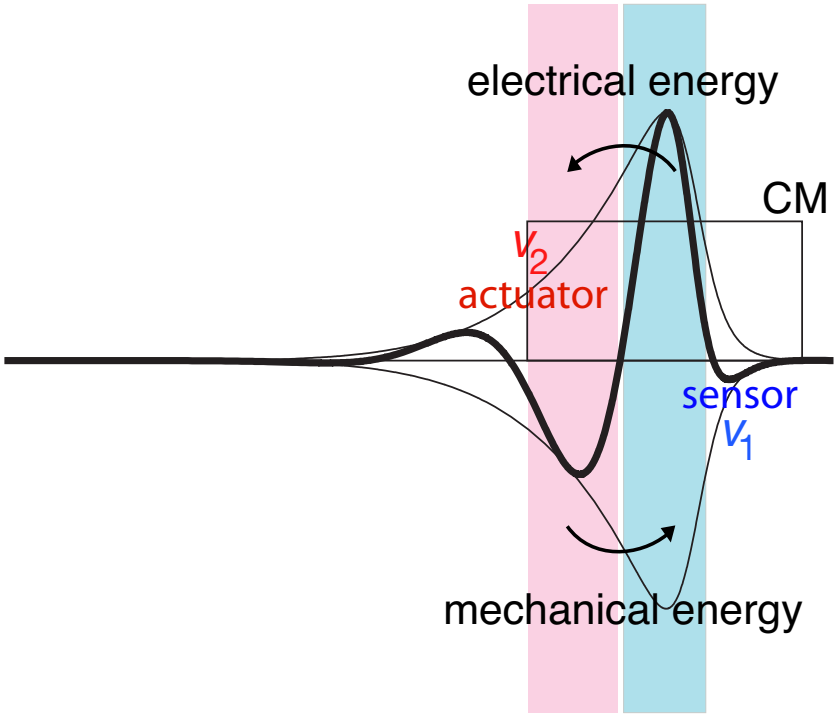

Figure 3.4: A simplified model showing lateral energy transfer. The bold line represents a traveling wave that propagate from the basal end (left). The sensor cells have the receptor potential (RP) V_1 and are in the zone of 1/2 wavelength (the shaded band on the right-hand side) centered at the characteristic location of the frequency, where the envelope (the thin line) peaks. The actuator cells have the pseudo-receptor potential (pRP) V_2 and are at a more basal zone of 1/2 wavelength (the shaded band on the left-hand side) centered at the point where traveling wave's phase is advanced by π. The spread of the CM is represented by the box centered at the sensor cells and extends 3/4 ($=\frac{1}{2} \cdot \frac{1}{2} + \frac{1}{2}$) wavelength in both directions.

higher efficiency of actuators in producing mechanical energy requires a larger amplitude of basilar membrane motion at the site of these cells.

2. Displacements of the basilar membrane generate receptor currents that contribute to the CM. For this reason, the amplitude of basilar membrane motion at the location of the actuator cells must be small enough not to diminish the CM by destructive interference.

3. The RP of actuator cells must interfere constructively with the CM. The zone of constructive interference is where phase advance is between $\pi/2$ and $3\pi/2$, optimally π. Without constructive interference, all electrical energy of a cell would be spent in counteracting the viscous drag at the location of the cell.

4. The efficiency of energy transmission decreases with the distance between sensors and actuators. Transmission of electrical energy depends on a space constant, which is $\sim$40 μm [52] or $<$300 μm [55], perhaps somewhat shorter than the wavelength of about 200 μm [124].

The condition 3 on the phase requires the actuator cells must be located between 1/4 and 3/4 wavelength basal to the characteristic location of the frequency. The most effective location is between 1/4 and 1/2 wavelength basal, where the amplitude is larger (the condition 1) and closer to the sensors (the condition 4).

To evaluate an upper bound of the efficiency with which actuator cells convert electrical energy associated with the CM, we make the following simplifications (Fig. 3.2). First, the sensor cells are OHCs in the 1/2 wavelength zone centered at the

location of the characteristic frequency. Second, the actuator cells are OHCs in the 1/2 wavelength zone centered at the location 1/2 wavelength more basal to the characteristic location. Third, the CM spreads 3/4 ($= \frac{1}{2} \cdot \frac{1}{2} + \frac{1}{2}$) wavelength in the basal direction from the characteristic location to cover the actuator cells and abruptly diminishes in a step. Because a space constant does not have directionality, the CM should spread in the apical direction symmetrically as it does in the basal direction. These assumptions lead to a value of 2 for the ratio n, which determines the attenuation of the CM. The exact value for n is not critical for our analysis as will be shown later. Fourth, the displacement amplitude of the actuator is equal to that of sensors. This condition maximizes the actuator output (condition 1) would reduce the CM (condition 2). However, we assume that the CM is not affected. These assumptions, each of which is too optimal, are again intended to give an upper bound of efficiency.

With these assumptions, an upper bound of the energy, $\overline{E}_{\mathrm{OHC}}$, generated by an OHC per cycle to counteract viscous drag is represented by

$$\overline{E}_{\mathrm{OHC}} = \int_0^{2\pi/\omega} dt\phi \cos^2(\omega t)(|v_1| + |v_2|)x, \tag{3.20}$$

where ϕ is the force generation per unit voltage change and x is the displacement of the basilar membrane at the characteristic location.

Since the CM is the product of the transducer current of OHCs through the extracellular space, its effect on enhancing electromotility requires introduction of an extracellular resistance R_e. However, the RP increases as $R_e \to 0$. As illustrated in Fig. 3.5, the reduction of the RP from v_0 to v_1 due to the external resistance is

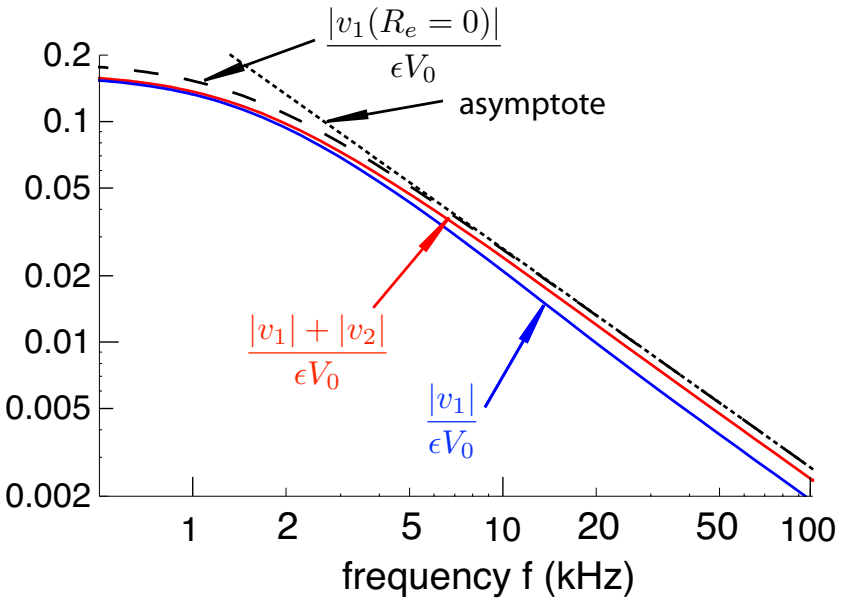

Figure 3.5: Relative magnitude of electromotility output, which is proportional to the electric potential plotted against the frequency. The combined magnitude $(|v_1| + |v_2|)/(\epsilon V_{10})$ is compared with $|v_1|/(\epsilon V_{10})$ and $|v_0|/(\epsilon V_{10})$ (dashed line), the magnitude of the sensor cell's receptor potential with and without (dashed line) the external resistance R_e, respectively. The asymptotic form of $|v_0|/(\epsilon V_{10})$ for high frequencies is $1/[\omega R_b(C_a + C_b)]$ (dotted line), was used in the previous treatment [118].

somewhat compensated by the effect of utilizing the CM under the most favorable condition. However, the combined amplitude $|v_1| + |v_2|$ still remains less than $|v_0|$, i.e. the RP without external resistance, throughout the frequency range (Fig. 3.5).

With Eq. (3.5), (3.17), and (3.18), the asymptotic form for high frequencies is

$$\overline{E}_{\mathrm{OHC}} \approx \pi\phi \frac{gR_0V_{10}}{R_K\omega(C_a + C_b)}x^2. \tag{3.21}$$

3.6 Limiting frequency revisited

Viscous drag in the gap between the tectorial membrane and the reticular lamina has been described in a previous analysis [118]. It showed that the drag is proportional to the velocity of shear motion and that the friction coefficient γ is expressed by $\gamma = \eta S/d$, where η is the viscosity of the fluid, S the area of the gap per OHC, and d the gap. The viscous loss per cycle per OHC at the characteristic location is then

$$E_{\mathrm{drag}} = \pi\gamma\omega x^2. \tag{3.22}$$

The condition for OHC electromotility to counteract viscous drag is $\overline{E}_{\mathrm{OHC}} \geq E_{\mathrm{drag}}$. This leads to a condition for the frequency ω,

$$\omega^2 \leq \alpha(n) \cdot \frac{\phi g V_0}{\gamma(C_a + C_b)} \tag{3.23}$$

with a factor

$$\alpha(n) \equiv \frac{V_{10}R_0}{V_0R_K} = \frac{R_0}{R_0 + R_K + (1+n)R_e}, \tag{3.24}$$

which is smaller than unity.

In the absence of extracellular resistance, the limiting frequency is somewhat higher because $\alpha(0) > \alpha(n)$ for $n > 0$.

Because $\alpha(n) < 1$, the inequality (3.23) gives a frequency limit lower than that given by

$$\omega^2 \leq \frac{\phi g V_0}{\gamma(C_a + C_b)}, \tag{3.25}$$

which was obtained assuming $R_0 \gg R_K$ and $R_e = 0$ [118]. With $\phi = 0.1$ nN/mV [76] and $\gamma = 1.4 \times 10^{-7}$ Ns/m [118], the condition (3.25) leads to the frequency limit of about 10 kHz for guinea pigs and chinchilla [118]. It should be noted that no single factor has a decisive effect on the frequency limit because the limit depends on the square root of each factor. Although the value for the friction coefficient γ of the subtectorial space, for example, is determined based on electron microscopy (EM) data that may need correction for shrinkage, such a correction has a relatively modest effect on the frequency limit because of the square root dependence.

3.7 Discussion

Our model is intended to estimate an upper bound of the CM's effect on enhancing electromotility and it is much simpler than the configuration for which most experimental data are obtained. Specifically, we evaluated the CM generated by the transducer current of OHCs in the location of the cochlea associated with basilar membrane motion with small amplitudes. However, in most experimental conditions, the transducer current contributing to the CM passes through OHCs over a much wider area with the contributions of these OHCs determined by a space constant. This explains why the calculated frequency dependence of the potential (Fig. 3.3) differs from that of experimentally observed one [52].

For an experimental condition where the cochlea is stimulated via stapes and a recording electrode for the CM is placed at a location in the organ of Corti, an increase in the frequency ω with constant stimulation intensity at the stapes shifts the location of maximum amplitude basally and changes the amplitude x of the basilar membrane motion at a given location, where the recording electrode is located.

If the stimulation frequency is increased from below the best frequency at the locus of recording, the peak of the traveling wave moves closer to the recording location from a more apical location. This basal shift of the current source advances the phase of the CM closer to π, from 130°to 164°in the reference [52], as the frequency approaches the optimal frequency. The phase of CM further advances when the frequency further increases beyond the best frequency, for stimulation intensity below 40 dB SPL [52]. This explanation is consistent with the interpretation given by the reference [52].

Our sensor cells are at the location of the highest characteristic frequency and we are only interested in high frequency response. We do not have to consider basal shifts of the current source as frequency increases. In addition, the phase of the CM experimentally observed near the best frequency is close to π [52], consistent with our model. For these reasons, our model is consistent with experimental data. The phase of CM only decreases with increasing frequency reflecting the RC filter of the circuit.

Finally, our result that the extracellular potential can improve the effectiveness of electromotility is consistent with a recent model evaluation [123] and an

experimental study [52]. Our result is further consistent with a conclusion of the latter [52] in that this factor alone is insufficient to make electromotility as the basis of cochlear amplifier.

3.8 Conclusions

We confirmed that the oscillatory potential in unstimulated OHCs induced by the extracellular potential can be greater the receptor potential and that this effect can increase the efficiency of electromotility as proposed by Dallos and Evans [30]. However, we do not find that this effect can extend the frequency limit of about 10 kHz, which was previously estimated [118]. The introduction of an extracellular resistance, which is needed to produce the CM, reduces the RP. Since the significance of prestin and electromotility has been established [33], our result indicates that there must be another factor, such as fast voltage-gated K-currents, in the basal turn where the characteristic frequencies exceed 10 kHz.

Acknowledgement

This work was directed by Dr. Kuni H. Iwasa and supported by NIDCD.

Chapter 4

Amplifying effect of a release mechanism for fast adaptation in the hair bundle

4.1 Introduction

Fast adaptation of the mechonoelectric transducer (MET) channel in hair bundles has been a focus of recent hair cell physiology because it is considered to be a reverse transduction mechanism with an amplifying effect [46, 72, 97, 165]. However, experimental examinations tend to show that the partial closure of the MET channel is accompanied by reduction of tension at the tip-link [97, 154], which is attributed to elongation of the link between the MET and an unconventional myosin that is responsible for adaptation[10, 59, 68, 112]. These observations are puzzling in view of presumed biological role of fast adaptation because such a delayed tension reduction is the property of an attenuator and not of an amplifier.

In this chapter, we show that this mechanism can have indeed an amplifying effect if it is associated with negative stiffness of the MET. In the following, we examine a specific example which is called a "release model" [97, 154] for fast adaptation. The conclusion drawn here is not limited to this particular model as it will become clear by the end of the chapter.

4.2 release mechanism

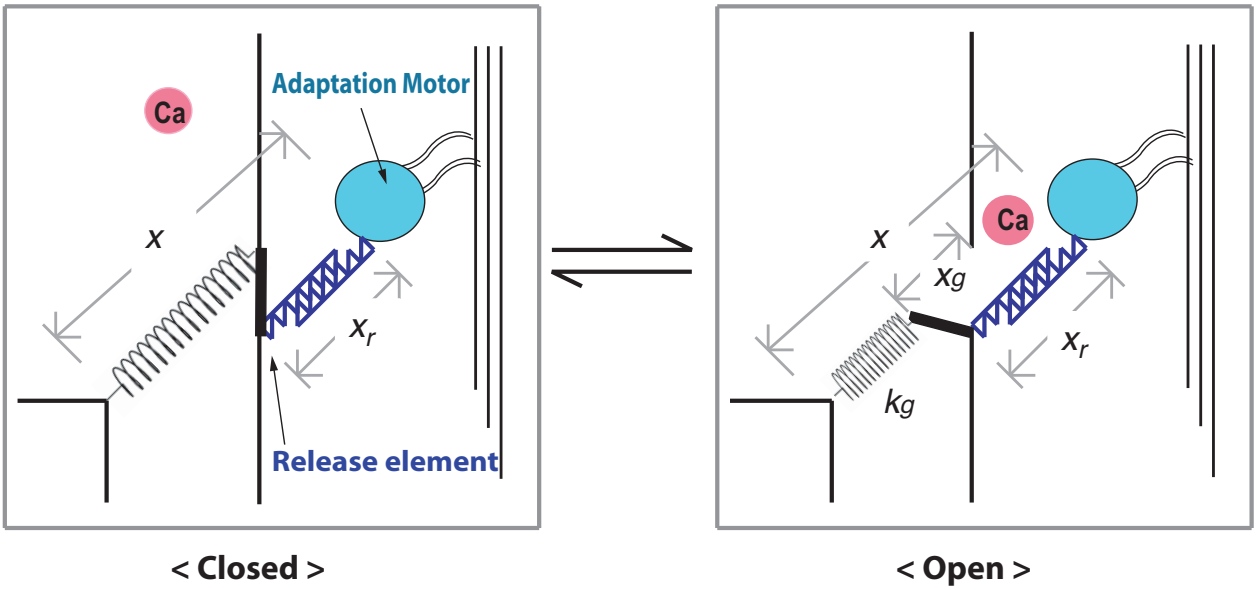

Figure 4.1: Schematic representation of two-state model for release mechanism. The mechano-electrical transducer MET channel is represented by the gating spring with stiffness k_g and gate size x_g. The release element connects the MET channel to the adaptation motor. The MET channel is either open or closed when displacement of hair bundle at the tip link and release element length are given by x and x_r, respectively. The model assumes that elongation of the release element takes place relatively slower than gating of the MET channels.

Here we give a brief description of the release mechanism. Let x_r be the length of the link, which serves as a release element that connects the MET and the slow adaptation motor (Fig. 4.1). In response to displacement x at tip link, the MET responds with force F, given by

$$F = -k_g(x - x_g P_o - x_r), \tag{4.1}$$

where k_g is the stiffness of the gating spring and x_g is the gating distance, which is the effective size of the gate of the channel. If the gating is much faster than relaxation, the open probability P_o of the channel is

$$P_o = \frac{1}{1 + \exp[-\beta k_g x_g (x - x_g - x_r)]} \tag{4.2}$$

where $\beta = 1/k_B T$ with Boltzmann's constant k_B and the temperature T. We assume the distance x_r obeys a relaxation equation with time constant τ,

$$\frac{d}{dt} x_r = (x_{max} P_r - x_r)/\tau. \tag{4.3}$$

Here $x_{max} P_r$ is the equilibrium distance for the intracellular Ca^{2+} concentration that corresponds to open probability P_o. If this release element has one Ca^{2+}-binding site, P_r may be expressed as,

$$P_r = \frac{P_o}{\nu + P_o}, \tag{4.4}$$

where ν is a constant.

4.3 Response to small displacements

Let us assume that displacement x has a time-dependent component Δx,

$$x = \bar{x} + \Delta x.$$

If this displacement Δx is small, it elicits small responses ΔP_o, ΔP_r, and Δx_r in the open probability, Ca^{2+}-binding, and the release distance, respectively. Eqs. 4.2 and 4.4 respectively lead to

$$\Delta P_o = \beta k_g x_g \bar{P}_o (1 - \bar{P}_o)(\Delta x - \Delta x_r), \tag{4.5}$$

$$\Delta P_r = \frac{\nu}{(\nu + \bar{P}_o)^2} \Delta P_o, \tag{4.6}$$

where $\bar{P}_o$ is the steady state open probability. Eq. 4.3 turns into

$$\begin{aligned} \frac{d}{dt}\Delta x_r &= (x_{max}\Delta P_r - \Delta x_r)/\tau \\ &= (C\Delta x - (1+C)\Delta x_r)/\tau \end{aligned} \tag{4.7}$$

with $C = \beta\nu x_{max} k_g x_g \bar{P}_o(1-\bar{P}_o)/(\nu+\bar{P}_o)^2$.

If Δx is sinusoidal, we can put $\Delta x = \delta x \cos\omega t = Re[\delta x e^{(i\omega t)}]$ and $\Delta x_r = \delta x_r \cos(\omega t + \phi_r) = Re[\delta x_r e^{i(\omega t+\phi_r)}]$. Then Eq. 4.7 can be expressed,

$$i\omega\tau\ \delta x_r e^{i(\omega t+\phi_r)} = C\ \delta X e^{i\omega t} - (1+C)\ \delta x_r e^{i(\omega t+\phi_r)},$$

which leads to

$$\delta x_r e^{i\phi_r} = \frac{C}{(1+C)+i\omega\tau}\ \delta x.$$

Thus, the imaginary part of this equation is

$$\delta x_r \sin\phi_r = -\frac{\omega\tau C\ \delta x}{(1+C)^2+(\omega\tau)^2}. \tag{4.8}$$

4.4 Work done during one cycle

For a given hair bundle displacement $x = \bar{x} + \delta x \cos\omega t$, the work W done by force F (Eq. 4.1) at the tip-link during one cycle is,

$$W = -k_g \int (x - x_g P_o - x_r) \cdot d\Delta x.$$

By using Eqs. 4.5 and 4.6, the integrand can be expressed by a sum of terms proportional to either Δx or Δx_r. Of these terms, only the ones proportional to Δx_r contribute, leading to,

$$W = k_g(1 - \beta k_g x_g^2 \bar{P}_o(1-\bar{P}_o)) \int \Delta x_r \cdot d\Delta x.$$

Here $k_g(1 - \beta k_g x_g^2 \bar{P}_o(1 - \bar{P}_o))$ is known as *gating stiffness* [71, 111] and will be denoted by $\tilde{k}_g$. This stiffness is reduced by the gating of the MET channel and can take negative values. Because the phase difference between Δx_r and Δx is ϕ_r, the integration over a cycle results in $\pi \sin \phi_r$. With the aid of Eq. 4.8, we then obtain

$$W = -\pi \tilde{k_g} \frac{\omega\tau C}{(1+C)^2 + (\omega\tau)^2} \delta x^2.$$

This result shows that the work done by the MET is negative as long as gating stiffness $\tilde{k}_g$ remains positive, implying that the MET functions as a damper for periodic stimuli. However, it should be also noted that the work done is positive, if gating stiffness is negative. Under this condition, the MET functions as an amplifier.

How can this be explained? Negative stiffness gives a 180° delay. An additional phase delay introduced by the release mechanism, in effect, gives a phase advance between 0 and 180°, providing amplification. A 90° phase delay due to the relaxation process, the condition for maximal damping, is also optimal for amplification if it is combined with negative stiffness. This observation is applicable to any relaxation process and is not specific to our model.

To take advantage of negative stiffness to do mechanical work, the system must expend energy to maintain itself in a state with negative stiffness. One such energy source is the Ca^{2+} concentration gradient across the plasma membrane and another is ATP for the myosin motor.

4.5 Discussion

We showed that the release model provides amplification when associated with negative stiffness. This property is not specific to this particular model but is applicable to any relaxation mechanism. An example is the model proposed by Tinevez et al. [162], which posits that fast adaptation is an epiphenomenon that arises from an interplay between the gating of the MET channel and the myosin motor that is responsible for slow adaptation. It includes viscoelastic relaxation and relaxation involving the movement of the myosin motor.

Here we have linearized the response for small stimuli and have not analyzed the stability of the system, specifically how the operating point of the MET channel, which makes gating stiffness negative can be maintained. It appears to us that the previously reported analysis [12] of the stability of the operating point of the MET would be applicable to our model.

Acknowledgement

This work was directed by Dr. Kuni H. Iwasa and supported by NIDCD.

Chapter 5

Effectiveness of Hair Bundle Motility as a Cochlear Amplifier

5.1 Introduction

With the mechanoelectric transducer (MET) channel in their hair bundles, hair cells effectively convert mechanical signal into electrical signal. This transduction is supported by reverse transduction in the hair cells that generates force in response to mechanical stimuli. Such a reciprocal process has been predicted by Gold [62] in 1948 as the requirement for counteracting damping of the mechanical stimuli in viscous fluid of the organ. In recent studies, this reciprocal process is recognized as the basis of the cochlear amplifier [35, 179], which is critical for the sensitivity and frequency selectivity of the ear in mammals [90, 98, 117, 177] and in other vertebrates [107, 110]. Those motile responses of hair cells include electromotility in the cell body of outer hair cells [2, 11, 142], which is specific to the mammalian ear, and the motility called fast adaptation in hair bundles themselves [6, 17, 27, 88, 126], which is not specific to any animal species.

For the mammalian ear where outer hair cells with two motile mechanisms could be involved in reverse transduction, the relative significance of the two mechanisms is an important issue [14, 99]. The importance of electromotility is supported

by experiments with mice that have mutant prestin, the protein essential for electromotility [176]. Mice with prestin mutated do not have electromotility in the physiological range of the membrane potential and their hearing threshold is significantly elevated [33]. The significance of fast adaptation is supported by an *in vitro* experiment that showed the importance of Ca^{2+} entry through the transducer channels into hair cells upon vibration of the basilar membrane [14]. Because the ear of non-mammalian vertebrates lacks electromotility, it has been assumed that hair bundle motility is an essential element for the cochlear amplifier in those animals [107, 110].

Here we examine the effectiveness of two models for hair bundle motility, which can function as the cochlear amplifier in the mammalian ear and the avian ear. One of the motile mechanisms, which is usually referred to as the "channel re-closure" model, assumes that Ca^{2+} binding to the cytosolic side of the MET channel on channel opening leads to closing of the channel [19]. It has been shown that this model can describe spontaneous oscillation and signal amplification by an individual hair bundle [19]. This motile mechanism uses chemical energy in the form of a Ca^{2+} gradient across the plasma membrane. This fast mechanism, which is called fast adaptation, is separate from myosin-based slow motility or slow adaptation [59, 64, 70], which controls the operating point of the MET channel.

Another model proposed by Tinevez *et al.* [162] assumes that fast adaptation is not an independent phenomenon but it is the result of interplay between gating of the MET channel and ATP-dependent myosin motor, which is responsible for slow adaptation [59, 64, 70]. This model [162] specifically assumes that myosin is a force

generator with a built-in viscoelastic property. Let us tentatively refer to this model as the "interplay" model.

To study the effectiveness with which hair bundles function as an amplifier, methods that solve the equations of motion for the hair bundle to obtain the amplitude of the hair bundle [19, 162] have been used previously. In those treatments, the amplitude of motion is determined by a nonlinear term that appears in the local resonance. Instead of solving equations of motion, we impose a small sinusoidal displacement of a fixed frequency on a hair bundle and evaluate the work done by the motor in the hair bundle. If the work done by hair bundles exceeds the energy loss by viscous damping, energy output is greater than energy input and the hair bundle can function as an amplifier. The validity of this condition is not limited to local resonance [148]. The method of this comparison is similar to a previous attempt to examine the efficiency of electromotility [118].

This approach has several advantages. First, it is much simpler than solving the equations of motion because we need to consider only linear terms in the perturbation method. Second, the effect of the cochlear amplifier is significant only for small amplitude displacements. Third, with small amplitude stimulation the operating point, from which the hair bundle is stimulated, will not be subjected to the effect of slow adaptation. This justifies omitting slow adaptation in the model. One limitation of our approach is that we only consider a necessary condition for amplification and not the sufficient condition and thus the actual frequency limit may be lower than our estimation. In addition, we cannot obtain the amplifier gain, which depends on the nonlinearity of the system. When energy output exceeds en-

ergy input at a small amplitude, the oscillation grows out of linear range until the growth is stopped by the nonlinearity of the system.

Initially we describe the basic assumptions and an outline of the method. Next, we examine the effectiveness of a simplified "channel re-closure" model and "interplay model" as the cochlear amplifier. After examining these two mechanisms, we discuss their implications.

5.2 Assumptions

In this section, we list and briefly describe our main assumptions. The assumptions specific to each model for hair bundle motility are described subsequently.

For the geometry of the hair bundle and the mechano-electric transducer (MET) channel, we make the following assumptions:

[1] The structure of the hair bundle imposes the same displacement for each tip-link in the bundle. This assumption allows the displacement of the hair bundle to be described as though it has one tip-link [71]. This condition can lead to negative stiffness of the hair bundles [77]. To be precise, this "tip-link displacement" is displacement of the tip-link assembly, which includes elements associated with the tip link such as the MET and elastic elements other than tip-link itself. We do not discuss how the complex structure of a hair bundle gives rise to such a property [42, 43, 93].

[2] One MET channel with two states, open and closed, is associated with each tip link. This assumption is required to explain gating compliance and is in line with

most theoretical treatments [71, 89, 96, 162]. Some experimental data are analyzed with one MET channel with three states, two closed and one open [25, 163], which can be re-interpreted as two interacting two state channels [164]. We do not consider such complex models here.

[3] One MET channel is connected in series with a myosin motor that interacts with actin filaments in the hair bundle and maintains the operating point of the MET channel.

In addition, we make the following assumptions to simplify our analysis regarding the effectiveness of hair bundle motility:

[4] The amplitude of tip-link displacement is periodic and small. We impose a tip-link displacement of angular frequency ω and amplitude δX,

$$X(t) = \bar{X} + \delta X \sin(\omega t), \tag{5.1}$$

where $\bar{X}$ is the steady state value before stimulation and $\delta X \ll \bar{X}$. The force F_{hb} elicited in the hair bundle depends on the model as will be described later. The leading term is linear in each model for the small amplitude stimulation. The mechanical energy generated by the hair bundle per cycle is then,

$$E_{hb} = \int F_{hb} \cdot dX, \tag{5.2}$$

which is proportional to δX^2.

[5] The dominant viscous drag is due to shear in the gap between the tectorial membrane and the reticular lamina (subtectorial gap). This has been suggested for the mammalian cochlea [1], where the surface of the tectorial membrane that faces the reticular lamina is smooth and planar. The morphology of the avian tectorical

membrane is not as certain. Electron micrographs (EM) show cavities (domes) in the avian tectorial membrane near its contact points with hair bundles and a thin structure of the tectorial membrane that descends to the microvilli surrounding each hair cell [63]. However, the avian tectorial membrane samples prepared for EM studies may have artifacts caused in the process of sample fixation [26, 135]. Here we evaluate the viscous loss in the avian ear in the manner similar to the mammalian ear. The assumptions involved are that the thin structure of the tectorial membrane surrounding each hair cell is thin enough to have negligible internal shear and the dome above each hair bundle has no significant effect on viscous drag. The former assumption would lead to underestimation and the latter to overestimation of the drag.

The tallest row stereocilia in the hair bundles of mammalian outer hair cells and the tallest row stereocilia of all avian hair cells are firmly attached to the tectorial membrane, capable of exerting force generated by those hair bundles. In those systems, the shear of the subtectorial gap is the same as the displacement X_s at the tip of the hair bundle, which is related to the displacement X at the tip-link by a geometrical factor g, i.e. $X_s = X/g$. For small displacements, we may use $g \approx s/h$ where s is rootlet separation, h the height of the tallest stereocilia (Fig. 5.1) [79].

The gap, which can be approximated with the height h of the tallest stereocilia, is less than the thickness of a boundary layer [118]. Thus viscous drag F_d of the

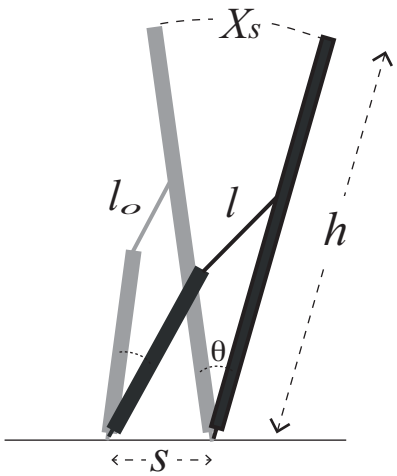

Figure 5.1: A schematic representation of hair bundle and geometrical factor g. Displacement of the tallest stereocilia at their tip is X_s and at the tip link where the MET channels are located is X. X is equivalent to $l - l_o$ where l and l_o are length of the tip link after and before displacement is given, respectively. For small angular displacement θ, X is proportional to X_s with a proportionality factor, geometrical factor g (i.e. $X = gX_s$). When h is length of the tallest stereocilia and s the distance between the rootlets of neighboring stereocilia, $g \simeq s/h$ [79].

subtectorial gap per hair cell is proportional to the shear velocity,

$$F_d = \eta \frac{A}{h} \frac{dX_s}{dt}. \tag{5.3}$$

Here η is the viscosity of an external medium, A the area of the subtectorial gap per hair cell. For sinusoidal hair bundle displacement X in Eq. 5.1, the viscous loss E_d, energy loss by viscous damping during one cycle of the displacement is

$$\begin{aligned} E_d &= \int F_d \cdot dX_s \\ &= \pi \eta A h \omega \, \delta X^2 / s^2. \end{aligned} \tag{5.4}$$

[6] Hair bundle energy must be greater than viscous loss. This condition,

$$E_{hb} \geq E_d, \tag{5.5}$$

leads to a frequency limit f_{lim} for the hair bundle motility to be able to counteract viscous drag. Note that it does not depend on the amplitude because both E_{hb} and E_d are proportional to δX^2. If this frequency limit does not exceed the auditory frequency, the motile mechanism described by the model does not satisfy a necessary condition for the cochlear amplifier.

5.3 Channel Re-closure Model

Now we examine the "channel re-closure" model [19]. This model assumes that an increase of cytosolic Ca^{2+} concentration due to opening of the MET channel, which does not have cation selectivity, leads to binding of Ca^{2+} to the cytosolic side of the channel, which in turn leads to channel re-closure [6, 17, 70, 71, 126],

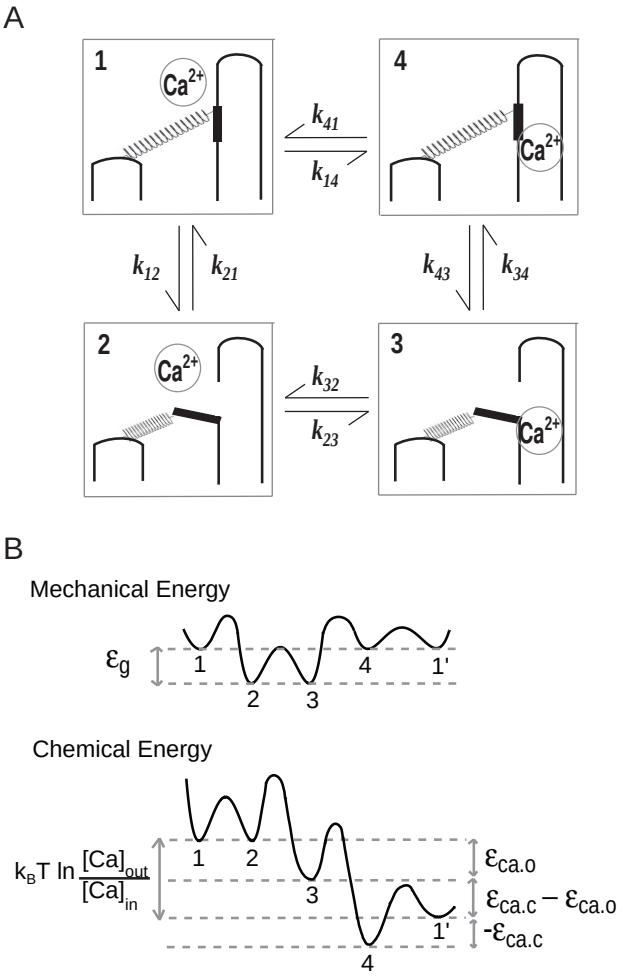

Figure 5.2: (A) Schematic representation of transitions, which the mechanoelectric transducer channel undergoes. An opening of the channel (2) elevates Ca^{2+} concentration on the cytosolic side of the channel. The resulting binding of Ca^{2+} to a binding site leads to closure of the channel (3). Closure of the channel (4) reduces the cytosolic Ca^{2+} concentration, leading to dissociation (1). (B) Schematic representation of energy levels of these states. The mechanical energy level of open states 2 and 3 are the same and differs from the closed states 1 and 4 by gating energy ϵ_g. States 3 and 4 differs in the binding energy. These levels differ from unbound states 1 and 4. Directed transitions of the channels are supported by the expenditure of the chemical energy $k_B T \ln([Ca]_{\rm out}/[Ca]_{\rm in})$ of Ca^{2+} after one cycle.

thereby increasing the tension on the tip-link. This delayed tension increase can have amplifying effect on an oscillator with which the tip-link is in contact. Indeed, this mechanism can lead to spontaneous oscillation of hair bundles [19]. The operating point of the MET channel is determined by a myosin motor, which is also triggered by an elevation of cytosolic Ca^{2+} concentration caused by channel opening.

Here we assume for simplicity that the MET channel has one Ca^{2+} binding site instead of two [19]. We assign a number to each channel state (Fig.5.2). The channel in the open state may be either Ca-unbound (state 2) or Ca-bound (state 3). Closed state is either Ca-unbound (state 1) or Ca-bound (state 4).

The probability P_i of the MET channel being in the ith state follows a set of differential equations,

$$\frac{d}{dt}P_i = -(k_{i\,i-1} + k_{i\,i+1})P_i + k_{i-1\,i}\,P_{i-1} + k_{i+1\,i}\,P_{i+1}, \tag{5.6}$$

where the index i runs from 1 to 4. Here the index value 0 and 5 are, respectively, identical to 4 and 1. The quantity k_{ij} represents the transition rate from ith state to jth state. Open probability P_o is given by $P_2 + P_3$. Here the transition rates are to be determined by the energy barriers (Fig.5.2B) in the manner consistent with Arrhenius-Eyring equation [5, 146], which is used for nonequilibrium systems [101, 146].

The transitions between states 1 and 2 involve gating of the MET channel. The ratio of the transition rates is given by the difference of the free energy in the two states,

$$\frac{k_{12}}{k_{21}} = \exp[\beta\epsilon_g], \tag{5.7}$$

where $\beta = 1/(k_B T)$ with Boltzmann's constant k_B and the temperature T. Gating energy ϵ_g can be expressed,

$$\epsilon_g = K_g X_g (X - \frac{1}{2} X_g). \tag{5.8}$$

Here X is the displacement at the tip-link, K_g stiffness of gating spring, and X_g gating distance.

States 2 and 3 are open states. The transitions between them involve Ca^{2+} binding and unbinding. We have

$$\frac{k_{23}}{k_{32}} = [Ca]_{out} \exp[\beta \epsilon_{ca,o}], \tag{5.9}$$

assuming that the cytosolic Ca^{2+} concentration near the channel can be approximated by that of the external medium, $[Ca]_{out}$. Ca^{2+} binding energy of the open configuration is represented by $-\epsilon_{ca,o}$ (< 0).

The transitions between state 3 and 4, both of which are Ca^{2+} bound, involve gating of the MET channel. However, the free energy of Ca^{2+} binding may depend on the conformation and may differ in these two states. On closing of the channel, Ca^{2+} level inside the cell ($[Ca]_{in}$) should immediately drop due to diffusion and Ca^{2+} buffers, aided by Ca^{2+} pumps in the hair bundle [103, 174], which maintain the low cytosolic Ca^{2+} concentration. Thus we obtain

$$\frac{k_{34}}{k_{43}} = \exp[\beta(\epsilon_{ca,c} - \epsilon_{ca,o})] \exp[-\beta \epsilon_g], \tag{5.10}$$

where $-\epsilon_{ca,c}$ (< 0) is Ca^{2+} binding energy of the channel when it is in closed configuration.

Transitions between states 4 and 1, which have closed, involve only Ca^{2+} binding and unbinding. They are similar to transitions between states 2 and 3 except that the Ca^{2+} concentration is lower because the channel is closed. The ratio of the transition rates is given by,

$$\frac{k_{41}}{k_{14}} = \frac{1}{[Ca]_{in}} \exp[-\beta\epsilon_{ca,c}]. \tag{5.11}$$

The free energy change ϵ_{cycle} after one cycle is then

$$\epsilon_{cycle} = k_B T \ln \frac{k_{12}k_{23}k_{34}k_{41}}{k_{21}k_{32}k_{43}k_{14}}. \tag{5.12}$$

Substitution of the transition rates using Eqs. 5.7, 5.9, 5.10, and 5.11 leads to

$$\epsilon_{cycle} = k_B T \ln \frac{[\mathrm{Ca}]_{out}}{[\mathrm{Ca}]_{in}}, \tag{5.13}$$

which is the difference of Ca^{2+} chemical potential inside and the outside of the cell. This result is consistent with nonequilibrium condition of this system, which uses chemical energy of a single Ca^{2+} per cycle.

These relationships between the transition rates allow us to replace eight transition rates by six new parameters.

$$\begin{aligned}
k_{12} &= k_1, \quad k_{21} = k_1 e^{-\beta\epsilon_g}, \\
k_{23} &= k_2, \quad k_{32} = r_2 k_2 \\
k_{34} &= k_3 e^{-\beta\epsilon_g}, \quad k_{43} = r_3 k_3, \\
k_{41} &= k_4, \quad k_{14} = r_4 k_4, \\
r_2 &= \frac{1}{r_3 r_4} \frac{[\mathrm{Ca}]_{in}}{[\mathrm{Ca}]_{out}}
\end{aligned}$$

5.3.1 Response of the MET channel

A small sinusoidal displacement X (See Eq. 5.1) of the hair bundle elicits a small periodic response in the channel. The probability P_i of the channel being in state i is, to the first-order terms,

$$P_i \simeq \bar{P}_i + \delta P_i \sin(\omega t + \phi_i), \tag{5.14}$$

where ϕ_i is the phase, $\bar{P}_i$ the probability of i state at the operating point (i.e. $\delta X = 0$), and the amplitude $\delta P_i/\bar{P}_i \ll 1$ for i = 1, 2, 3, and 4.

The applied displacement changes the transition rates k_{21} and k_{34} through its effect on the gating energy $\Delta\epsilon_g$ ($\equiv K_g X_g \delta X \sin\omega t$). The linearized forms are given by

$$k_{ij} \simeq \bar{k}_{ij} + \delta k_{ij} \ \sin\omega t \tag{5.15}$$

where $\bar{k}_{ij} = \kappa_{ij} \exp[-\beta K_g X_g (\bar{X} - \frac{1}{2} X_g)]$ and $\delta k_{ij} = -\bar{k}_{ij} \ \beta K_g X_g \delta X$ with κ_{ij} being a prefactor.

With Eq. 5.14 and 5.15, Eq.5.6 leads to

$$\delta P_i = \beta K_g X_g \delta X \theta_i, \tag{5.16}$$

where θ_i is a constant. The open probability P_o ($= P_2 + P_3$) is then expressed by

$$\begin{aligned} P_o &= \bar{P}_o + \delta P_o \sin(\omega t + \phi_o) \\ &= \bar{P}_o + \beta K_g X_g \delta X \theta_o \sin(\omega t + \phi_o). \end{aligned} \tag{5.17}$$

Constants θ_o and ϕ_o depend on the rates k_1, ..., k_4, r_3, r_4, the ratio $[Ca]_{out}/[Ca]_{in}$, and the open probability $\bar{P}_o$ at the operating point.

5.3.2 Limiting frequency

The force F_{hb} produced by a hair bundle with N tip-links in response to the displacement X at each tip-link is expressed by

$$F_{hb} = -NK_g(X - X_g P_o) - NK_s X, \tag{5.18}$$

where X_g is gating distance, K_g the stiffness of the gating spring of each MET channel, and K_s the stiffness due to rootlet and side links.

The work E_{hb} done by the hair bundle during one cycle of stimulation is

$$E_{hb} = NK_g X_g \int_0^T P_o \cdot dX, \tag{5.19}$$

because the work done by elastic elements drops off at the end of one cycle, leaving components of force with phase shifts. With Eq. 5.17, we obtain

$$\begin{aligned} E_{hb} &= NK_g X_g \delta P_o \delta X \int_0^T \sin(\omega t + \phi_o) \cos \omega t \, d(\omega t) \\ &= \beta N (K_g X_g \delta X)^2 \Phi \end{aligned} \tag{5.20}$$

where $\Phi = \pi \theta_o \sin \phi_o$, which we call the *phase factor*.

With the aid of Eq. 5.4, the assumption [6] that mechanical energy E_{hb} produced by the hair bundle must be larger than viscous loss E_d leads to a condition for the limiting frequency $f_{\lim}$,

$$f_{\lim} = \beta M (K_g X_g)^2 \Phi / (2\pi^2 \eta) \tag{5.21}$$

below which viscous drag can be overcome. This limiting frequency is obtained by dividing the corresponding angular frequency by 2π. A factor M is defined by

$$M = \frac{Ns^2}{Ah}. \tag{5.22}$$

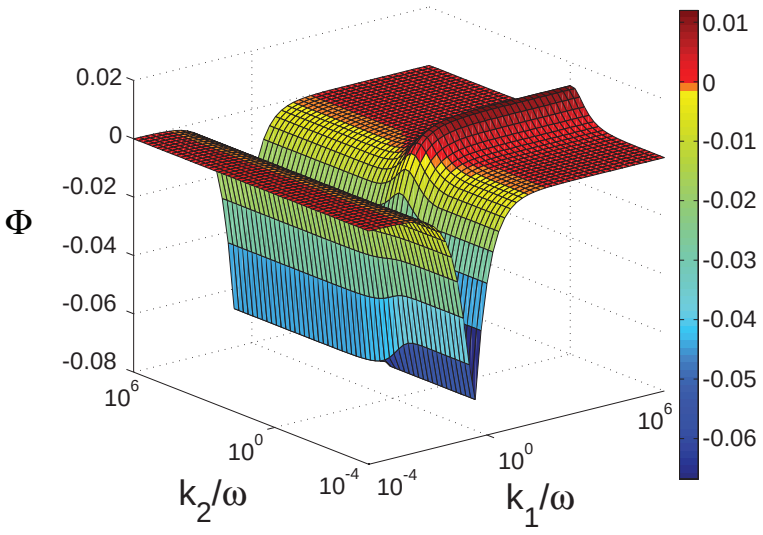

Figure 5.3: The phase factor Φ is plotted against k_1/ω and k_2/ω under the constraints $k_3 = k_1$ and $k_4 = k_2$. The range of the parameter values is in table 5.1. Each point represents the maximum value with respect to r_3 and r_4. The maximum value of Φ is 0.0086 at $k_2/\omega = 1.00$. $[\mathrm{Ca}]_{out}/[\mathrm{Ca}]_{in} = 100$ and $\bar{P}_o = 0.1$.

Notice that M can be determined by morphological data alone. For this reason we call it the *morphological factor*.

The limiting frequency f_{lim} (Eq.5.21) for the channel re-closure model is determined by gating force $K_g X_g$, the morphological factor M, and the phase factor Φ. Among these factors, the limiting frequency is particularly sensitive to gating force because of its quadratic dependence.

5.3.3 Optimal value of the phase factor

Since we are interested in the frequency limit, we seek the maximum value for the phase factor Φ. First we normalized the four parameters k_1, k_2, k_3, and k_4, with

Parameter	Range
k_1/ω	10^{-5} — 10^{11}
k_2/ω	10^{-5} — 10^{5}
k_3/ω	10^{-5} — 10^{11}
k_4/ω	10^{-5} — 10^{5}
r_3	0.0005 — 100
r_4	0.0005 — 100

Table 5.1: The range of the transition rates examined for optimizing Φ. The parameter r_2 is determined from these parameters and the ratio $[\mathrm{Ca}]_{out}/[\mathrm{Ca}]_{in}$, which is $\sim$100 for the mammalian ear and $\sim$1000 for the avian ear (see text).

respect to the operating frequency ω at which hair bundle displacement is driven. Then we performed numerical calculation, using SciLab program (http://www.scilab.org) on Biowulf at the NIH (http://biowulf.nih.gov). The range of parameter values examined is shown in the table 5.1.

Since the value for the steady state open probability $\bar{P}_o$ is fixed, the steady state bundle displacement must be determined by solving a nonlinear equation for every set of transition rate values and the steady state open probability $\bar{P}_o$. We found that inclusion of displacement dependence in k_1 and k_3 renders the solution too lengthy to be accepted by the computer program. For this reason, we assume that k_1 and k_3 are constants. That is equivalent to assuming that the energy barriers for channel opening does not change with the tip-link displacement [25]. This assumption may

not be valid where channel gating speed is important. However, it will be much less significant when the phase factor is insensitive to the details of gating.

Preliminary optimization calculations (data not shown) show that the phase factor Φ is a monotonically increasing function of k_1/ω and k_3/ω although it is virtually flat beyond 10^6. This is illustrated in figure 5.3 where Φ is plotted for the constraints of $k_1 = k_3$ (= parameters involved in gating) and $k_2 = k_4$ (= parameters involved in Ca^{2+}-binding and unbinding). The figure shows that channel gating with a rate close to the operating frequency has a damping effect. That is intuitively obvious because gating is a mechanical relaxation. On the other hand, Ca^{2+}-binding and unbinding at a rate near the operating frequency is effective in causing a phase delay that has an amplifying effect.

We can maximize Φ with respect to only four parameters, while giving large fixed values for k_1/ω and k_3/ω (i.e. $k_1/\omega = 10^6$, $k_3/\omega = 10^6$). The grid is iteratively recast in the optimal zone until the relative increment of the maximum value for Φ between the iteration falls below 1%.

If we assume that open probability at the operating point is $\bar{P}_o$ of 0.1, the optimal value of Φ is 0.05 for the mammalian ear, which has the Ca2+ concentration ratio of 10^2 (Table.5.2). The corresponding optimal parameter values are $k_2 = 2.1$, $k_4 = 0.3$, $r_3 = 5 \times 10^{-4}$, $r_4 = 0.26$. For the avian ear, which has about 10 times higher endolymphatic Ca^{2+} concentration [145], the optimal value is 0.07. The corresponding optimal parameter values are $k_2 = 2.5$, $k_4 = 0.4$, $r_3 = 5 \times 10^{-4}$, $r_4 = 0.08$. The phase factor Φ also depends on the open probability of hair bundle at rest, $\bar{P}_o$. It has a maximum at $\bar{P}_o = 0.5$, and the optimal Φ values are higher for

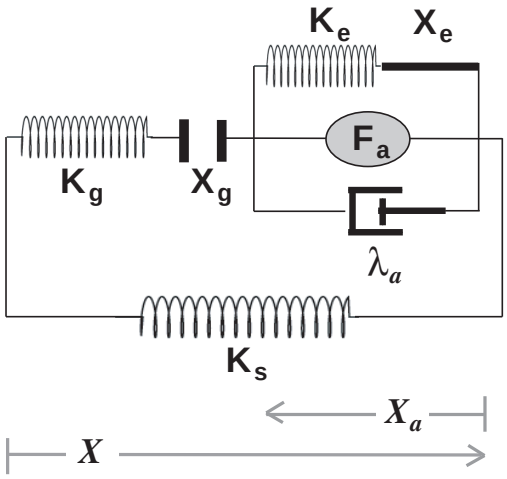

Figure 5.4: Gating of the MET channel is characterized by the stiffness K_g and distance X_g of the gate. Myosin, which produces force F_a, is connected with the MET channel through an element with stiffness K_e and friction coefficient λ_a. A parallel element has stiffness K_s.

$\bar{P}_o = 0.5$ by about 25% than that for $\bar{P}_o = 0.1$.

5.4 Interplay model

In this section, we investigate another mechanism for hair bundle motility that described by "interplay model". The interplay model, proposed by Tinevez *et al.* [162], assumes that fast adaptation is not based on a special structure or a mechanism but is a result of interplay between the MET channel and the myosin motor, which is a force generator and responsible for slow adaptation (See chapter 1.

hair bundle motility.). While a "release" model [97, 154] assumes that an element, which links the myosin motor with the MET channel, undergoes Ca^{2+}-activated fast elongation, the interplay model assumes the actomyosin system that produces force has viscoelasticity. In the following we give a brief description of this model.

The distance X_a of the myosin motor from actin filaments obeys a differential equation,

$$\lambda_a \frac{dX_a}{dt} = K_g(X - X_a - X_g P_o) - K_e(X_a - X_e) - F_a \tag{5.23}$$

where the myosin motor which generates isometric force F_a has an intrinsic pre-stressed Voigt-type viscoelastic element with viscosity λ_a and stiffness K_e [162] (Fig.5.4). The degree of pre-stress is represented by X_e, which can serve as an adjustable parameter.

The force F_a generated by myosin1c, which is unconventional myosin, is a decreasing function of the cytosolic Ca^{2+} concentration, which is approximately proportional to open probability P_o of the MET channel [162]. Hence it can be expressed to the first-order term,

$$F_a = F_{max}(1 - SP_o). \tag{5.24}$$

The coefficient S can be expressed by

$$S = -\frac{[Ca^{2+}]_{max}}{F_{max}} \frac{dF_a}{d[Ca^{2+}]}|_{ref}. \tag{5.25}$$

Here F_{max} is maximum force generated by myosin motor when open probability P_o is zero. The channel's open probability P_o, that affects the cytosolic Ca^{2+} concen-

tration, is expressed by a two-state Boltzmann function [162],

$$P_o = \frac{1}{1 + B\exp[-\beta K_g X_g (X - X_a)]} \tag{5.26}$$

where B determines the open probability at rest.

5.4.1 Linearized response

A small sinusoidal displacement of the hair bundle, represented by Eq. 5.1, should give rise to a small displacement of the position X_a of the motor. This can be expressed,

$$X_a = \bar{X}_a + \delta X_a \sin(\omega t + \phi), \tag{5.27}$$

where $\bar{X}_a$ is the position at rest. For small periodical displacements, Eq. 5.26 becomes

$$P_o = \bar{P}_o + \beta K_g X_g \bar{P}_o (1 - \bar{P}_o)(\delta X \sin \omega t - \delta X_a \sin(\omega t + \phi)), \tag{5.28}$$

where the open probability $\bar{P}_o$ at the operating point is given by $\bar{P}_o = 1/(1 + B\exp[-\beta K_g X_g (\bar{X} - \bar{X}_a)])$.

Substitution of X_a and P_o into the differential equation Eq. 5.23, using Eqs. 5.27 and 5.28, leads to an expression for the amplitude δX_a of the motor displacement,

$$\delta X_a \ \sin\phi_a = -\frac{(\tilde{K_g} + K_{ca})\ \omega\lambda_a}{(\tilde{K_g} + K_{ca} + K_e)^2 + (\omega\lambda_a)^2}\delta X \tag{5.29}$$

where

$$\tilde{K_g} = K_g[1 - \beta K_g X_g^2 \bar{P}_o(1 - \bar{P}_o)], \tag{5.30}$$

which is the familiar form of gating stiffness [71] and can take negative values. The quantity K_{ca} defined by

$$K_{ca} = \beta K_g X_g^2 \bar{P}_o(1 - \bar{P}_o) SF_{max}/X_g \tag{5.31}$$

is the sensitivity of force production by the myosin motor to displacement. That is because a displacement X_g at the tip-link increases the open probability by $\beta K_g X_g^2 \bar{P}_o(1 - \bar{P}_o)$ and in turn it rises the cytosolic Ca^{2+} concentration as described by Eq. 5.24, decreasing the motor force by the efficiency factor of SF_{max}.

5.4.2 Energy balance and frequency limit

In this section, we calculate work done by hair bundle, described by the interplay model, in response to sinusoidal hair bundle displacement X. In response to a tip-link displacement X, N tip-links of a hair bundle produce total force F_{hb} ,

$$F_{hb} = -NK_g(X - X_a - X_g P_o) - NK_s X. \tag{5.32}$$

For small periodical displacement Eq. 5.1, the work done by the hair bundle per cycle depends only on terms that include X_a and P_o because elastic terms do not contribute. Only the term that is proportional to δX_a is non-elastic and remains in Eq. 5.28 after a full cycle. Thus, we have

$$\begin{aligned} E_{hb} &= N\tilde{K_g} \int X_a \cdot dX \\ &= N\tilde{K_g}\, \delta X \delta X_a \int_0^T \sin(\omega t + \phi_a) \cos \omega t \, d(\omega t) \\ &= \pi N \tilde{K_g}\, \delta X \delta X_a \sin \phi_a \end{aligned} \tag{5.33}$$

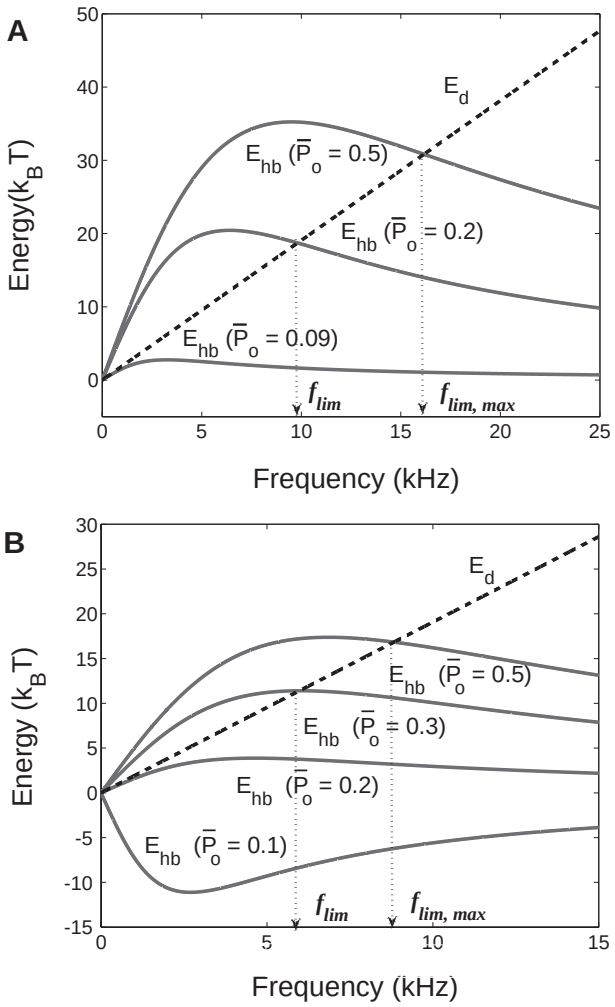

Figure 5.5: Examples of E_d (dotted) and E_{hb}. (A) $\bar{P}_o$=0.09 (or 0.91), 0.2 (or 0.8), and 0.5. $E_{hb} > 0$ requires $0.08 < \bar{P}_o < 0.92$. $E_{hb} > E_d$ requires $0.09 < \bar{P}_o < 0.91$. (B) $\bar{P}_o$=0.1 (or 0.9), 0.2 (or 0.8), 0.3 (or 0.7), and 0.5. $E_{hb} > 0$ requires $0.17 < \bar{P}_o < 0.83$. $E_{hb} > E_d$ requires $0.2 < \bar{P}_o < 0.8$. Assumed parameter values: $N = 60$, $K_g = 1.2$ mN/m, $X_g = 7$ nm for (A) , 5 nm for (B), $F_m = 3$ pN, $S = 4$, $\lambda_a = 0.1$ μN.s/m, $K_e = 0.13$ mN/m, $\eta = 1$ mPa.s, $A = 100$ μm^2, $h = 1$ μm, and $s = 0.5$ μm.

With the aid of Eq. 5.29, we obtain

$$E_{hb} = -\frac{\pi N \tilde{K_g}(\tilde{K_g} + K_{ca})\omega\lambda_a}{(\tilde{K_g} + K_{ca} + K_e)^2 + (\lambda_a\omega)^2}\,\delta X^2. \tag{5.34}$$

Notice that the work E_{hb} done by the hair bundle can be negative. Under such conditions, the hair bundle behaves as a damper. The condition $E_{hb} > 0$ requires $\tilde{K_g}(\tilde{K_g} + K_{ca}) < 0$. Since $K_{ca} > 0$ as shown in Eq. 5.31, This condition leads to,

$$-K_{ca} < \tilde{K_g} < 0. \tag{5.35}$$

This means that negative stiffness must be always the case for the hair bundle to function as an amplifier.

The condition for being an amplifier $E_{hb} > E_d$ leads to $\omega > 2\pi f_{\text{lim}}$ with a linear limiting frequency f_{lim},

$$f_{\text{lim}} = \frac{1}{2\pi\lambda_a}\sqrt{-\tilde{K_g}(\tilde{K_g} + K_{ca})\,\frac{\lambda_a}{\eta}\,M - (\tilde{K_g} + K_{ca} + K_e)^2}. \tag{5.36}$$

For a limiting frequency f_{lim} to exist, the terms inside the square root must be positive,

$$-\frac{(\tilde{K_g} + K_{ca} + K_e)^2}{\lambda_a\,\tilde{K_g}\,(\tilde{K_g} + K_{ca})}\,\frac{\eta}{M} < 1. \tag{5.37}$$

5.4.3 Factors that determine the limiting frequency

The frequency limit f_{lim} for the interplay model depends on many parameters. Its sensitivity to operating point $\bar{P}_o$ enters through $\tilde{K_g}$ and K_{ca}. An example of the dependence on the operating point is shown in Fig. 5.5. Notice that E_{hb} has a symmetry axis $\bar{P}_o = 0.5$, where it has the maximum. The hair bundle energy E_{hb} is negative if $\bar{P}_o$ is small. For a limiting frequency f_{lim} to exist, $\bar{P}_o$ must be large

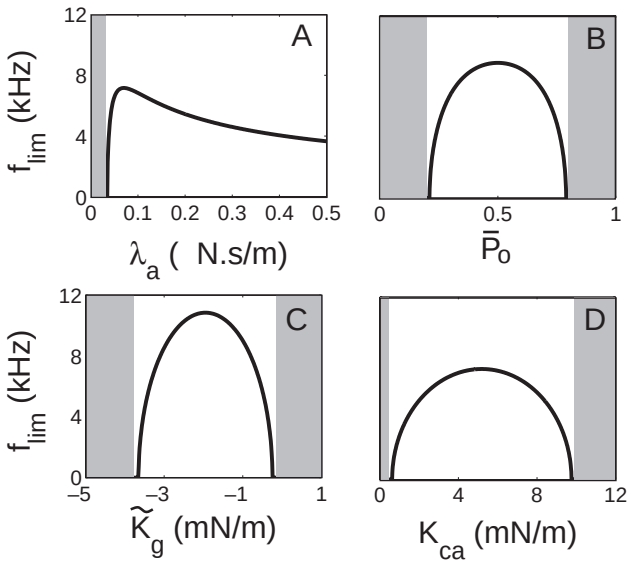

Figure 5.6: An example of parameter dependence of limiting frequency. The dependence on (A) λ_a, (B) $\bar{P}_o$, (C) $\tilde{K}_g$, and (D) K_{ca}. Limiting frequency $f_{\rm lim}$ does not exist in the shaded areas. Assumed parameter values are same as Fig.5.5(B).

enough to make E_{hb} greater than E_d, which is positive. The dependence of $f_{\rm lim}$ on its parameters is illustrated in Fig. 5.4.3.

The morphological factor M (Eq. 5.22) that appears in the channel re-closure model also appears in the frequency limit of the interplay model. Here we observe that the limiting frequency is an increasing function of this factor. The limiting frequency obtained is, however, quite sensitive to other factors (Fig. 5.4.3).

5.5 Morphological factor

The morphological features of the cochlea are represented by a single factor M in the limiting frequency for each of the two models. How do the values for this factor in the mammalian ear compare with those in the avian ear? The mammalian ear differs from the avian ear in having lower bundle height h and smaller number N of tip-links per bundle (see Table 5.2). These two factors do not have significant influences on the morphological factor M because they work in the opposite directions in Eq. 5.22. The most important factor is the area A of the subtectorial gap per hair cell, which is much larger in the mammalian ear. For this reason, the morphological factor M for the avian cochlea is $\sim$10 times of that for the mammalian cochlea.

Audible frequency limit of the avian ear is 1/10th the mammalian one and our estimation shows that f_{lim} is an increasing function of the morphological factor in the two models. Thus, the large morphological factor M for the avian ear indicates that hair bundle motility is more important in the avian ear than in the mammalian ear. For this reason it is of interest to compare the mapping of the morphological

notation	quantity	mammal	chicken	unit
$K_g X_g$	gating force	4.4 [a]	> 0.43 [b]	pN
h	height of tallest cilia	0.7 [100]	1.54 [157]	μm
s	rootlet separation	0.5 [121]	0.45 [92]	μm
N	number of tip-links/cell	60 [c]	187 [d]	
A	subtectorial gap area/hair cell	125 [100]	19 (neural) [157]	μm^2
			23 (abneural)[157]	
$[Ca]_{out}$	endolymphatic [Ca^{2+}]	23.7 [139]	240 [145]	μM
$[Ca]_{in}$	cytosolic [Ca^{2+}]	0.2 [e]	0.2 [e]	μM

Table 5.2: Parameter values for the basal end of the cochlea

[a]Obtained from 500 fN of [163] force at the tip of mouse outer hair cell and the geometric factor for $h \simeq 4.4\mu$m [56]. [b]Obtained from the value 40 fN [149, 175] at the tip and $h \simeq 4.8\mu m$ (at the apex). [c]At the mid-turn of the cochlea [7]. [d]The number of stereocilia [157] multiplied by a ratio 0.8 [160]. [e]Median of estimated 60nM and 300nM [103]. The viscosity coefficient η of the medium is assumed 1 mPa·s, same as water.

factor along the avian basilar papilla with that of the characteristic frequency [1]. In the chicken cochlea each quantity that contributes to this factor has been carefully mapped along its longitudinal axis [157, 160] although morphological data obtained from electron microscopy may need correction for sample shrinkage, which could be $\sim 30\%$ in length [44, 92] for scanning electron microscopy (SEM).

It has been shown that the height h of the tallest cilia in a hair bundle (Fig.5.1) shows monotonic decrease from the apex to the base (Fig.5.8B). The number of stereocilia shows monotonic increases [157]. The number N of tip-links in a hair bundle, which can be estimated by multiplying by a factor 0.8 [160], to the number of stereocilia, is therefore an increasing function of the distance from the apex (Fig.5.8A). The surface area A of a single hair cell on the reticular lamina does not show a monotonic dependence on the distance from the apex (Fig.5.8C) [157]. It has a maximum at about 50% from the apex on the abneural side (i.e. abneural hair cells [2]) and it is relatively constant on the neural side (neural hair cells [3])[157].

The morphological factor M for the avian ear obtained from these experimental data is an increasing function of the distance from the apical end (Fig.5.8D), similar to the mapping of the characteristic frequency (Fig.5.8D). This observation is somewhat surprising because our condition to introduce the morphological factor is simply a necessary condition for an upper bound of characteristic frequency. However, this factor is always greater on the neural side than the abneural side at

[1]Characteristic frequency means frequency at which the hair cell at a particular location is stimulated most

[2]Abneural hair cells are also called short hair cells. Fig. 5.7

[3]Neural hair cells are also called tall hair cells. Fig. 5.7

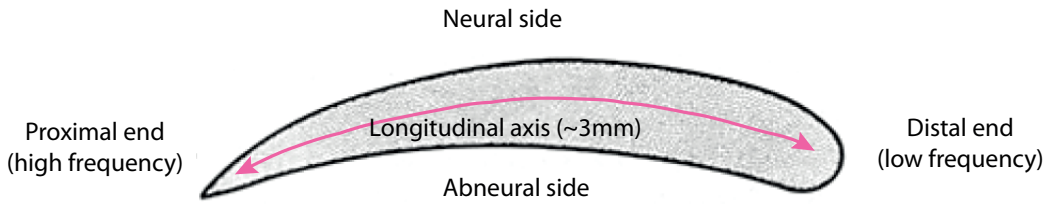

Figure 5.7: Diagram of chicken cochlea viewed from above. Hair cells in the abneural side are called abneural hair cells or short hair cells and in the neural side are called neural hair cells or tall hair cells. Similar to in the mammalian cochlea, hair cells near the proximal end and near the distal end of cochlea respond to high and low frequency, respectively.

each longitudinal location. If one assumes that the role of abneural hair cells is similar to that of outer hair cells, this observation is somewhat paradoxical because larger values of the morphological factor correspond to a greater effectiveness of the amplifier if other parameters are the same.

If we assume that achieving high frequency sensitivity is biologically costly, limiting frequency may have a correlation with the characteristic frequency. Then a relatively good correspondence of the morphological factor and the characteristic frequency along the longitudinal axis of the chicken ear appears consistent with the channel re-closure model, which predicts a limiting frequency proportional to the morphological factor. The difference in the morphological factor for neural and abneural cells could be attributed to either systematic differences in the gating force in those cells or in the open probability of the MET channel. The gating force $K_g X_g$ or the resting open probability $\bar{P}_o$ of the channel could be somewhat larger

in abneural cells than in neural cells.

The implication of the mapping of the morphological factor on the interplay model is more equivocal. The square root dependence of the limiting frequency on the morphological factor indicates that the frequency limit predicted by the interplay model does not rise as sharply as the characteristic frequency along the longitudinal axis if all other parameters are constant throughout the cochlea. However, with so many parameters to which the limiting frequency is sensitive, such an assumption may not be realistic. Rather it could imply that other parameters need to change along the axis to make the rise of the limiting frequency sharper.

Alternatively, it is possible that the limiting frequencies that we obtained could be significantly higher than the characteristic frequency. If that is the case, the present analysis is more effective in examining the validity of the re-closure model than in examining the interplay model because the re-closure model is more constrained by a smaller number of parameters.

5.6 Limiting frequency

For the channel re-closure model, the gating force $K_g X_g$ and the morphological factor M can be used to predict the limiting frequency if we can assume that the phase factor Φ is optimized. For hair cells at the basal turn of the mammalian cochlea, which respond to high frequency signals, the gating force $K_g X_g$ is 4.4 pN for mice [163], and the morphological factor at the base is 0.17 μm^{-1} for animal chichilla. If we can use mouse gating force value for chincilla, the limiting frequency

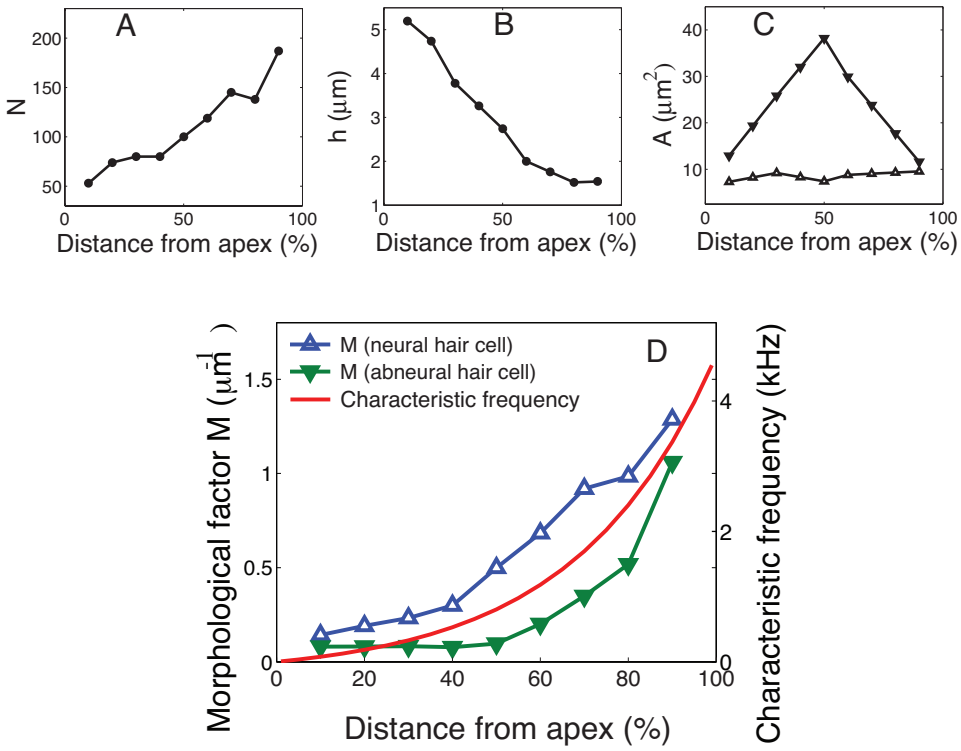

Figure 5.8: (A) Hair bundle height h, (B) the number N of tip-links, and (C) apical surface area A per hair cell on the neural (unfilled) and abneural (filled) sides are plotted against the distance from the apex. Adopted from ref. [157] N is obtained by multiplying a factor 0.8 [160] to the number of stereocilia [157]. Shrinkage factor is not considered. (D) Morphological factor M $(= Ns^2/A\,h)$ on the neural (blue) and abneural sides (green) are plotted together with the best frequency (red line). s is assumed $0.45\mu m$ [92] (Table. 5.2). The best frequencies are adopted from ref. [61]

is $\sim$ 2 kHz, much lower than the auditory frequency of 20 kHz for chinchilla, 40 kHz for guinea pig and gerbil. It is also lower than the limiting frequency of $\sim$ 10 kHz, obtained from the condition for electromotility of outer hair cells to locally counteract viscous drag [78, 118].

If we can assume that the gating force for the chicken is $\sim$ 4.3 pN, similar to that of other animals, including $\sim$ 5.2 pN for frog [96], $\sim$ 4.1 pN for turtle [128] (these values are based on $s/h = 0.11$), we obtain the limiting frequency of 20 kHz on the neural side and 17 kHz for the abneural side at the basal end. These frequencies are higher than the auditory range of $\sim$4 kHz, even after correcting for EM sample shrinkage that would reduce the morphological factor and thereby the limiting frequency by 50%. This observation is consistent with the hypothesis that hair bundles function as the cochlear amplifier in the avian ear. However, experimental values for the gating force measured at the tip of the hair bundle of the chicken are $\sim$ 40 fN [149, 175], about 1/10 of those in other animals, leading to 0.43 pN at the tip-link by considering the geometrical factor $g \approx h/s$ (Table5.2). This lower value for gating force leads to the limiting frequency of 200 Hz for the neural side and 170 Hz for the abneural side, without correcting for sample shrinkage.

Why are the current values for gating force of the chicken hair bundle so small compared with those from other animals? A possible reason could be technical difficulties in experiments, specifically the time resolution must be high enough compared with measuring gating force in frogs [9]. Alternatively, it is possible that gating of channels in a single hair bundle may not be stimulated by the same degree, broadening channel opening with respect to bundle displacement [42, 43]. If

the channel re-closure model, which predicts a quadratic power dependence of the limiting frequency on gating force, is correct, the gating force of chicken hair cells must be as high as that of other animals.

The predictions of the interplay model on the limiting frequency are difficult to make. It depends on a greater number of parameters such as λ_a, F_m, and S, which are related to the myosin motor and show considerable variability in their values [162]. In addition, a relatively small uncertainty in some parameter values tends to lead to a large uncertainty in the limiting frequency. For example, a 10% difference in either gating distance or gating stiffness can lead to $> 100\%$ difference in the limiting frequency.

5.7 Conclusions

We assumed that viscous drag in the subtectorial gap must be counteracted by hair bundle motility for small periodic stimulation and derived limiting frequencies of the ear for two models, the "channel re-closure" model [19] and the "interplay" model [162], of hair bundle motility, each of which works as an amplifier.

The limiting frequency obtained from the channel re-closure model is proportional to the phase factor, the morphological factor, and the square of gating force. The limiting frequency obtained from the interplay model is much more complex. Although it depends on the morphological factor, it is very sensitive to factors that characterize the gating of the mechanoelectric transducer channel as well as force production by the myosin motor.

The morphological factor is much larger for the avian ear than for the mammalian ear. For the chicken ear, this factor shows a similar dependence along the longitudinal axis of the cochlea to characteristic frequency. Such properties of the morphological factor can be derived by the channel re-closure model. However, gating force for the chicken must be larger than reported values. The limiting frequency predicted by the interplay model is not so specific, involving numerous parameters.

Acknowledgement

This work was directed by Dr. Kuni H. Iwasa and supported by NIDCD.

Chapter 6

Hair bundle motility in the avian ears

In this chapter [1], we study the possible contribution of hair bundle motility, described by channel re-closure model (See chapter 5), for avian ears. In the chapter 5, we saw that the hair bundle motility is more effective in the avian ears than in mammalian ears, mainly due to morphological advantages of the avian ears (See chapter 5). Here we examine the hair bundle motility for the barn owl, which are known to operate at high frequencies (= ∼10 kHz), in comparison of chicken hair cell morphology.

6.1 Methods

We make three basic assumptions: 1. Hair bundles produce force based on channel re-closure due to the binding of Ca^{++} introduced during channel opening. 2. The energy generated by the channel re-closure must be sufficient to counteract viscous loss in the subtectorial space. 3. The mechanical stimulus is a continuous sinusoid with infinitesimal amplitude. With these assumptions, the limiting frequency [2] is expressed by

$$f_{lim} = \frac{\Phi N h (\gamma f_g)^2}{2\pi^2 \eta A k_B T} \tag{6.1}$$

[1] This is a collaborative work with Dr. Christine Köppl who provided experimental data.

[2] The method used to estimate the limiting frequency f_{lim} is same as in the chapter 5.3 Channel re-closure model.

where k_B is Boltzmann's constant, T the temperature, Φ a phase factor, determined by channel kinetics ($\sim$0.07), η the viscosity of the fluid, N the number of tip links, h the height of the tallest stereovilli, A the surface area of the hair cell exposed to the subtectorial space, and f_g the gating force of the MET channel. The factor γ is the geometric factor, which is approximately s/h [79], where s is the separation of stereovillar rootlets. Thus, the dependence of the limiting frequency on the morphological factor M is given by

$$M = \frac{Ns^2}{hA}. \tag{6.2}$$

We made an effort to use, wherever possible, experimentally avian values for the various parameters in the model, and also to take into account differences between chicken and owl and between different locations within the basilar papilla. We supplemented published data with new scanning-electron microscopy data, obtained by routine methods. Hair cell samples were taken at defined, positions both along and across the papilla. Stereovillar counts were carried out in 4 barn owl and 2 chicken basilar papillae, from images taken at a minimal magnification of $\times$8500. Hair cell surface areas were determined in one barn owl papilla (aged P41), from images taken at $\times$2500. Custom-made modifications to the SEM stage ensured a perpendicular surface view onto the strongly curved owl papilla at all locations evaluated.

6.2 Results

Two birds for which hosts of morphological and physiological data are available, were contrasted; The chicken is a bird with unspecialized hearing and the barn owl is a high-frequency specialist.

6.2.1 Values for morphological parameters

We first summarize the sources of data used, as well as uncertainties associated with them that have important consequences for the model.

- Hair cell surface area (A). In the chicken, presumed tall hair cells (at neural positions) are smallest, while presumed short hair cells (at abneural positions) are larger at all longitudinal positions and reach a peak midway between apex and base [109, 157]. In the barn owl, the relative sizes of tall and short hair cells uniquely reverse in the basal end of the cochlea, high-frequency regions [50]. While there is agreement on these species-specific patterns, data sets for the same species differ by a factor of about 1.5 in their absolute values. We believe this is due to the difficulties of obtaining a perfectly perpendicular view of the curved surface of the basilar papilla, leading to an underestimate of surface areas. For model calculations, we have adopted Manley *et al.*'s [109] larger values for the chicken and our own for the owl, all corrected for 30% linear shrinkage due to SEM processing.

- Height of tallest stereovilli (h). Bundle heights reported for both chicken and owl are in very good agreement between different studies. In the chicken,

bundle height decreases nearly linearly from apex to base of the cochlea. We adopted the most comprehensive dataset by Tilney et al. [161] (SEM data, corrected for 30% linear shrinkage). In the owl, stereocilia height decreases linearly over the apical half of the papilla, but, uniquely, stays nearly constant within the basal half [91]. We used the transmission electron micrograph (TEM) measurements of Fischer [49] without correction.

- Number of MET channels per hair bundle (N). The number of tip links was obtained by subtracting the number of stereovilli in one row from the total count of stereocilia. In birds, stereocilia numbers typically increase both from apex to base of the cochlea and, at a given longitudinal position, from abneural to neural; absolute numbers, however, differ substantially between different studies. For the chicken, our own counts are intermediate between the reported extremes, which differ by a factor of about 1.5 [157, 159]. For the owl, Fischer *et al.* [50] first showed the pronounced non-linear pattern along the basilar papilla which correlates with the foveal frequency representation [91]. Our own counts indicated, in addition, an extraordinarily steep rise in stereovillar numbers towards the neural edge of the papilla which had previously been missed. Numbers up to 350 stereovilli were typical for hair cells at the neural edge. For the model, we adopted our own data, supplemented by Tilney and Tilney [158] for the most apical positions in the chicken.

- Stereocilia rootlet separation (s). Very few data are available for bird hair cells. Pickles [121] gave a value of 0.67 μm for a chicken tall hair cell. Our

own estimates from published TEM micrographs indicate 0.27–0.39 μm for chicken basilar-papilla hair cells [48], his Figs. 2, 4) and 0.36–0.53 μm for the barn owl [49], his Fig.3). We therefore assumed a constant stereovillar separation of 0.45 μm for both chicken and owl.

6.2.2 The morphological factor for upper frequency limit

We plotted the morphological factor M ($=Ns^2/(hA)$ in Eq. 6.2) as a function of longitudinal (tonotopic) position and compared it with the known frequency maps for the chicken ("Greenwood" map from review [61]) and for the owl [91] (Fig. 6.1). The morphological factor reproduced the characteristic features of the tonotopic map [3] for both birds. While, in the barn owl, the characteristic frequency and M rise sharply in the apical part and then flatten off, the reverse pattern is seen in the chicken. The values for M, however, did not reflect the factor-of-two difference in the upper limits of the tonotopic maps of these birds.

6.2.3 Predicted upper frequency limit of effective hair-bundle forces

The morphological factor M was converted into frequency by assuming a gating force f_g of 4.3 pN at the MET channel and a phase factor Φ of 0.07 (see Eq. 6.1). The value for f_g was based on Le Goff *et al.* [96] who measured 470 fN at the tip of the tallest stereovilli in bullfrog saccular hair cells. This converts to 4.3

[3] Tonotopy (from Greek tono- and topos = place) refers to the spatial arrangement of where sounds of different frequency stimulate the cochlea and are processed in the brain. [www.wikipedia.org]

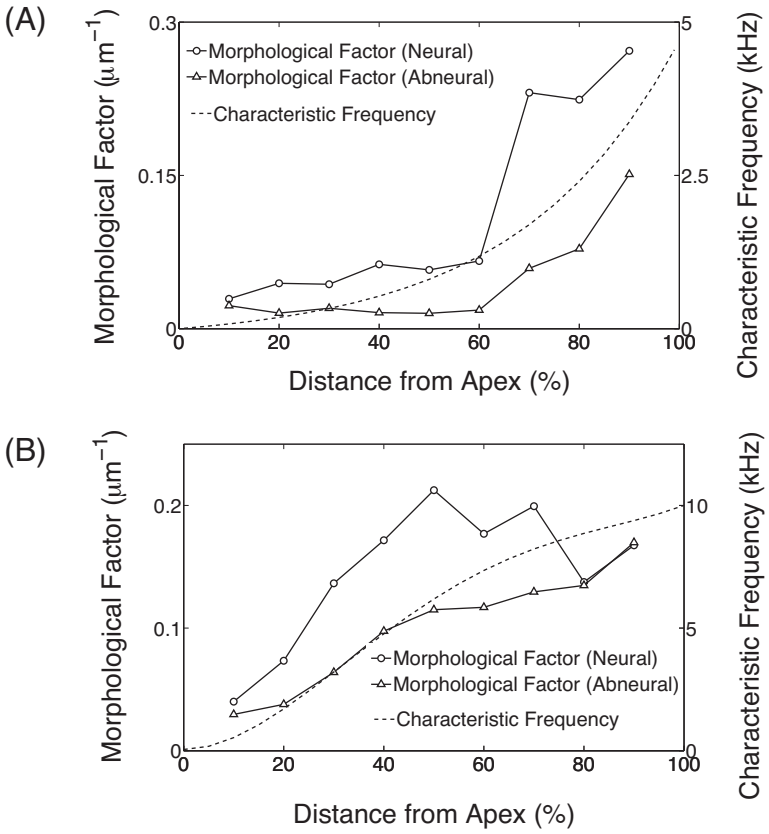

Figure 6.1: Morphological factor as a function of longitudinal (tonotopic) position, separately for neural and abneural positions across the papilla (cochlea), and compared to the known tonotopic frequency (characteristic frequency) gradient. (A) chicken and (B) owl.

pN at the tip-link due to the geometrical factor [79]. Using that value, we obtained 4.3 kHz and 2.6 kHz for the frequency limits of the most basal-neural hair cells in chicken and owl, respectively.

6.3 Discussion

6.3.1 Are hair-bundle forces likely to be effective in the avian frequency range?

The estimated frequency limits, using parameter values that we judged to be the most realistic, were close to the known upper tonotopic limits of birds with average hearing, such as the chicken. We conclude that hair-bundle forces remain a realistic candidate mechanism for the cochlear amplifier in birds. Preliminary data indicate that chicken hair bundles display pronounced mechanical oscillations in response to step displacements, i.e. show evidence of such an active process [73]. We observe that the frequency range highly depends on the value of the gating force. The gating force F_g measured at the top of the hair bundle has determined in a number of hair-cell preparations. Most of reported values are $\sim$400 fN (Table 6.1). For preparations whose geometrical factor γ (Fig. 5.1) can be estimated, the gating force f_g at the MET channel is about 4 pN [79]. Oddly, estimates for F_g for chicken basilar-papilla hair cells are unusually low, at about 40 fN [149, 175]. The low values could be due to incoherence in the gating of MET channels because the temporal resolution for observing synchronous gating is very high (Bozovic, personal communication). We assume here that the gating mechanism is shared between all

types of hair cells and that a realistic value for the gating force of bird hair cells is nearer the high end of the measured scale (review in [46]). An even higher value of the order of 10 pN has been suggested as plausible [130]. This would be more than adequate for explaining the hearing range of the barn owl.

Table 6.1: Gating force values

	mouse	turtle	frog	chicken
Gating force F_g (fN)	300 – 500 [163]	250 – 370 [127]	470 [96]	40 [149, 175]

6.3.2 Can the model account for species-specific differences?

Our predictions of upper frequency limits for chicken and owl reproduced the species-specific shapes of the known tonotopic maps very well. Importantly, the combination of a number of salient parameters produced the match, which goes beyond the individual correlations with bundle height and stereovillar number that have previously been shown. In absolute terms, however, the estimated frequency limits approximated only the auditory range up to ∼5 kHz in the chicken, while the estimate for the barn owl was significantly lower and contradicted the fact that the auditory range for the barn owl is twice as wide, reaching to 10 kHz. As pointed out above, some of the data that form the basis of the model calculations show significant variation across studies. While we resolved several uncertainties by obtaining additional data, two parameters remain with large ranges of uncertainty: stereovillar rootlet separation and MET channel gating force. If chicken and owl

hair cells should differ in one or both respects, it could reverse the predicted upper frequency limits and thus match the real situation. We believe the most likely possibility for obtaining a realistic frequency limit near 10 kHz in the owl is a higher MET channel gating force.

Acknowledgement

This work was directed by Dr. Kuni H. Iwasa and Dr. Christine Köppl and supported by NIDCD.

Chapter 7

Conclusions

In this thesis, we made theoretical investigations on functions of hair cells, which are mechano-electrical transducers and amplifiers in the cochlea.

In the chapter 2, we addressed discrepancy between recent experimental findings [7, 8] and earlier theoretical models for gating of mechano-electrical transducer (MET) channels [18, 71, 162]; the earlier theoretical models assume one MET channel per tip link, however the recent experiments found about two MET channels exist per tip link. To be consistent with the recent findings, we developed models that assume two identical MET channels connected either in series or in parallel.

We found that series connection of the two channels predicts a critical value for the minimum of effective stiffness for gating elements. The effective stiffness for gating elements has a single minimum with respect to hair bundle displacement if the minimum is larger than the critical value and double minima if the minima are smaller than the critical value. In contrast, parallel connection of the two channels predicts that the effective stiffness for gating elements has a single minimum always. We found that within the physiological range of parameters, the parallel connection of the two channels predicts similar to an earlier model assuming one channel with two states per tip link [71]. This explains why the earlier models have been successful in describing the most of experimental data even though they assumed a single

channel for each tip link.

To check the connectivity of the two channels, we compared our models with experimental data. We found that for rat and frog hair cells, hair bundle stiffness data are reasonably described by the parallel connection model, not by the series connection model. Parallel connection of MET channels is, therefore, a reasonable assumption to explain experimental observations for rat and frog hair cells.

The compatibility with series connection, however, cannot be ruled out for experimental data on turtle hair cells even though distinction between the series and the parallel connection models is not as clear as for rat and frog hair cells. Among the existing hair bundle stiffness data for turtle hair cells, only one data set has minimum value for the effective hair bundle stiffness below the critical point, which enables to distinguish the two models in the number of minima for the effective hair bundle stiffness. This data set shows slightly better fit with the series connection model. The rest data sets have the minimum value for the hair bundle stiffness above the critical value and, thus, distinction between the two models is only possible by comparing goodness of the curve-fits, not by the number of minima for the hair bundle stiffness. Thus our model suggests the importance of further studies on the connectivity between the tip link and the MET channels in turtle hair cells.

In the chapter 3, we estimated the efficiency of electromotility as an amplifier in the cochlea. We examined a proposal [30] that the cochlear microphonic, the voltage drop across the extracellular medium by the receptor current, contributes to overcome the RC time constant problem. We considered two kinds of outer hair cells (OHCs), stimulated OHCs which are located in the cochlear partition of

the characteristic, and unstimulated OHCs, which are in the locus of the cochlear partition of the characteristic frequency.

We confirmed that the oscillatory potential in unstimulated OHCs induced by the extracellular potential can be greater than the receptor potential and that this effect can increase the efficiency of electromotility as the earlier proposal [30]. However, we found that this effect alone is too small to enhance the effectiveness of electromotility beyond 10 kHz in the mammalian ear. The introduction of an extracellular resistance, which is needed to produce the cochlear microphonic, reduces the receptor potential. Since the significance of prestin and electromotility has been experimentally proven [33], our result indicates that there must be another factor, such as fast voltage-gated K-currents, in the basal turn where the characteristic frequencies exceed 10 kHz.

In the chapter 4, we investigated how hair bundle motility based on the release mechanism can work for amplification even though it appears to have a similar property of a damper. With a perturbation method for small sinusoidal displacement of hair bundle, we found that the release mechanism can indeed have a role in amplification, if it is associated with negative stiffness due to the gating of the mechaoelectric transducer channel. This result is applicable to any relaxation mechanism because the validity of our analysis is not limited to a particular release mechanism.

Our analysis shows that if hair bundle motility is operated in the domain of negative stiffness, direction of force generation becomes opposite. This suggests that relaxation-like phenomena in the hair bundle be observed experimentally because experiments were done in the domain of positive stiffness. Because negative stiffness

is intrinsically unstable, certain mechanisms must be present in the hair bundle to maintain negative stiffness. If such mechanisms are disturbed during the experiments, observations will be made in the domain of positive stiffness and relaxation phenomena will be observed.

In the chapter 5, we studied the effectiveness of hair bundle motility in mammalian and avian ears. We examined energy balance between energy gain and loss for a small sinusoidal displacement of the hair bundle and obtained an upper bound of frequency that can be supported by hair bundle motility. We considered two mechanisms for hair bundle motility, the channel re-closure model and the interplay model. The channel re-closure model assumes that calcium binding to MET channel causes channel re-closure and the interplay model assumes that fast adaptation is an interplay between gating of the channel and the myosin motor.

We found that the upper bound of frequency obtained for both models is an increasing function of a factor, called morphological factor, that is determined by the morphology of hair bundles and the cochlea. While the upper bound of frequency for the channel re-closure model is proportional to the morphological factor, the interplay model is very sensitive to factors that characterize the gating of the MET channel as well as force production by the myosin motor.

Primarily due to the higher density of hair cells in the avian inner ear, this factor is about 10-fold greater for the avian ear than the mammalian ear, which has much higher auditory frequency limit. This result is consistent with a much greater significance of hair bundle motility in the avian ear than that in the mammalian ear. For the chicken ear, this factor shows a similar dependence along the length of

the cochlea to characteristic frequency. Such properties of the morphological factor is more consistent with the channel re-closure model.

In the chapter 6, we expanded a scope of investigation on hair bundle motility in avian ears, with the same method used in the chapter 5. We found that the morphological factor, which is proportional to the upper bound of the frequency estimated for the channel re-closure model, for chicken and owl reproduced the species-specific shapes of the known tonotopic maps very well. It is noteworthy that the combination of parameters produced the match, which goes beyond the individual correlations with bundle height and stereocillar number that have previously been shown.

We found that the value of the morphological factor for owl is lower than for chicken. This contradicts the fact that the auditory range for owl is as twice high as chicken. This issue may be related to uncertainties in parameters such as stereocilliar rootlet separation and MET channel gating force. Even though the frequency limits have quadratic dependence on these parameters, we assumed that these parameter values are the same across the species because of lack of experimental data available for such parameters. If owl has a bigger separation between the stereocilliar rootlets than chicken, owl's morphological factor can be easily bigger than chicken's and can cover its auditory limit. Another example is gating force of owl. We assumed that owl has the same gating force of chicken because data are not available to determine gating force of owl. If owl has a bigger gating force than chicken, even when owl's morphological factor is not bigger than chicken's, owl's upper bound of frequency can be higher than chicken's. Therefore our result that chicken has bigger

morphological factor than owl shows importance of experimental studies to be done on owl hair cells.

While gating force values for other animals, such as mouse [163] , turtle [127], and frog [96], are similar to each other, reported values for chicken gating force [149, 175] are almost 10 times smaller than those animals. The smaller value of chicken gating force may be due to experimental errors, rather than chicken MET channels being unique. Errors may come from misinterpretation of experimental condition. Reported values were obtained assuming that all the MET channels were stimulated by the same degree in the experiments. However if all the MET channels in hair bundles are not displaced by the same amount in experiments, plot of open probability of the MET channels–hair bundle displacement does not only represent a property of a single MET channel but also a superposition of each gating event of a single MET channel. This results in underestimation of gating force. In fact, we found that the same data for chicken can be explained with a gating force value similar to other animals if we consider a certain distribution of displacement given to MET channels in the experiment. Experimental studies to verify whether or not chicken has smaller gating force seems important because gating force has significance in estimating effectiveness of hair bundle motility.

Appendix A

Appendix

A.1 Derivation of Eqs. 2.17–2.19

Let the total displacement of the system x and the displacement of the channel elements x'. The displacement of the shared spring k_b is then $x - x'$ (See Fig. 2.1B). The energy of the system in each state is

$$\epsilon_{oo} = k_g(x' - x_g)^2 + \frac{1}{2}k_b(x - x')^2, \tag{A.1}$$

$$\epsilon_{oc} = \frac{1}{2}k_g(x' - x_g)^2 + \frac{1}{2}k_g x'^2 + \frac{1}{2}k_b(x - x')^2, \tag{A.2}$$

$$\epsilon_{cc} = k_g x'^2 + \frac{1}{2}k_b(x - x')^2. \tag{A.3}$$

Displacement x' is determined by the equation for force balance,

$$2k_g x' - n_j k_g x_g = k_b(x - x')$$

where n_j is the number of open channels, i.e. 2 for {o,o}, 1 for {o,c}, and 0 for {c,c}. This condition leads to

$$x' = \frac{k_b x + n_j k_g x_g}{k_b + 2k_g}. \tag{A.4}$$

By substituting x' in Eqs. A.1–A.3 by Eq. A.4, we obtain Eqs. 2.17–2.19.

A.2 Condition for negative stiffness for parallel connectivity

By introducing a parameter D $(= \gamma/(\alpha + 2))$ into Eq. 2.26, the condition $\kappa_{p,min} < 0$ can be expressed as

$$\kappa_{p,min} = 1 - (\gamma - 2D)\,\frac{1}{1 + e^{-D}} < 0. \tag{A.5}$$

This inequality can be rewritten as

$$e^{-D} < -2D + \gamma - 1. \tag{A.6}$$

This inequality can be illustrated by plotting $y_1 = e^{-D}$ and $y_2 = -2D + \gamma - 1$ together against D (Fig. A.1). To satisfy $y_1 < y_2$, the condition $\gamma - 1 > 1$ is required because $D > 0$. Thus negative stiffness exists if $\gamma > 2$ and $0 < D < D_{lim}$, where D_{lim} is the solution of the equation $e^{-D} = -2D + \gamma - 1$.

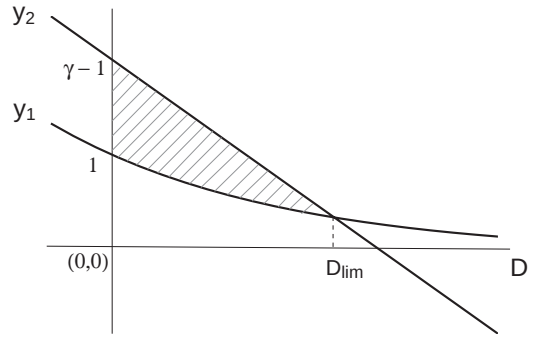

Figure A.1: Parameter ranges of γ and D $(\equiv \gamma/(\alpha + 2))$ giving negative stiffness in the parallel connection model. Negative stiffness exists where y_1 $(\equiv e^{-D}) > y_2$ $(\equiv -2D + \gamma - 1)$. This condition leads to $\gamma > 2$ and $0 < D < D_{lim}$.

A.3 Cooperative gating of two channels connected in parallel

For stiff elastic element k_a that anchors the two channels (i.e. $\alpha \to \infty$), we have a limiting value $\kappa_{p,min} \to 1 - \gamma/2$, which is same as gating of a single channel. To examine the presence of optimal $\kappa_{p,min}$ minimized by α, we put $d\kappa_{p,min}/d\alpha = 0$. This leads to

$$e^D = -D + \frac{\gamma}{2} - 1 \tag{A.7}$$

with $D = \gamma/(\alpha+2)$. The left-hand-side is an increasing function and the right-hand-side is a decreasing function of D. Because $D > 0$, a root exists only if $\gamma/2 - 1$ (i.e. the right-hand-side value at $D = 0$) is greater than unity (i.e. the left-hand-side value at $D = 0$). This leads to $\gamma > 4$.

By putting Eq. A.7 in Eq. 2.26, we obtain $\kappa_{p,min}$ optimized by α such that

$$\kappa_{p,min} = 3 - \gamma + \frac{2\gamma}{\alpha + 2}. \tag{A.8}$$

Thus for infinitely large γ, the ratio of optimized $\kappa_{p,min}$ to $1 - \gamma/2$ is $2 - 4/(\alpha + 2)$ and this value approaches 2 for large α.

Bibliography

[1] J. Allen. Cochlear micromechanics—a physical model of transduction. *J. Acoust. Soc. Am.*, 68:1660–1670, 1980.

[2] J. F. Ashmore. A fast motile response in guinea-pig outer hair cells: the molecular basis of the cochlear amplifier. *J. Physiol.*, 388:323–347, 1987.

[3] J. F. Ashmore. Forward and reverse transduction in guinea-pig outer hair cells: the cellular basis of the cochlear amplifier. *Neurosci. Res. Suppl.*, 12: S39–S50, 1990.

[4] J. A. Assad and D. P. Corey. An active motor model for adaptation by vertebrate hair cells. *J Neurosci*, 12(9):3291–3309, Sep 1992.

[5] P. Atkins and J. de Paula. *Atkins' physical chemistry*. Oxford University Press, 2002.

[6] M. E. Benser, R. E. Marquis, and A. J. Hudspeth. Rapid, active hair bundle movements in hair cells from the bullfrog's sacculus. *J Neurosci*, 16:5629–5643, 1996.

[7] M. Beurg, M. G. Evans, C. M. Hackney, and R. Fettiplace. A large-conductance calcium-selective mechanotransducer channel in mammalian cochlear hair cells. *J Neurosci*, 26:10992–11000, 2006. doi: 10.1523/JNEUROSCI.2188-06.2006.

[8] M. Beurg, R. Fettiplace, J.-H. Nam, and A. J. Ricci. Localization of inner hair cell mechanotransducer channels using high-speed calcium imaging. *Nat Neurosci*, 12(5):553–558, May 2009. doi: 10.1038/nn.2295. URL `http://dx.doi.org/10.1038/nn.2295`.

[9] D. Bozovic, 2008. personal communication.

[10] D. Bozovic and A. J. Hudspeth. Hair-bundle movements elicited by transepithelial electrical stimulation of hair cells in the sacculus of the bullfrog. *Proc Natl Acad Sci U S A*, 100(3): 958–963, Feb 2003. doi: 10.1073/pnas.0337433100. URL `http://dx.doi.org/10.1073/pnas.0337433100`.

[11] W. Brownell, C. Bader, D. Bertrand, and Y. Ribaupierre. Evoked mechanical responses of isolated outer hair cells. *Science*, 227:194–196, 1985.

[12] S. Camalet, T. Duke, F. Jülicher, and J. Prost. Auditory sensitivity provided by self-tuned critical oscillations of hair cells. *Proc. Natl. Acad. Sci. USA*, 97: 3183–3188, 2000.

[13] D. K. Chan and A. J. Hudspeth. Ca2+ current-driven nonlinear amplification by the mammalian cochlea in vitro. *Nat Neurosci*, 8(2):149–155, Feb 2005. doi: 10.1038/nn1385. URL `http://dx.doi.org/10.1038/nn1385`.

[14] D. K. Chan and A. J. Hudspeth. Ca^{2+} current-driven nonlinear amplification by the mammalian cochlea in vitro. *Nature Neurosci.*, 8:149–55, 2005.

[15] M. A. Cheatham, K. H. Hynh, J. Gao, J. Zuo, and P. Dallos. Cochlear function in prestin knockout mice. *J. Physiol.*, 560:821–30, 2004.

[16] M. A. Cheatham, J. Zheng, K. H. Huynh, G. G. Du, R. M. Edge, C. T. Anderson, J. Zuo, A. F. Ryan, and P. Dallos. Evaluation of an independent prestin mouse model derived from the 129s1 strain. *Audiol Neurootol*, 12(6):378–390, 2007. doi: 10.1159/000106481. URL `http://dx.doi.org/10.1159/000106481`.

[17] E. L. Cheung and D. P. Corey. Ca^{2+} changes the force sensitivity of the hair-cell transduction channel. *Biophys. J.*, 90:124–139, 2006.

[18] E. L. M. Cheung and D. P. Corey. Ca2+ changes the force sensitivity of the hair-cell transduction channel. *Biophys J*, 90 (1):124–139, Jan 2006. doi: 10.1529/biophysj.105.061226. URL `http://dx.doi.org/10.1529/biophysj.105.061226`.

[19] Y. Choe, M. O. Magnasco, and A. J. Hudspeth. A model for amplification of hair-bundle motion by cyclical binding of Ca^{2+} to mechanoelectrical-transduction channel. *Proc. Natl. Acad. Sci. USA*, 95:15321–15326, 1998.

[20] A. P. Christensen and D. P. Corey. Trp channels in mechanosensation: direct or indirect activation? *Nat Rev Neurosci*, 8(7):510–521, Jul 2007. doi: 10.1038/nrn2149. URL `http://dx.doi.org/10.1038/nrn2149`.

[21] A. R. Cody and I. J. Russell. The response of hair cells in the basal turn of the guinea-pig cochlea to tones. *J. Physiol.*, 383:551–569, 1987.

[22] D. P. Corey. What is the hair cell transduction channel? *J Physiol*, 576(Pt 1):23–28, Oct 2006. doi: 10.1113/jphysiol.2006.116582. URL `http://dx.doi.org/10.1113/jphysiol.2006.116582`.

[23] D. P. Corey. Cell biology of mechanotransduction in inner-ear hair cells. *F1000 Biology reports*, 1:58, 2009.

[24] D. P. Corey and A. J. Hudspeth. Ionic basis of the receptor potential in a vertebrate hair cell. *Nature*, 281(5733):675–677, Oct 1979.

[25] D. P. Corey and A. J. Hudspeth. Kinetics of the receptor current in bullfrog saccular hair cells. *J Neurosci*, 3(5):962–976, May 1983.

[26] D. A. Cotanche. Video-enhanced DIC images of the noise-damaged and regenerated chick tectorial membrane. *Exp Neurol*, 115(1):23–26, Jan 1992.

[27] A. C. Crawford, M. G. Evans, and R. Fettiplace. Activation and adaptation of transducer currents in turtle hair cells. *J Physiol*, 419:405–434, Dec 1989.

[28] A. C. Crawford, M. G. Evans, and R. Fettiplace. The actions of calcium on the mechano-electrical transducer current of turtle hair cells. *J Physiol*, 434: 369–398, Mar 1991.

[29] P. Dallos and M. A. Cheatham. Production of cochlear potentials by inner and outer hair cells. *J Acoust Soc Am*, 60(2):510–512, 1976.

[30] P. Dallos and B. N. Evans. High-frequency outer hair cell motility: corrections and addendum. *Science*, 268(5216):1420–1421, 1995.

[31] P. Dallos and B. N. Evans. High-frequency motility of outer hair cells and the cochlear amplifier. *Science*, 267(5206):2006–2009, Mar 1995.

[32] P. Dallos and D. Harris. Properties of auditory nerve responses in absence of outer hair cells. *J Neurophysiol*, 41(2):365–383, Mar 1978.

[33] P. Dallos, X. Wu, M. A. Cheatham, J. Gao, J. Zheng, C. T. Anderson, S. Jia, X. Wang, W. H. Y. Cheng, S. Sengupta, D. Z. Z. He, and J. Zuo. Prestin-based outer hair cell motility is necessary for mammalian cochlear amplification. *Neuron*, 58(3):333–339, May 2008. doi: 10.1016/j.neuron.2008.02.028.

[34] P. Dallos, X. Wu, M. A. Cheatham, J. Gao, J. Zheng, C. T. Anderson, S. Jia, X. Wang, W. H. Y. Cheng, S. Sengupta, D. Z. Z. He, and J. Zuo. Prestin-based outer hair cell motility is necessary for mammalian cochlear amplification. *Neuron*, 58(3):333–339, May 2008. doi: 10.1016/j.neuron.2008.02.028. URL `http://dx.doi.org/10.1016/j.neuron.2008.02.028`.

[35] H. Davis. An active process in cochlear mechanics. *Hear Res*, 9(1):79–90, Jan 1983.

[36] E. de Boer. On active and passive cochlear models–toward a generalized analysis. *J Acoust Soc Am*, 73(2):574–576, Feb 1983.

[37] L. Déak, J. Zheng, A. Orem, G. G. Du, S. Aguinaga, K. Matsuda, and P. Dallos. Effects of cyclic nucleotides on the function of prestin. *J. Physiol.*, 563: 483–496, 2005.

[38] W. Denk, J. R. Holt, G. M. Shepherd, and D. P. Corey. Calcium imaging of single stereocilia in hair cells: localization of transduction channels at both ends of tip links. *Neuron*, 15:1311–1321, 1995.

[39] X. X. Dong, D. Ehrenstein, and K. H. Iwasa. Fluctuation of motor charge in the lateral membrane of the cochlear outer hair cell. *Biophys. J.*, 79:1876–1882, 2000.

[40] T. Duke and F. Jülicher. Active traveling wave in the cochlea. *Phys. Rev. Lett.*, 90:158101, 2003.

[41] R. A. Dumont, Y.-D. Zhao, J. R. Holt, M. Bähler, and P. G. Gillespie. Myosin-i isozymes in neonatal rodent auditory and vestibular epithelia. *J Assoc Res Otolaryngol*, 3(4):375–389, Dec 2002. doi: 620020049. URL `http://dx.doi.org/620020049`.

[42] R. K. Duncan, H. N. Hernandez, and J. C. Saunders. Relative stereocilia motion of chick cochlear hair cells during high-frequency water-jet stimulation. *J. Aud. Neurosci.*, 1:321–329, 1995.

[43] R. K. Duncan, M. D. Eisen, and J. C. Saunders. Distal separation of chick cochlear hair cell stereocilia: analysis of contact-constraint models. *Hear Res*, 127(1-2):22–30, Jan 1999.

[44] R. K. Duncan, K. E. Ile, M. G. Dubin, and J. C. Saunders. Hair bundle profiles along the chick basilar papilla. *J Anat*, 198(Pt 1):103–116, Jan 2001.

[45] J. Fang, C. Izumi, and K. H. Iwasa. Sensitivity of prestin-based membrane motor to membrane thickness. *Biophys J*, 98 (12):2831–2838, Jun 2010. doi: 10.1016/j.bpj.2010.03.034. URL `http://dx.doi.org/10.1016/j.bpj.2010.03.034`.

[46] R. Fettiplace. Active hair bundle movements in auditory hair cells. *J Physiol*, 576(Pt 1):29–36, Oct 2006. doi: 10.1113/jphysiol.2006.115949. URL `http://dx.doi.org/10.1113/jphysiol.2006.115949`.

[47] R. Fettiplace and C. M. Hackney. The sensory and motor roles of auditory hair cells. *Nat. Rev. Neurosci.*, 7:19–29, 2006.

[48] F. P. Fischer. Quantitative analysis of the innervation of the chicken basilar papilla. *Hear Res*, 61(1-2):167–178, Aug 1992.

[49] F. P. Fischer. Quantitative tem analysis of the barn owl basilar papilla. *Hear Res*, 73(1):1–15, Feb 1994.

[50] F. P. Fischer, C. Köppl, and G. A. Manley. The basilar papilla of the barn owl tyto alba: a quantitative morphological sem analysis. *Hear Res*, 34(1): 87–101, Jul 1988.

[51] G. Frank, W. Hemmert, and A. W. Gummer. Limiting dynamics of high-frequency electromechanical transduction of outer hair cells. *Proc. Natl. Acad. Sci. USA*, 96:4420–4425, 1999.

[52] A. Fridberger, J. B. de Monvel, J. Zheng, N. Hu, Y. Zou, T. Ren, and A. Nuttall. Organ of corti potentials and the motion of the basilar membrane. *J Neurosci*, 24:10057–10063, 2004. doi: 2004.

[53] J. E. Gale and J. F. Ashmore. An intrinsic frequency limit to the cochlear amplifier. *Nature*, 389:63–66, 1997.

[54] J. A. Garcia, A. G. Yee, P. G. Gillespie, and D. P. Corey. Localization of myosin-ibeta near both ends of tip links in frog saccular hair cells. *J Neurosci*, 18(21):8637–8647, Nov 1998.

[55] C. D. Geisler, G. K. Yates, R. B. Patuzzi, and B. M. Johnstone. Saturation of outer hair cell receptor currents causes two-tone suppression. *Hear Res*, 44 (2-3):241–256, Mar 1990.

[56] G. S. Géléoc, G. W. Lennan, G. P. Richardson, and C. J. Kros. A quantitative comparison of mechanoelectrical transduction in vestibular and auditory hair cells of neonatal mice. *Proc Biol Sci*, 264:611–621, 1997. doi: 10.1098/rspb.1997.0087.

[57] P. G. Gillespie and A. J. Hudspeth. Adenine nucleoside diphosphates block adaptation of mechanoelectrical transduction in hair cells. *Proc Natl Acad Sci U S A*, 90(7):2710–2714, Apr 1993.

[58] P. G. Gillespie and U. Müller. Mechanotransduction by hair cells: models, molecules, and mechanisms. *Cell*, 139 (1):33–44, Oct 2009. doi: 10.1016/j.cell.2009.09.010. URL `http://dx.doi.org/10.1016/j.cell.2009.09.010`.

[59] P. G. Gillespie, M. C. Wagner, and A. J. Hudspeth. Identification of a 120 kd hair-bundle myosin located near stereociliary tips. *Neuron*, 11(4):581–594, Oct 1993.

[60] P. G. Gillespie, R. A. Dumont, and B. Kachar. Have we found the tip link, transduction channel, and gating spring of the hair cell? *Curr Opin Neurobiol*, 15(4):389–396, Aug 2005. doi: 10.1016/j.conb.2005.06.007. URL `http://dx.doi.org/10.1016/j.conb.2005.06.007`.

[61] O. Gleich and G. A. Manley. The hearing organ of birds and crocodilia. In R. J. Dooling, R. R. Fay, and P. A. N., editors, *Comparative Hearing: Birds and Reptiles*, pages 70–138. Springer, New York, 2000.

[62] T. Gold. Hearing. II. the physical basis of the action of the cochlea. *Proc. Roy. Soc., B*, 135:492–498, 1948.

[63] R. J. Goodyear and G. P. Richardson. Extracellular matrices associated with the apical surfaces of sensory epithelia in the inner ear: molecular and structural diversity. *J Neurobiol*, 53(2):212–227, Nov 2002. doi: 10.1002/neu.10097. URL `http://dx.doi.org/10.1002/neu.10097`.

[64] N. Hacohen, J. A. Assad, W. J. Smith, and D. P. Corey. Regulation of tension on hair-cell transduction channels: displacement and calcium dependence. *J. Neurosci.*, 9:3988–3997, 1989.

[65] T. Hasson, P. G. Gillespie, J. A. Garcia, R. B. MacDonald, Y. Zhao, A. G. Yee, M. S. Mooseker, and D. P. Corey. Unconventional myosins in inner-ear sensory epithelia. *J Cell Biol*, 137(6):1287–1307, Jun 1997.

[66] D. Z. Z. He, S. Jia, and P. Dallos. Mechanoelectrical transduction of adult outer hair cells studied in a gerbil hemicochlea. *Nature*, 429(6993):766–770, Jun 2004. doi: 10.1038/nature02591.

[67] M. C. Holley and J. F. Ashmore. On the mechanism of a high-frequency force generator in outer hair cells isolated from the guinea pig cochlea. *Proc R Soc Lond B Biol Sci*, 232(1269):413–429, Jan 1988.

[68] J. R. Holt, S. K. H. Gillespie, D. W. Provance, K. Shah, K. M. Shokat, D. P. Corey, J. A. Mercer, and P. G. Gillespie. A chemical-genetic strategy implicates myosin-1c in adaptation by hair cells. *Cell*, 108(3):371–381, Feb 2002.

[69] G. D. Housley and J. F. Ashmore. Ionic currents of outer hair cells isolated from the guinea-pig cochlea. *J. Physiol.*, 448:73–98, 1992.

[70] J. Howard and A. J. Hudspeth. Mechanical relaxation of the hair bundle mediates adaptation in mechanoelectrical transduction by the bullfrog's saccular hair cell. *Proc. Natl. Acad. Sci. USA*, 84:3064–3068, 1987.

[71] J. Howard and A. J. Hudspeth. Compliance of the hair bundle associated with gating of mechanoelectrical transduction channels in the bullfrog's saccular hair cell. *Neuron*, 1:189–199, 1988.

[72] A. J. Hudspeth. Making an effort to listen: mechanical amplification in the ear. *Neuron*, 59(4):530–545, Aug 2008. doi: 10.1016/j.neuron.2008.07.012. URL `http://dx.doi.org/10.1016/j.neuron.2008.07.012`.

[73] A. J. Hudspeth, Y. Choe, A. D. Mehta, and P. Martin. Putting ion channels to work: mechanoelectrical transduction, adaptation, and amplification by hair cells. *Proc. Natl. Acad. Sci. USA*, 97:11765–11772, 2000.

[74] K. H. Iwasa. A membrane model for the fast motility of the outer hair cell. *J. Acoust. Soc. Am.*, 96:2216–2224, 1994.

[75] K. H. Iwasa. Electromotility of outer hair cells. In P. A. Fuchs, editor, *The Oxford Handbook of Auditory Science: The Ear*, chapter 179–212. Oxford University Press, 2010.

[76] K. H. Iwasa and M. Adachi. Force generation in the outer hair cell of the cochlea. *Biophys. J.*, 73:546–555, 1997.

[77] K. H. Iwasa and G. Ehrenstein. Cooperative interaction as the physical basis of the negative stiffness in hair cell stereocilia. *J. Acoust. Soc. Am.*, 111: 2208–2212, 2002.

[78] K. H. Iwasa and B. Sul. Effect of the cochlear microphonic on the limiting frequency of the mammalian ear. *J Acoust Soc Am*, 124(3):1607, Sep 2008. doi: 10.1121/1.2953317. URL http://dx.doi.org/10.1121/1.2953317.

[79] R. A. Jacobs and A. J. Hudspeth. Ultrastructural correlates of mechanoelectrical transduction in hair cells of the bullfrog's internal ear. *Cold Spring Harb Symp Quant Biol*, 55:547–561, 1990.

[80] F. Jaramillo and A. J. Hudspeth. Localization of the hair cell's transduction channels at the hair bundle's top by iontophoretic application of a channel blocker. *Neuron*, 7(3):409–420, Sep 1991.

[81] S. Jia and D. Z. Z. He. Motility-associated hair-bundle motion in mammalian outer hair cells. *Nat Neurosci*, 8(8):1028–1034, Aug 2005. doi: 10.1038/nn1509. URL http://dx.doi.org/10.1038/nn1509.

[82] B. M. Johnstone, R. Patuzzi, J. Syka, and E. Sykov. Stimulus-related potassium changes in the organ of corti of guinea-pig. *J Physiol*, 408:77–92, Jan 1989.

[83] B. Kachar, M. Parakkal, M. Kurc, Y. Zhao, and P. G. Gillespie. High-resolution structure of hair-cell tip links. *Proc Natl Acad Sci U S A*, 97: 13336–13341, 2000. doi: 10.1073/pnas.97.24.13336.

[84] F. Kalinec, M. Holley, K. H. Iwasa, D. J. Lim, and B. Kachar. A membrane-based force generation mechanism in auditory sensory cells. *Proc. Natl. Acad. Sci. USA*, 89:8671–8675, 1992.

[85] K. D. Karavitaki and D. P. Corey. Sliding adhesion confers coherent motion to hair cell stereocilia and parallel gating to transduction channels. *J Neurosci*, 30(27):9051–9063, Jul 2010. doi: 10.1523/JNEUROSCI.4864-09.2010. URL http://dx.doi.org/10.1523/JNEUROSCI.4864-09.2010.

[86] P. Kazmierczak, H. Sakaguchi, J. Tokita, E. M. Wilson-Kubalek, R. A. Milligan, U. Mller, and B. Kachar. Cadherin 23 and protocadherin 15 interact to form tip-link filaments in sensory hair cells. *Nature*, 449(7158):87–91, Sep 2007. doi: 10.1038/nature06091. URL http://dx.doi.org/10.1038/nature06091.

[87] D. T. Kemp. Stimulated acoustic emissions from within the human auditory system. *J Acoust Soc Am*, 64(5):1386–1391, Nov 1978.

[88] H. J. Kennedy, M. G. Evans, A. C. Crawford, and R. Fettiplace. Fast adaptation of mechanoelectrical transducer channels in mammalian cochlear hair cells. *Nat Neurosci*, 6:832–836, 2003. doi: 10.1038/nn1089.

[89] H. J. Kennedy, A. C. Crawford, and R. Fettiplace. Force generation by mammalian hair bundles supports a role in cochlear amplification. *Nature*, 433: 880–883, 2005.

[90] D. O. Kim, S. T. Neely, C. E. Molnar, and J. W. Matthews. An active cochlear model with negative damping in the partition: comparison with Rhode's ante- and post-mortem observations. In G. van den Brink and F. A. Bilsen, editors, *Psychological, physiological and behavioral studies of hearing*, pages 7–14. Delft University Press, Delft, the Netherlands, 1980.

[91] C. Köppl, O. Gleich, and G. Manley. An auditory fovea in the barn owl cochlea. *J. Comp. Physiol. A*, 171:695–704, 1993.

[92] C. Köppl, K. H. Iwasa, and B. Sul. Big and powerful: a model of the contribution of bundle motility to mechanical amplification in hair cells of the bird basilar papilla. In N. P. Cooper and T. Kemp, D., editors, *Concepts and challenges in the biophysics of hearing*, pages 444–450, Singapore, 2009. World Scientific.

[93] A. S. Kozlov, T. Risler, and A. J. Hudspeth. Coherent motion of stereocilia assures the concerted gating of hair-cell transduction channels. *Nat Neurosci*, 10:87–92, 2007. doi: 10.1038/nn1818.

[94] C. J. Kros. Physiology of mammalian cochlear hair cells. In P. Dallos, A. N. Popper, and R. R. Fay, editors, *The Cochlea*, pages 318–385. Springer, New York, 1996.

[95] C. J. Kros, A. Rüsch, and G. P. Richardson. Mechano-electrical transducer currents in the hair cells of the cultured mouse cochlea. *Proc. Roy. Soc. Lond. B*, 249:185–193, 1992.

[96] L. Le Goff, D. Bozovic, and A. J. Hudspeth. Adaptive shift in the domain of negative stiffness during spontaneous oscillation by hair bundles from the internal ear. *Proc. Natl. Acad. Sci. USA*, 102:16996–17001, 2005.

[97] M. LeMasurier and P. G. Gillespie. Hair-cell mechanotransduction and cochlear amplification. *Neuron*, 48:403–415, 2005.

[98] M. C. Liberman and L. W. Dodds. Single neuron labeling and chronic cochlear pathology. III. stereocilia damage and alterations of threshold tuning curves. *Hearing Res.*, 16:55–74, 1984.

[99] M. C. Liberman, J. Gao, D. Z. He, X. Wu, S. Jia, and J. Zuo. Prestin is required for electromotility of the outer hair cell and for the cochlear amplifier. *Nature*, 419:300–304, 2002.

[100] D. J. Lim. Cochlear anatomy related to cochlear micromechanics. a review. *J. Acoust. Soc. Am.*, 67:1686–1695, 1980.

[101] P. Luger. Dynamics of ion transport systems in membranes. *Physiol Rev*, 67 (4):1296–1331, Oct 1987.

[102] A. N. Lukashkin, M. N. Walling, and I. J. Russell. Power amplification in the mammalian cochlea. *Curr Biol*, 17:1340–1344, 2007. doi: 061.

[103] E. A. Lumpkin and A. J. Hudspeth. Regulation of free Ca^{2+} concentration in hair-cell stereocilia. *J Neurosci*, 18(16):6300–6318, Aug 1998.

[104] F. Mammano and J. F. Ashmore. Differential expression of outer hair cell potassium currents in the isolated cochlea of the guinea-pig. *J. Physiol.*, 496: 639–646, 1996.

[105] F. Mammano and R. Nobili. URL `147.162.36.50/cochlea`.

[106] G. A. Manley. Cochlear mechanisms from a phylogenetic viewpoint. *Proc. Natl. Acad. Sci. USA*, 97:11736–11743, 2000.

[107] G. A. Manley. Evidence for an active process and a cochlear amplifier in nonmammals. *J Neurophysiol*, 86(2):541–549, Aug 2001.

[108] G. A. Manley and C. Köppl. Phylogenetic development of the cochlea and its innervation. *Curr Opin Neurobiol*, 8(4):468–474, Aug 1998.

[109] G. A. Manley, B. Meyer, F. P. Fischer, G. Schwabedissen, and O. Gleich. Surface morphology of basilar papilla of the tufted duck aythya fuligula, and domestic chicken gallus gallus domesticus. *J Morphol*, 227(2):197–212, Feb 1996. doi: 3.0.CO;2-6. URL `http://dx.doi.org/3.0.CO;2-6`.

[110] G. A. Manley, D. L. Kirk, C. Köppl, and G. K. Yates. In vivo evidence for a cochlear amplifier in the hair-cell bundle of lizards. *Proc Natl Acad Sci U S A*, 98(5):2826–2831, Feb 2001. doi: s.041604998.

[111] P. Martin, A. D. Mehta, and A. J. Hudspeth. Negative hair-bundle stiffness betrays a mechanism for mechanical amplification by the hair cell. *Proc. Natl. Acad. Sci. USA*, 97:12026–12031, 2000.

[112] P. Martin, D. Bozovic, Y. Choe, and A. J. Hudspeth. Spontaneous oscillation by hair bundles of the bullfrog's sacculus. *J Neurosci*, 23(11):4533–4548, Jun 2003.

[113] M. M. Merzenich, P. L. Knight, and G. L. Roth. Representation of cochlea within primary auditory cortex in the cat. *J Neurophysiol*, 38(2):231–249, Mar 1975.

[114] D. C. Mountain and A. E. Hubbard. Computational analysis of hair cell and auditory nerve processes. In H. L. Hawkins, T. A. McMullen, A. N. Popper, and R. R. Fay, editors, *Auditory Computation*, pages 121–156. Springer, New York, 1995.

[115] D. Navaratnam, J.-P. Bai, H. Samaranayake, and J. Santos-Sacchi. N-terminal-mediated homomultimerization of prestin, the outer hair cell motor protein. *Biophys J*, 89:3345–3352, 2005. doi: 10.1529/biophysj.105.068759.

[116] S. T. Neely and D. O. Kim. An active cochlear model showing sharp tuning and high sensitivity. *Hear Res*, 9(2):123–130, Feb 1983.

[117] S. T. Neely and D. O. Kim. A model for active elements in cochlear biomechanics. *J. Acoust. Soc. Am.*, 79:1472–1480, 1986.

[118] M. Ospeck, X.-X. Dong, and K. H. Iwasa. Limiting frequency of the cochlear amplifier based on electromotility of outer hair cells. *Biophys. J.*, 84:739–749, 2003.

[119] M. Ospeck, X.-X. Dong, J. Fang, and K. H. Iwasa. Electromotility in outer hair cells: a supporting role for fast potassium conductance. *ORL J Otorhinolaryngol Relat Spec*, 68(6):373–377, 2006. doi: 10.1159/000095280.

[120] J. O. Pickles. *An introduction to the physiology of hearing, 2nd edition.* Academic Press, London, 1988.

[121] J. O. Pickles. A model for the mechanics of the stereociliar bundle on acousticolateral hair cells. *Hear Res*, 68(2):159–172, Aug 1993.

[122] R. Probst. Otoacoustic emissions: an overview. *Adv Otorhinolaryngol*, 44: 1–91, 1990.

[123] S. Ramamoorthy, N. V. Deo, and K. Grosh. A mechano-electro-acoustical model for the cochlea: response to acoustic stimuli. *J Acoust Soc Am*, 121: 2758–2773, 2007.

[124] T. Ren. Longitudinal pattern of basilar membrane vibration in the sensitive cochlea. *Proc Natl Acad Sci U S A*, 99(26):17101–17106, Dec 2002. doi: 10.1073/pnas.262663699.

[125] W. S. Rhode. Observations of the vibration of the basilar membrane in squirrel monkeys using the Mössbauer technique. *J. Acoust. Soc. Am.*, 49:1218–1231, 1971.

[126] A. J. Ricci, A. C. Crawford, and R. Fettiplace. Active hair bundle motion linked to fast transducer adaptation in auditory hair cells. *J. Neurosci.*, 20: 7131–7142, 2000.

[127] A. J. Ricci, A. C. Crawford, and R. Fettiplace. Mechanisms of active hair bundle motion in auditory hair cells. *J Neurosci*, 22(1):44–52, Jan 2002.

[128] A. J. Ricci, A. C. Crawford, and R. Fettiplace. Mechanisms of active hair bundle motion in auditory hair cells. *J. Neurosci.*, 22:44–52, 2002.

[129] A. J. Ricci, A. C. Crawford, and R. Fettiplace. Tonotopic variation in the conductance of the hair cell mechanotransducer channel. *Neuron*, 40:983–990, 2003.

[130] A. J. Ricci, B. Kachar, J. Gale, and S. M. V. Netten. Mechano-electrical transduction: new insights into old ideas. *J Membr Biol*, 209(2-3):71–88, 2006. doi: 10.1007/s00232-005-0834-8. URL `http://dx.doi.org/10.1007/s00232-005-0834-8`.

[131] L. Robles and M. A. Ruggero. Mechanics of the mammalian cochlea. *Physiol Rev*, 81(3):1305–1352, Jul 2001.

[132] L. Robles, M. A. Ruggero, and N. C. Rich. Basilar membrane mechanics at the base of the chinchilla cochlea. i. input-output functions, tuning curves, and response phases. *J Acoust Soc Am*, 80(5):1364–1374, Nov 1986.

[133] M. A. Ruggero and N. C. Rich. Furosemide alters organ of corti mechanics: evidence for feedback of outer hair cells upon the basilar membrane. *J. Neurosci.*, 11:1057–1067, 1991.

[134] M. A. Ruggero, N. C. Rich, A. Recio, S. S. Narayan, and L. Robles. Basilar-membrane responses to tones at the base of the chinchilla cochlea. *J Acoust Soc Am*, 101(4):2151–2163, Apr 1997.

[135] G. Runhaar. The surface morphology of the avian tectorial membrane. *Hear Res*, 37(2):179–187, Jan 1989.

[136] I. J. Russell. Origin of the receptor potential in inner hair cells of the mammalian cochlea–evidence for davis' theory. *Nature*, 301(5898):334–336, Jan 1983.

[137] A. Ryan and P. Dallos. Effect of absence of cochlear outer hair cells on behavioural auditory threshold. *Nature*, 253(5486):44–46, Jan 1975.

[138] V. Rybalchenko and J. Santos-Sacchi. Cl^- flux through a non-selective, stretch-sensitive conductance influences the outer hair cell motor of the guinea-pig. *J Physiol*, 547:873–891, 2003. doi: 34.

[139] A. N. Salt, N. Inamura, R. Thalmann, and A. Vora. Calcium gradients in inner ear endolymph. *Am. J. Otol.*, 10:371–375, 1989.

[140] J. Santos-Sacchi. Reversible inhibition of voltage-dependent outer hair cell motility and capacitance. *J. Neurophysiol.*, 11:3096–3110, 1991.

[141] J. Santos-Sacchi. On the frequency limit and phase of outer hair cell motility: effects of the membrane filter. *J Neurosci*, 12:1906–1916, 1992.

[142] J. Santos-Sacchi and J. P. Dilger. Whole cell currents and mechanical responses of isolated outer hair cells. *Hearing Res.*, 65:143–150, 1988.

[143] J. Santos-Sacchi, S. Kakehata, T. Kikuchi, Y. Katori, and T. Takasaka. Density of motility-related charge in the outer hair cell of the guinea pig is inversely related to best frequency. *Neurosci Lett.*, 256:155–158, 1998.

[144] J. Santos-Sacchi, L. Song, J. Zheng, and A. L. Nuttall. Control of mammalian cochlear amplification by chloride anions. *J Neurosci*, 26:3992–3998, 2006. doi: 10.1523/JNEUROSCI.4548-05.2006.

[145] G. Sauer, C. P. Richter, and R. Klinke. Sodium, potassium, chloride and calcium concentrations measured in pigeon perilymph and endolymph. *Hear Res*, 129(1-2):1–6, Mar 1999.

[146] S. K. Scott. *Oscillations, Waves, and Chaos in Chemical Kinetics*. Oxford University Press, USA, 1994.

[147] P. M. Sellick, R. Patuzzi, and B. M. Johnstone. Measurement of basilar membrane motion in the guinea pig using the mssbauer technique. *J Acoust Soc Am*, 72(1):131–141, Jul 1982.

[148] C. A. Shera. Mammalian spontaneous otoacoustic emissions are amplitude-stabilized cochlear standing waves. *J Acoust Soc Am*, 114(1):244–262, Jul 2003.

[149] F. Si, H. Brodie, P. G. Gillespie, A. E. Vazquez, and E. N. Yamoah. Developmental assembly of transduction apparatus in chick basilar papilla. *J Neurosci*, 23(34):10815–10826, Nov 2003.

[150] G. P. Sinha, F. Sabri, E. K. Dimitriadis, and K. H. Iwasa. Organization of membrane motor in outer hair cells: an atomic force microscopic study. *Pflugers Arch*, 459(3):427–439, Feb 2010. doi: 10.1007/s00424-009-0742-3. URL `http://dx.doi.org/10.1007/s00424-009-0742-3`.

[151] M. Sotomayor, D. P. Corey, and K. Schulten. In search of the hair-cell gating spring elastic properties of ankyrin and cadherin repeats. *Structure*, 13(4):669–682, Apr 2005. doi: 10.1016/j.str.2005.03.001. URL `http://dx.doi.org/10.1016/j.str.2005.03.001`.

[152] A. A. Spector, W. E. Brownell, and A. S. Popel. Effect of outer hair cell piezoelectricity on high-frequency receptor potentials. *J Acoust Soc Am*, 113 (1):453–461, Jan 2003.

[153] K. J. Spinelli and P. G. Gillespie. Bottoms up: transduction channels at tip link bases. *Nat Neurosci*, 12(5):529–530, May 2009. doi: 10.1038/nn0509-529. URL `http://dx.doi.org/10.1038/nn0509-529`.

[154] E. A. Stauffer, J. D. Scarborough, M. Hirono, E. D. Miller, K. Shah, J. A. Mercer, J. R. Holt, and P. G. Gillespie. Fast adaptation in vestibular hair cells requires myosin-1c activity. *Neuron*, 47:541–553, 2005.

[155] P. S. Steyger, P. G. Gillespie, and R. A. Baird. Myosin ibeta is located at tip link anchors in vestibular hair bundles. *J Neurosci*, 18(12):4603–4615, Jun 1998.

[156] B. Sul and K. H. Iwasa. Amplifying effect of a release mechanism for fast adaptation in the hair bundle. *J Acoust Soc Am*, 126(1):4–6, Jul 2009. doi: 10.1121/1.3143782. URL `http://dx.doi.org/10.1121/1.3143782`.

[157] L. G. Tilney and J. C. Saunders. Actin filaments, stereocilia, and hair cells of the bird cochlea. I. length, number, width, and distribution of stereocilia of each hair cell are related to the position of the hair cell on the cochlea. *J. Cell Biol.*, 96:807–821, 1983.

[158] L. G. Tilney and M. S. Tilney. The actin filament content of hair cells of the bird cochlea is nearly constant even though the length, width, and number of stereocilia vary depending on the hair cell location. *J Cell Biol*, 107(6 Pt 2): 2563–2574, Dec 1988.

[159] L. G. Tilney, M. S. Tilney, J. S. Saunders, and D. J. DeRosier. Actin filaments, stereocilia, and hair cells of the bird cochlea. iii. the development and differentiation of hair cells and stereocilia. *Dev Biol*, 116(1):100–118, Jul 1986.

[160] L. G. Tilney, D. A. Cotanche, and M. S. Tilney. Actin filaments, stereocilia and hair cells of the bird cochlea: vi. how the number and arrangement of stereocilia are determined. *Development*, 116(1):213–226, Sep 1992.

[161] M. Tilney, L. Tilney, and D. DeRosier. The distribution of hair cell bundle lengths and orientations suggests an unexpected pattern of hair cell stimulation in the chick cochlea. *Hear Res*, 25:141–151, 1987.

[162] J.-Y. Tinevez, F. Jülicher, and P. Martin. Unifying the various incarnations of active hair-bundle motility by the vertebrate hair cell. *Biophys J*, 93:4053–4067, 2007. doi: 10.1529/biophysj.107.108498.

[163] S. M. van Netten and C. J. Kros. Gating energies and forces of the mammalian hair cell transducer channel and related hair bundle mechanics. *Proc. R. Soc. Lond. B Biol. Sci.*, 267:1915–1923, 2000.

[164] S. M. van Netten, C. J. W. Meulenberg, G. W. T. Lennan, and C. J. Kros. Pairwise coupling of hair cell transducer channels links auditory sensitivity and dynamic range. *Pflugers Arch*, 458(2):273–281, Jun 2009. doi: 10.1007/s00424-008-0617-z. URL `http://dx.doi.org/10.1007/s00424-008-0617-z`.

[165] M. A. Vollrath, K. Y. Kwan, and D. P. Corey. The micromachinery of mechanotransduction in hair cells. *Annu Rev Neurosci*, 30:339–365, 2007. doi: ro.29.051605.112917. URL `http://dx.doi.org/ro.29.051605.112917`.

[166] G. von Békésy. The variation in phase along the basilar membrane with sinusoidal vibration. *J Acous Soc Am*, 19:452–460, 1947.

[167] G. von Békésy. On the resonance curve and the decay period at various points on the cochlear partition. *J Acoust Soc Am*, 21:245–254, 1949.

[168] G. von Békésy. Description of some mechanical properties of the organ of corti. *J Acoust Soc Am*, 25:770–785, 1953.

[169] G. von Békésy. *Experiments in Hearing*. MacGraw-Hill, 1960.

[170] R. G. Walker and A. J. Hudspeth. Calmodulin controls adaptation of mechanoelectrical transduction by hair cells of the bullfrog's sacculus. *Proc Natl Acad Sci U S A*, 93(5):2203–2207, Mar 1996.

[171] P. Wangemann. Supporting sensory transduction: cochlear fluid homeostasis and the endocochlear potential. *J Physiol*, 576(Pt 1):11–21, Oct 2006. doi: 10.1113/jphysiol.2006.112888. URL `http://dx.doi.org/10.1113/jphysiol.2006.112888`.

[172] S. Xue, D. C. Mountain, and A. E. Hubbard. Direct measurement of electrically evoked basilar membrane motion. In H. J. v. D. P. . v. N. S. Duifuis, H., editor, *Biophysics of hair cell sensory systems.*, pages 361–369. Singapore: World Scientific, 1993.

[173] E. N. Yamoah and P. G. Gillespie. Phosphate analogs block adaptation in hair cells by inhibiting adaptation-motor force production. *Neuron*, 17(3):523–533, Sep 1996.

[174] E. N. Yamoah, E. A. Lumpkin, R. A. Dumont, P. J. Smith, A. J. Hudspeth, and P. G. Gillespie. Plasma membrane Ca^{2+}-ATPase extrudes Ca^{2+} from hair cell stereocilia. *J Neurosci*, 18(2):610–624, Jan 1998.

[175] Y. Zhao, E. N. Yamoah, and P. G. Gillespie. Regeneration of broken tip links and restoration of mechanical transduction in hair cells. *Proc Natl Acad Sci U S A*, 93(26):15469–15474, Dec 1996.

[176] J. Zheng, W. Shen, D. Z.-Z. He, K. B. Long, L. D. Madison, and P. Dallos. Prestin is the motor protein of cochlear outer hair cells. *Nature*, 405:149–155, 2000.

[177] G. Zweig. Finding the impedance of the organ of Corti. *J. Acoust. Soc. Am.*, 89:1229–1254, 1991.

[178] G. Zweig and C. A. Shera. The origin of periodicity in the spectrum of evoked otoacoustic emissions. *J Acoust Soc Am*, 98(4):2018–2047, Oct 1995.

[179] E. Zwicker. A model describing nonlinearities in hearing by active processes with saturation at 40 dB. *Biol Cybern*, 35(4):243–250, Dec 1979.